Multivalent Molecular Motors for Surface Attachment

Chen, Kuang-Yen

Multivalent Molecular Motors For Surface Attachment

Kuang-Yen Chen

The research described in this thesis was carried out at the Stratingh Institute for chemistry, University of Groningen, The Netherlands.

This work was financially supported by the Ubbo Emmius Scholarship.

Cover designed by Kuang-Yen Chen
Photo credits to Kuang-Yen Chen and Flora van der Wei

Printed by Ipskamp Drukkers BV, Enschede, The Netherlands

ISBN: 978-90-367-7239-6
eISBN: 978-90-367-7240-2

university of groningen

Multivalent Molecular Motors For Surface Attachment

PhD Thesis

to obtain the degree of PhD at the
University of Groningen
on the authority of the
Rector Magnificus Prof. E. Sterken
and in accordance with
the decision by the College of Deans.

This thesis will be defended in public on

Friday 28 November 2014 at 16.15 hours

by

Kuang-Yen Chen

born on 11 March 1986
in Taipei, Taiwan

Supervisor
Prof. B. L. Feringa

Assessment committee
Prof. W. R. Browne
Prof. P. Rudolf
Prof. J. Huskens

Table of contents

Chapter 1: Light-Driven Molecular Motors on Surfaces

Chapter 2: Towards Dynamic Control of Wettability by Using Functionalized Altitudinal Molecular Motors on Solid Surfaces

Chapter 3: Control of Surface Wettability Using Tripodal Light-Activated Molecular Motors

Chapter 4: Tetrapodal Molecular Switches and Motors: Synthesis and Photochemistry

Chapter 5: Facile Assembly of Light-Driven Molecular Motors onto a Solid Surface

Chapter 1
Light-Driven Molecular Motors on Surfaces

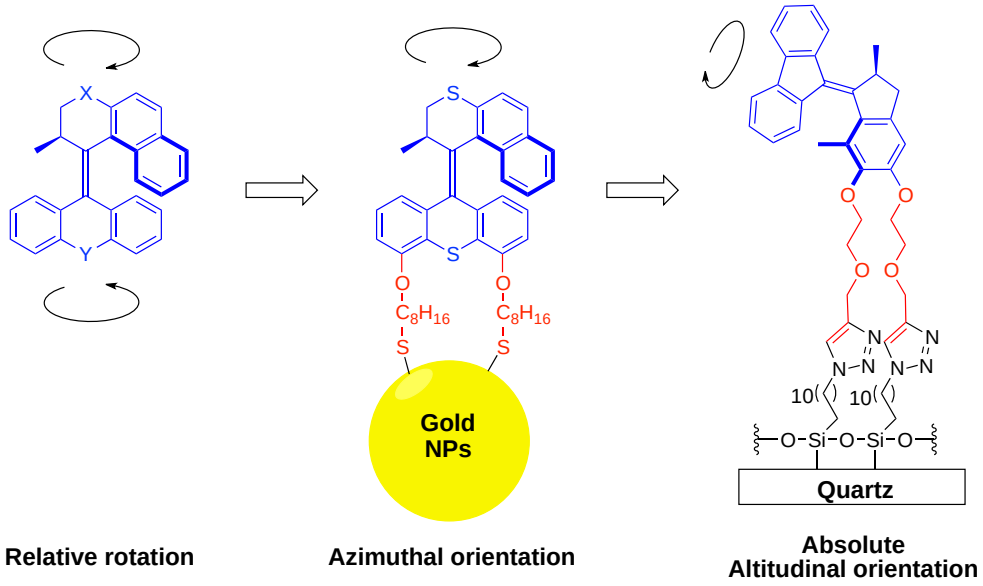

Confining light-driven molecular motors on surfaces could inhibit the Brownian motion and hence, the relative rotation of one part of the molecule with respect to the other can be converted into absolute rotation.

1.1 Introduction

The design and construction of molecular-level devices *e.g.*, molecular switches and machines for the control over macroscopic phenomena is of great importance to future nanotechnologies.[1,2,3,4,5,6,7] Nature provide chemists with fascinating examples of nanoscale rotary motors, F_1-ATP synthase,[8] of which solvated form is able to hydrolyze adenosine tri-phosphate (ATP), the cell's energy currency, and convert the energy into rotary motion of its central stalk.[9,10] Inspired by the dynamic systems like naturally occurring ATP synthase and the machines of the macroscopic world, scientists have developed molecular tweezers,[11] propellers,[12] brakes,[13] elevators,[14] nanocars,[15,16] and muscles[2] over the past decades.[7,17,18] Moreover, it has been demonstrated that molecular switches can be used to perform specific functions, such as reversible change in supramolecular organization,[19] synthesizing a peptide in a sequence-specific manner,[20] rotating microscale objects,[21] and control of singlet oxygen generation for photodynamic therapy.[22]

While in the solution phase, any directed motion generated by the molecular machines is overwhelmed and dissipated by the uncontrolled Brownian motion, which makes it challenging to harness the collective motion of molecular machines to perform work. Immobilizing molecules on the interface inhibits the Brownian motion and allows not only for tuning the surface with tailored properties *e.g.*, wettability,[23,24] optical property,[25,26] conductance,[27,28] chirality,[29,30] and catalytic activity[31,32] but also for performing work at the molecular level through externally induced reversible structural changes.[33,34,35]

In recent years, increasing attention has therefore been focused on surface-immobilized systems containing molecules that are capable of undergoing reversible structural changes in response to external stimuli.[36,37] Spiropyrans, azobenzenes, dithienylethenes, and molecular motors based on overcrowded alkenes have proven to be particularly versatile stimuli-responsive molecules in surface-immobilized systems.[3,4,7] Various types of external stimuli *e.g.*, chemical,[38,39] electric,[40] or light[36] can be applied to change the structure of these molecules on the surfaces. Among these stimuli the use of light, which allows spatial temporal control,[26] is of particular interest due to the potential fast response times of photochemical processes and because light provides a clean, noninvasive, and tunable energy input.[41] In this chapter, we focus on various approaches for the control of surface wettability using surface-immobilized

systems based on photochromic molecular switches. Furthermore a detailed review and analysis of the recent progress in photoresponsive surface based on molecular motors, and their potential applications in the control of surface wettability is presented.

1.2 Photochromic molecular switches

1.2.1 Spiropyrans

The ring-closed form of spiropyran is consisting of an indoline and a chromene moiety bound together *via* a spiro junction making the two moieties oriented perpendicularly to with each other (Scheme 1). Spiropyran could undergo photoisomerization from a ring-closed form (SP) to a zwitterionic merocyanine isomer (MC) upon irradiation with UV light, which is accompanied with a large change in dipole moment (~15 Debye).[7,42,43]

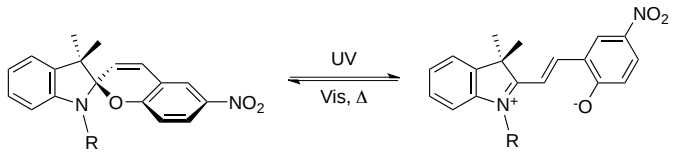

Spiropyran (SP) Spiropyran (MC)

Scheme 1 Reversible isomerization between ring-closed form and merocyanine form of spiropyrans.[*]

1.2.2 Azobenzenes

Azobenzenes are among the most studied photochromic units and have received substantial attention due to their simple molecular structure, relatively facile synthesis, and fatigue resistant *trans*→*cis* photoisomerization.[7,44,45] When the thermodynamically stable *trans* isomer of azobenzene is exposed to UV light, it isomerize to the *cis* isomer (Scheme 2); the two isomers have noticeable difference in molecular geometry, electronic properties, and dipole moment, making azobenzene an attractive candidate for construction of photoswitchable systems

[*] For consistency, the name "spiropyran" in this chapter applies to both isomers, and the ring-closed form is abbreviated as "SP", ring-open form as "MC".

and materials. The *cis* isomer is metastable, hence it undergo thermal *cis*→*trans* isomerization at room temperature once the UV light source is removed and this may be the drawback in the construction of photoresponsive surfaces based on azobenzenes.

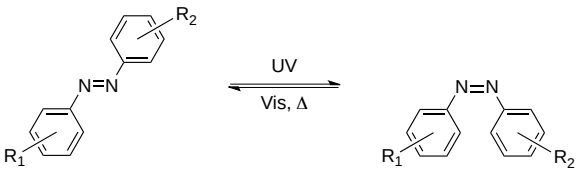

Scheme 2 Reversible photoisomerization of azobenzene moieties upon UV-vis irradiation.

1.2.3 Dithienylethenes

Dithienylethenes undergo photocyclization from ring-open to closed form by irradiation with UV light ($300 < \lambda < 400$ nm); while the reverse process occurs with visible light ($500 < \lambda < 700$ nm).[7] In the ring-closed form of dithienylethene, the π-conjugation extends through the entire molecule; while in the ring-open form, it is restricted to each half of the molecule (Scheme 3). Compared to other photochromic compounds, dithienylethenes display excellent thermal stability for both isomers as well as superb resistance to photodegradation.[46,47]

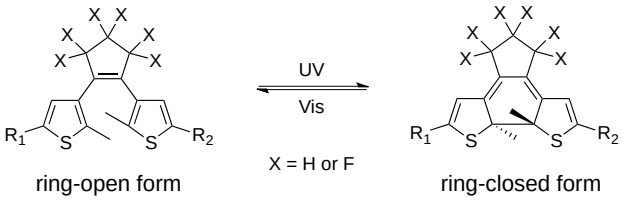

Scheme 3 Photoswitching of dithienylethenes.

1.2.4 Alkenes

Olefins can undergo *trans*→*cis* photoisomerization through a geometrical isomerization of the C=C double bond.[48] The best known switch among these systems are stilbenes, which can be switched reversibly between *trans* and *cis* isomers upon irradiation with light (Scheme 4).[7,49] However, the application of stilbenes for the construction of a photoresponsive surface is limited due to side

reactions. Photochemical reaction of *cis*-stilbene results in an oxidative cyclization to provide phenanthrene, a side product that could not be reverted to its original form. This side reaction could be prevented by *ortho*-substitution of the benzene rings which forms the basis for the construction of molecular motors based on overcrowded alkenes (see section 1.4 for discussions on molecular motors).

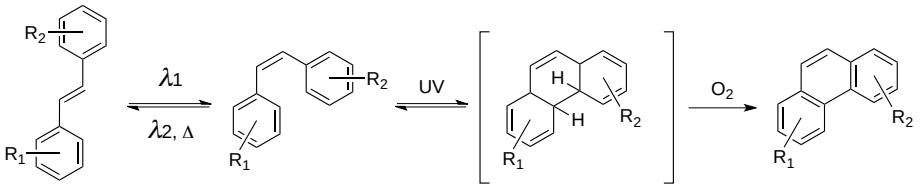

trans-stilbene *cis*-stilbene phenanthrene

Scheme 4 Photoisomerization of stilbenes and the side reaction: oxidative photocyclization.

1.3 Controlling of surface wettability with molecular switches

One of the simplest way to demonstrate that the photoinduced switching of a surface-bound layer of molecular switches can collectively influence interactions with an overlayer material is to monitor the contact angle of a liquid on top of the monolayer of molecular switches.[23,24] Changes in the contact angle (CA) of a liquid droplet at the surface of the monolayer can be correlated to collective changes in the orientation or morphology of the switches with respect to the surface.[50,51] Numerous examples of surfaces functionalized with photo-responsive molecular switches and machines for reversible light-induced wettability changes have been reported and representative examples are discussed below.

1.3.1 Spiropyran-functionalized surfaces

Spiropyrans can be converted from a relatively hydrophobic ring-closed form (SP) to a hydrophilic zwitterionic merocyanine isomer (MC) accompanied with a higher dipole moment (Scheme 1). This unique feature makes spiropyrans ideal candidates for controlling surface wettability by light. Rasario *et al.* demonstrated that the water contact angle (WCA) of a droplet on a surface functionalized with mixed monolayers of spiropyrans and alkylsilanes can be switched reversibly upon irradiation with UV and visible light (Figure 1).[52] They further demonstrated that by coating a similar monolayer in the inner wall of a 500 μm diameter capillary, the water in the capillary tubes rose up for ~2.8 mm upon UV irradiation, while the

water did not rise using a control capillary tube.[52]

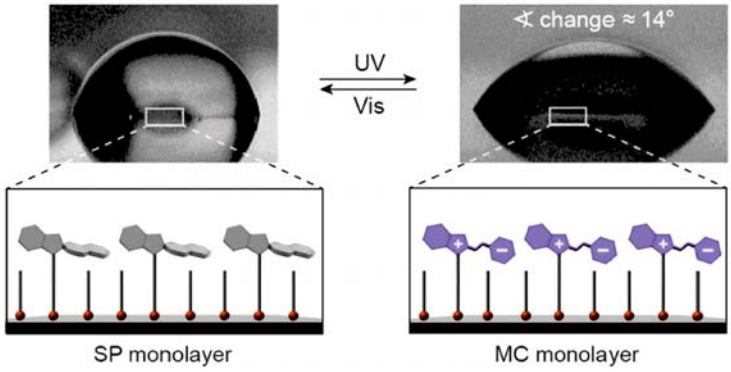

Figure 1 Water droplet on a spiropyran-functionalized surface after irradiation with visible light (left) and UV light (right). The magnitude of the WCA change was found to be 11º–14º. Reproduced from Ref. [42,52].

However, the control of WCA on flat and smooth surfaces functionalized with photoresponsive organic monolayers remains challenging. The change of the WCA of spiropyran monolayers on flat surfaces is typically in the order of 5-14º.[42,52] Therefore, different strategies have been applied in an effort to amplify the contact angle variation. Locklin *et al.* reported a surface modified with covalently attached spiropyran-based polymer films which could be used to switch the WCA reversibly for up to 15º upon UV irradiation.[53] By simply adding $CoCl_2$ to the water droplet lying on the same polymer film, the WCA variation could be enhanced from 15º to 35º upon UV irradiation (Figure 2). This amplification of WCA change is attributed to the photoisomerization from SP→MC•Co(II) instead of SP→MC; with the MC•Co(II) being a more hydrophilic complex. A drawback of this approach is the potential contamination of the surface with $CoCl_2$ salt.

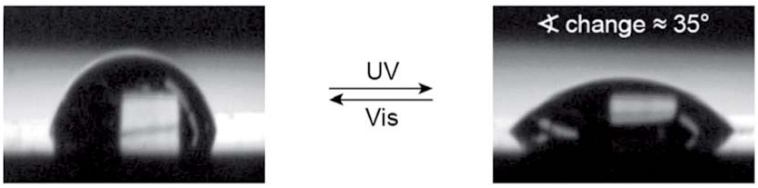

Figure 2 $CoCl_{2(aq.)}$ solution in water droplet on a spiropyran-functionalized surface after irradiation with visible light (left) and UV light (right). Reproduced from Ref. [53].

Inspired by the naturally occurring superhydrophobic surfaces,[54] *e.g.* lotus leaves,[55] butterfly wings,[56] and water striders,[57] an alternative approach to enhance the contact angle change is achieved by combining two features together: the chemical composition of the surface and the surface roughness. A rough surface could be prepared by modifying the surface either with Si-nanowires (20-50 nm diameter; Figure 3, left)[58] or polymeric nanorods (Figure 3, right).[59] It is generally assumed that for rough surfaces with water repellent properties, the liquid droplets rest on top of the rough features with air trapped in the nanopores (Cassie wetting),[60] while for the enhanced wettability of a hydrophilic surface, the droplets penetrate and wet the rough features of the surfaces (Wenzel wetting).[61]

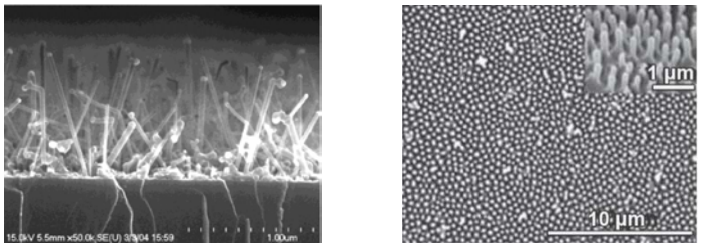

Figure 3 SEM images of Si nanowire grown on a silicon substrate (left) and polymer nanorods based surfaces (right). Adapted from Ref. [58,58].

Yang *et al.* found that by grafting polymers with spiropyran side chains on a silicon substrate, the WCA of this rough surface could be changed from 140º to 43º upon UV irradiation and be changed back after 20 min of irradiation with visible light (Figure 4).[62] Chen *et al.* demonstrated a synergistic system based on cross-linked poly(*N*-Isopropyl Acrylamide) copolymer film containing covalently

attached spiropyrans (pNIPAAm-SP).[59] The surface was initially rich in pNIPAAm-MC•H^+ in the hydrated form in dark environment, the photoisomerization of pNIPAAm-MC•H^+→pNIPAAm-SP upon irradiation with visible light triggered the dehydration of the main chain of pNIPAAm, resulting the WCA to change from 49º to 73º. The authors further demonstrated that by incorporating microstructures[63] or nanostructures with nanorods[64] to the surface, the WCA variation could be enhanced from ~24º to ~79º and ~118º, respectively.

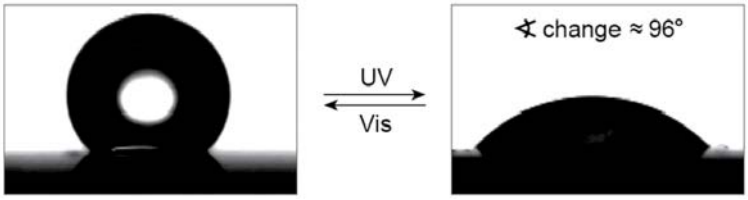

Figure 4 Water droplet on silicon substrates functionalized with spiropyran polymers before (left) and after (right) UV irradiation. Reproduced from Ref. [62].

1.3.2 Azobenzene-functionalized surface

Azobenzene exhibits changes in conformation and dipole moment upon *trans*→*cis* photoisomerization, resulting in changes to the inherent polarity and accordingly the surface wettability while attached to the interface (Scheme 2). Generally the WCA of *trans*-azobenzene monolayers decrease after UV irradiation, since the photoinduced *cis* isomer usually has a higher dipole moment, which is attributed to the asymmetric bent structure and the electron withdrawing properties of the N=N moiety of the azobenzenes in the *cis* form.[44,65]

Tamaki *et al.* compared the WCA changes of self-assembled monolayers (SAMs) based on azobenzenes bearing different substituents at their *para* positions (Scheme 5). In the case of *trans*-**1** SAMs or *trans*-**2** SAMs on gold, the WCA of the surfaces decreased for 5º or 7º upon UV irradiation, respectively.[65] However, the dipole moment of *cis*-**3** (2.77 D) was calculated to be lower than that of *trans*-**3** (4.93 D) because of the electron withdrawing properties of the N=N moiety and the cyano group cancelled partially each other, leading to the unusual increase of the WCA of *trans*-**3** SAMs after UV irradiation.

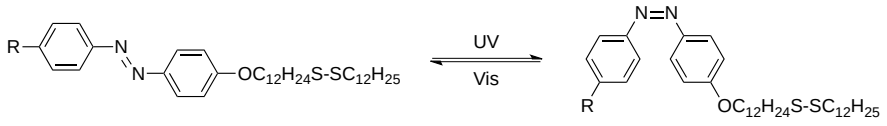

R = C_6H_{13} *trans*-**1**
R = H *trans*-**2**
R = CN *trans*-**3**

R = C_6H_{13} *cis*-**1**
R = H *cis*-**2**
R = CN *cis*-**3**

Scheme 5 Structure of asymmetric disulfides for producing SAMs on gold surfaces.

Unfortunately, the change in WCA of azobenzene monolayers on flat surfaces is typically in the order of 2-14º.[66,67,68,69] Larger changes are required for the construction of photoswitchable surface with tailored properties. It was already discussed in section 1.3.1 that the surface wettability variation could be enhanced by the introduction of surface roughness. Cho *et al.* developed an organic-inorganic hybrid deposition technique with layer-by-layer porous structures on silicon wafer terminated with amine functional groups. These amines were further functionalized *via* covalently attachment of azobenzenes bearing a trifluoromethyl (CF_3) group at the *para* position.[70,71] Increasing the number of deposition cycles enhances the surface roughness and nanoporosity, hence the WCA difference of the azobenzene film before and after UV irradiation could be increased from 5º for the flat surface to 150º for the surface after 9 deposition cycles. This is the first photoresponsive surface based on azobenzene which could be switched from superhydrophobic (WCA=152º) to superhydrophilic (WCA<5º).

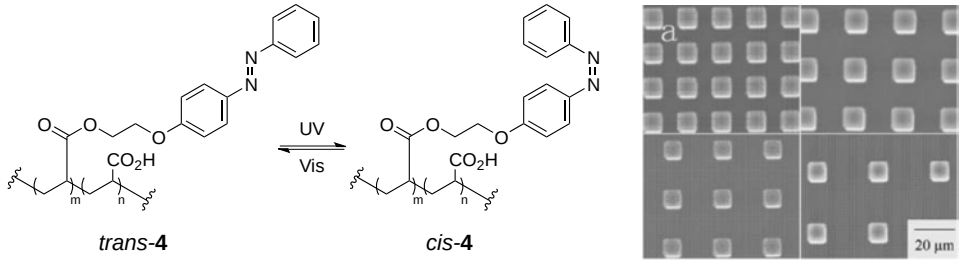

trans-**4** *cis*-**4**

Scheme 6 The *trans* and *cis* structures of polymeric azobenzenes (left); SEM images of silicon wafers patterned with micropillars (right). Adapted from Ref. [72].

Similarly, an azobenzene polyelectolyte **4** for fabricating organic films through electrostatic interaction on a silicon substrate was reported by Jiang *et al.* (Scheme 6, left).[72] A WCA change of 66º of the **4** monolayer after UV irradiation was achieved by introducing patterned square pillars on flat silicon substrate

through photolithography (Scheme 6, right)[73]; this difference is 33 times larger than the difference of a flat silicon substrate covered with the same polymeric **4** after irradiation (ΔWCA=2º). The amplification of WCA changes is attributed to the increased surface roughness by the micropillars on the patterned silicon substrates, and the trapped air in the microgrooves leading to a more hydrophobic surface (Cassie wetting, see section 1.3.1).[60]

The effect of surface roughness was also examined by using SAMs of a photocontrollable molecular shuttle on the basis of an *α*-cyclodextrin/azobenzene (*α*-CD/AB) inclusion complex (Figure 5).[74] The mixed monolayer of *n*-C_4H_9SH and the *α*-CD/*trans*-AB complex was assembled on a rough gold surface with the hydrophilic *α*-CD ring exposed to the interface (Figure 5 upper left, WCA= 70º). Upon UV irradiation, the *α*-CD cavity cannot include the bulky *cis*-AB anymore due to the the mismatch between the host and guest in shape, forcing the hydrophilic *α*-CD to be hidden from the interface by the *cis*-AB (Figure 5 lower left), hence an increase of WCA from 70º to 120º was observed. It should be noted that the WCA change of the same mixed-monolayer on flat gold surface upon UV irradiation is only ~2º, demonstrating the importance of surface roughness in constructing photoresponsive surface with larger wettability change.

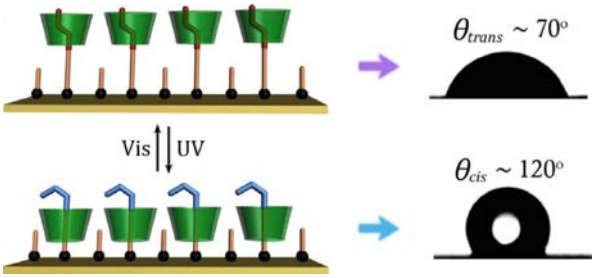

Figure 5 Schematic representation of an α-cyclodextrin/azobenzene inclusion complex (left, green cylinder = *α*-CD) and the corresponding change in WCA (right). Adapted from Ref. [44].

In a similar approach photocontrollable SAMs consisting of an calix[4]arene/*trans*-**5** inclusion complex grafted on rough silicon wafer by click chemistry was reported by Li *et al.* (Scheme 7, left).[75] The N atoms of the dimethylamino groups are electronegative and have affinity for the carboxylic acid group of the *trans*-**5**. Upon *trans*→*cis* photoisomerization by irradiation with UV light, *cis*-**5** was released from the calix[4]arene cavity (Scheme 7, right) due to the geometrical mismatch between the host and guest, caused the exposure of the

hydrophobic dimethylamino groups to the interface and hence an increase of WCA from 24º to 140º. The micro/nanostructured silicon surface again played an important role in the amplification of the WCA variation.

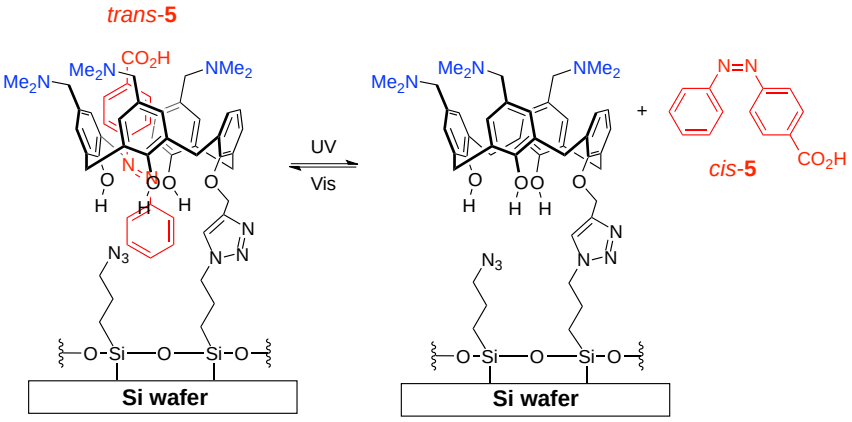

Scheme 7 Reversible switching of the host-guest system of calix[4]arene and azobenzenes.

The first example of macroscopic movement of liquid droplet on a flat solid surface modified with an azobezene monolayer was reported by Ichimura *et al.* who used aminosilylated silica substrated functionalized with azobenzene-containing calix[4]resocrinarene (Figure 6a).[67,76]

The calix[4]resocrinarene moiety dictates the orientation of the azobenzenes and increase the space between the azobezenes in the surface-bound assembly sufficiently to ensure efficient photoisomerization of the photochromic units. UV irradiation (365 nm) of the *trans*-**6** functionalized surface resulted in formation of the *cis*-**6** which has a larger dipole moment, hence the spreading of the droplet was observed after *trans*→*cis* photoisomerization. Macroscopic movement of the droplet was achieved by exposing the *cis*-**6** riched surface to blue light (436 nm) in a spatially controlled manner with a gradient of intensity (Figure 6b) to create gradients in surface free energy, which results in a directional transport of a liquid droplet at a constant velocity (35 μm/s for olive oil). This system has the advantage that the direction and the speed of the movement is tunable by varying the direction and steepness of the gradient in light intensity.

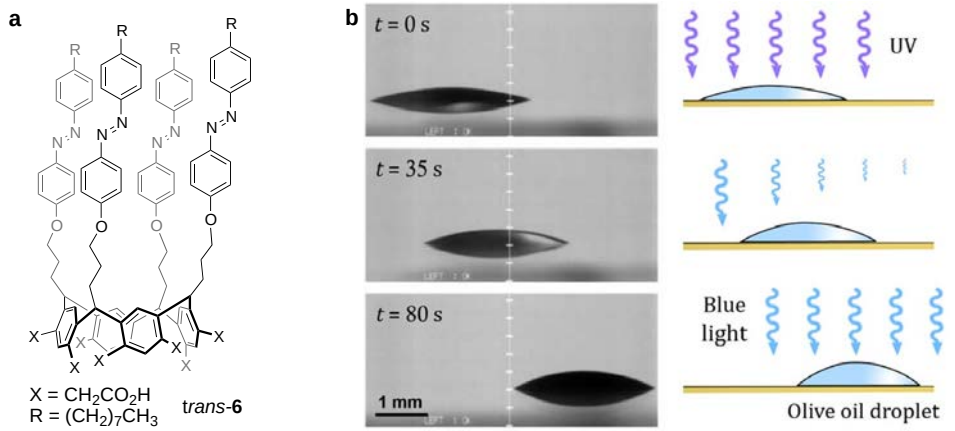

Figure 6 (a) A calix[4]resorcinarene derivative with azobenzene units. (b) Light-induced motion of an olive oil droplet on silica substrate decorated with *cis*-**6**. The droplet on the *cis*-rich surface moves in the direction of the higher surface energy area by exposure to blue light with a gradient in intensity. Adapted from Ref. [44].

1.3.3 Dithienylethene based thin films

There are two major approaches to control surface wettability: one is to change the polarity of the surface with photochromic azobenzene and spiropyran units as described in the previous sections. The other is to change the morphology of the surface, since the increase in surface roughness results in an enhancement in surface hydrophobicity (see section 1.3.1 and 1.3.2).

Irie *et al*. reported surface morphology changes upon UV irradiation due to the formation of needle-shape crystals on a glass substrate coated with dithienylethenes in the ring-open form (Figure 7a).[77] The WCA of this dithienylethenes film was initially 120º, upon UV irradiation (254 nm) the color of the film turned deep blue indicating photocylization of the dithienylethene from the ring-opened form to the ring-closed form, and the surface became superhydrophobic (WCA = 163º). SEM images showed that the surface was covered with microfibrils after UV irradiation (diameter around 1 μm; Figure DTE 1b). Upon irradiation of the substrate with visible light (λ > 500 nm), the surface became flat (Figure DTE 1c) and its initial WCA of 120º was recovered.

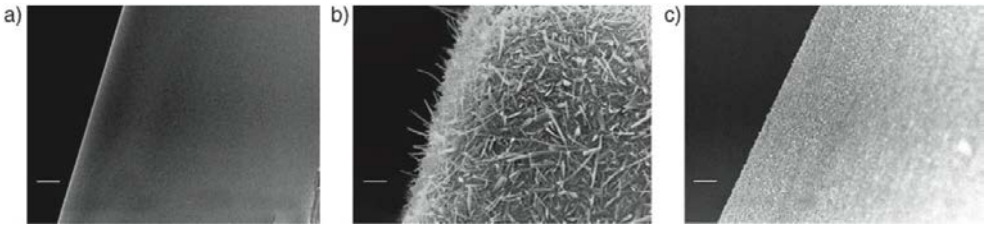

Figure 7 SEM images of the dithienylethene coated glass (Scale bar: 10 μm). (a) Before UV irradiation; (b) After UV irradiation and keeping the surface in dark for 24 h; (c) After irradiation with visible light and keeping the surface in dark for 24 h. Adapted from Ref. [77].

However, in Irie's system, the change in WCA is relatively small (120º ↔ 163º) and it took 24 h to form the rough surface by the formation of the fine fibril structures. To generate a larger WCA change, Uchida *et al.* designed new surface coated with dithienylethene derivative **7o** with a SO_2 group on one of the thiophenes to enhance the polarity of the surfaces (Scheme 8). In this system, the superhydrophobic rough surface (WCA > 150º) could be converted to hydrophilic flat surface (WCA < 90º) upon UV irradiation in 1 h due to the melting of the microcrystalline **7o**. This flat surface could be switched back to its original morphology by irradiation with visible light. The faster change in surface morphology in combination with larger change in WCA makes this system suitable for application in lithography and in biological environment.[78]

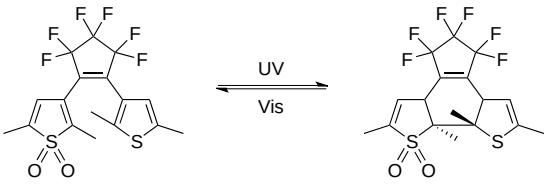

7o **7c**

Scheme 8 Molecular structure of the asymmetric diaryethenes.

1.3.4 Rotaxane-functionalized surface

Macroscopic liquid transport by surface functionalized with photoresponsive rotaxanes were reported by Leigh, Rudolf, and Zerbetto *et al*.[79] They designed a rotaxane consists of a macrocycle in a shuttle with perfluoroethyl segment on one side and a fumaramide moiety on the other (Scheme 9). The pyridine containing rotaxanes could be grafted to a monolayer of *n*-$C_{10}H_{20}CO_2H$ on gold film by physical adsorption.[25,80]

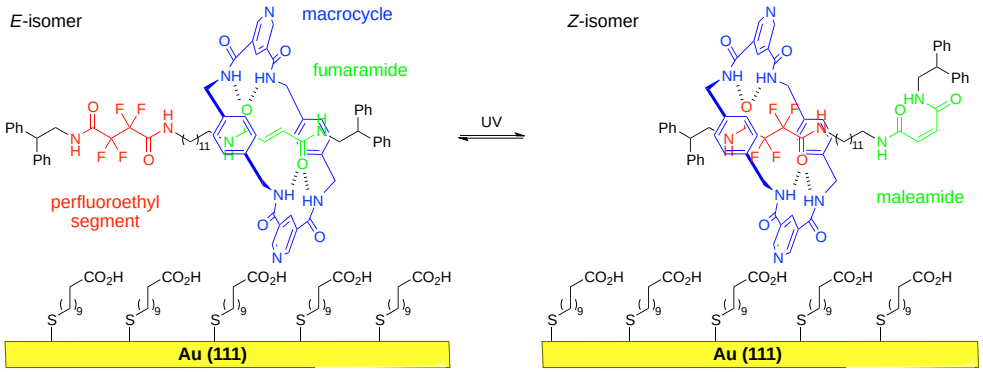

Scheme 9 Molecular shuttle based on rotaxanes.

In the *E*-isomer of the rotaxane, the macrocycle is positioned at the fumaramide station, hence the perfluoroethyl chain at the other end of the thread is exposed to the surface, making the interface hydrophobic. Upon UV irradiation, the fumaramide (which has higher affinity to the macrocycle) is converted to maleamide (which has lower affinity to the macrocycle), as a consequence, the macrocycle ring moves to the perfluoroethyl segment of the thread (*Z*-isomer). The relocation of the macrocycle cause the shielding effect of the perfluoroethyl chain, hence the interface could be changed from hydrophobic to less hydrophobic.

Macroscopic liquid transport was achieved by UV irradiation on one side of a CH_2I_2 droplet (1.25 μL) on the surface grafted with *E*-isomers to create a surface energy gradient across the length of the droplet (Figure 8, a), resulting in millimeter-scale directional transport of the droplet at a mean speed of ~1 μm s^{-1} (Figure 8, a→d). Zerbetto *et al.* further demonstrated that this molecular shuttle could do macroscopic work against gravity by moving a droplet up a 12º incline (Figure 8, e→h). This technique may prove useful for transporting chemicals in lab-on-a-chip environment, or carrying out chemical reactions without vessels by

bringing individual droplets with different chemical reagents together by the use of light.[67]

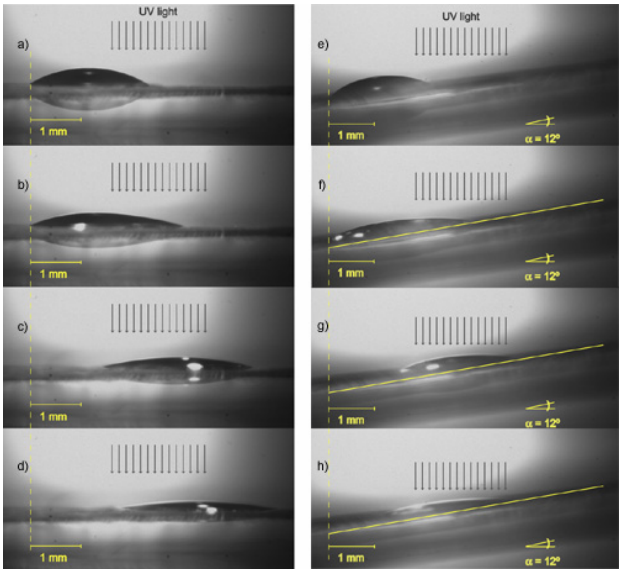

Figure 8 Light-driven directional transport of droplet across the rotaxane-functionalized surface, both flat (a→d) and up a 12º incline (e→h). Adapted from Ref. [79]

1.4 Potential of molecular motors in control of surface wettability

1.4.1 Light-driven molecular motors

Molecular motors are a unique group of photoresponsive organic molecules that are able to convert light energy into repetitive unidirectional rotary motion which is controlled by the stereogenic center in the rotor moiety.[7,81]

The full 360º unidirectional rotary cycle occurs through a four-step switching cycle. These steps involve two energetically uphill photochemical isomerization steps (Scheme 10, step 1 and 3), each followed by an energetically downhill and irreversible thermal isomerization step (Scheme 10, step 2 and 4), resulting in a full 360º rotation of the rotor respected to the relative stator. The irreversibility of the thermal isomerization steps is the key to the unidirectionality of the rotary cycle.

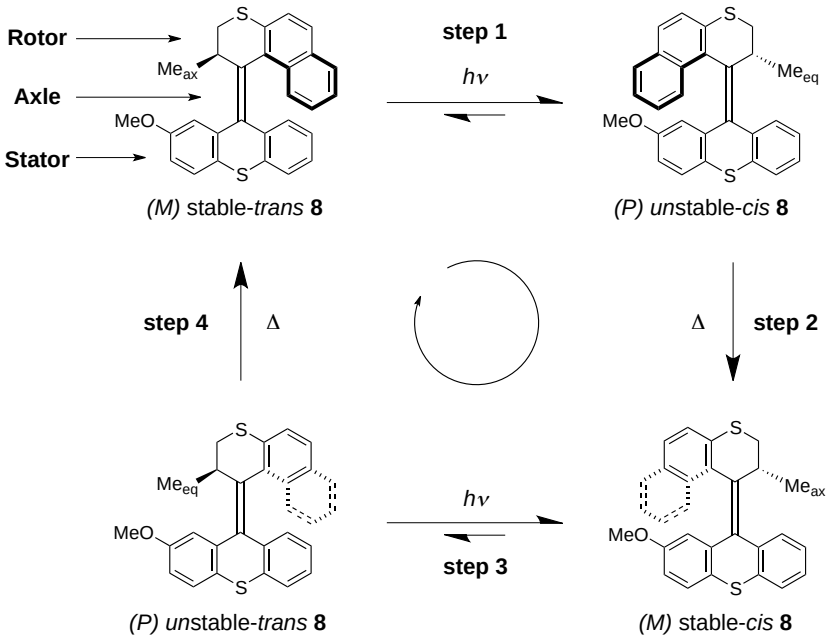

Scheme 10 Photochemical and thermal isomerization processes of molecular motors.

Since the rate of the photoisomerization steps (Scheme 10, step 1 and 3) was found to be much higher (on picosecond timescale)[82] than the thermal isomerization steps (Scheme 10, step 2 and 4), the latter is considered as the rate-determining step of the rotary cycle. Our group have designed, synthesized, and studied a series of molecular motors leading to a better understanding how different substituents and ring sizes influence the rotation rate (Scheme 11).[83]

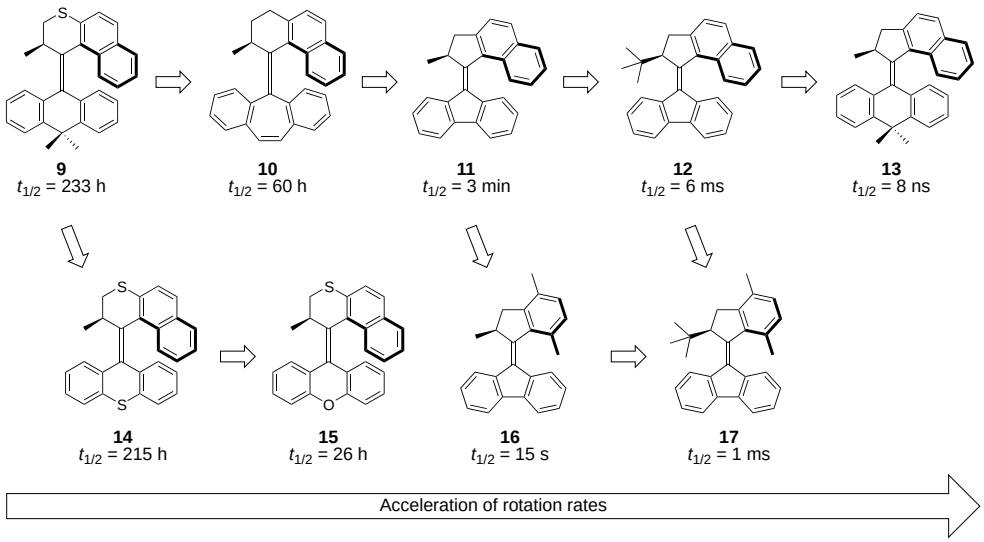

Scheme 11 Representative molecular motors and their rotation rates expressed in terms of the half-life ($t_{1/2}$) of the thermal isomerization step at room temperature (rt).

Molecular motors are promising candidates in photochemically-driven systems as multi-stage switches. It has already been shown that molecular motors can be used to perform various tasks, such as propelling single molecules in a controlled manner,[15] inducing the rotation of liquid crystal's surface texture or a micro-object,[84] and controlling the chiral space in which a catalytic reaction occurs.[85]

1.4.2 From relative to absolute rotation

A key challenge in developing photo-driven systems based on molecular motors is to exploit their collective rotary motion in order to interact with external, micro- or macro-objects in a dynamic manner. However, the rotary motion of molecular motors is overwhelmed by Brownian motion while the molecules are in solution.

Confining molecular motors to surfaces could inhibit Brownian motion and hence the relative rotation of one part of the molecule with respect to the other could be converted to absolute rotation of the rotor relative to the surface.

When molecular motors are attached to the surface, two kinds of orientations can be envisioned: azimuthal and altitudinal (Figure 9).[86] In the azimuthal orientation the axis of rotation is perpendicular to the surface, while in the altitudinal orientation it is parallel to the surface.

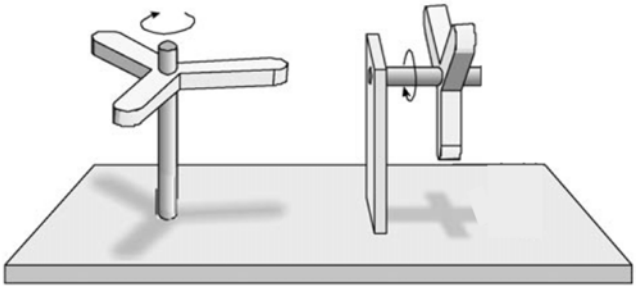

Figure 9 A schematic view of azimuthal (left) and altitudinal (right) orientations. Reproduced from Ref. [86].

1.4.3 Azimuthal molecular motors on surfaces

The first example of unidirectional rotary motion on a surface using azimuthal molecular motors was reported by van Delden *et al.*[87,88] In this design, molecular motors **18** with two thiol-terminated legs were attached to gold nanoparticles (NPs) by sulfur-gold bonds (Scheme 12). The two attachment points prevent the uncontrolled thermal rotation of the whole system with respect to the surface and hence upon UV irradiation the relative rotation of the rotor with respect to the stator (Scheme 10) can be converted to the rotation of the rotor relative to the surface of the NPs.

The self-assembly on gold NPs facilitates monitoring the repetitive rotary process of the motors using standard solution analysis techniques, including UV/vis absorption, circular dichroism (CD), and ^{1}H NMR spectroscopies. The half-life ($t_{1/2}$) of the thermal isomerization step from (*P*) unstable **18** to (*M*) stable **18** (Scheme 12, step 2 and 4) while anchored on the gold NPs was 12×10^{3} s at rt, which is almost double than that of its parent motor (5.6×10^{3} s at rt). The longer $t_{1/2}$ indicates that the rotation speed of the surface-bound motor slows down and is attributed to the reduction in degree of freedom when motors are attached to the

surface. Although the rotary motion of the motors is preserved while grafted to the gold NPs, these NPs are still in the solution phase, hence the rotary motion of the motor is still overwhelmed by Brownian motion *via* rotational and translational motion, making it challenging to harness work from this system.

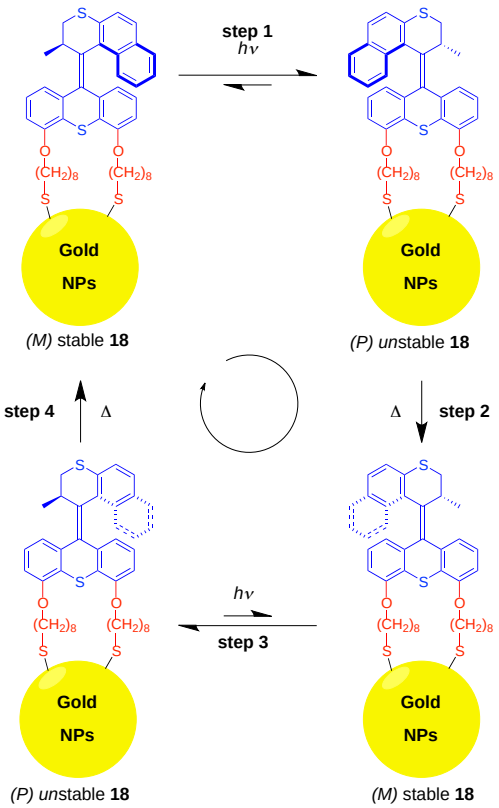

Scheme 12 Full rotary cycle of molecular motor **18** anchored on gold nanoparticles.

The uncontrolled Brownian motion was later overcome by immobilizing motors **19** on quartz[89] or **20** on gold films[90] (Scheme 13). The attachment of azimuthal motor **19** to quartz through two attachment points was verified by X-ray photoelectron spectroscopy (XPS). By using CD spectroscopy, the photochemical and thermal behavior of the motors on the quartz and gold films were correlated to

their solution analogues and is consistent with unidirectional rotary motion, indicating that the rotary motion is preserved while attached to solid substrates.[†]

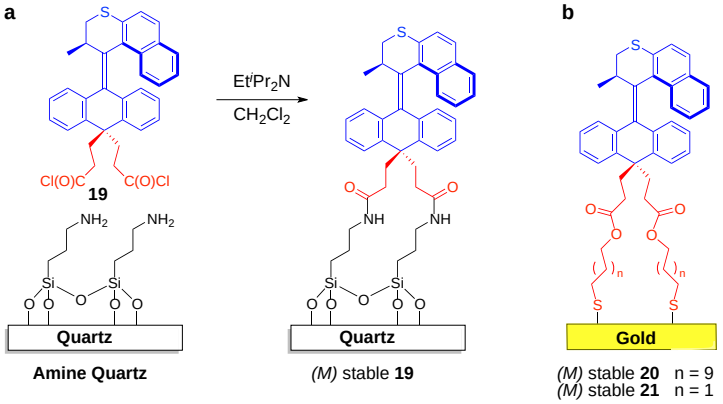

Scheme 13 Azimuthal molecular motors on amine-functionalized quartz (a) and gold films (b).

To harness the rotary motion of the molecular motors, two key issues should be taken into account: (a) Their rotary speed should be fast enough to compete with the Brownian motion; (b) To limit the positional and orientational degrees of freedom of the motors, they need to be immobilized on macroscopic surfaces. These two issues were addressed by grafting a monolayer of ultrafast motors on solid surfaces. In this design, an ultrafast molecular motor **22** with $t_{1/2}$ of 38 ns at rt (measured by ns-pulsed laser transient absorption spectroscopy)[91,92] was attached to azide-functionalized quartz by a click approach (Scheme 14).[93]

The quartz surface was first functionalized with a monolayer of azides, followed by immersing this azide substrate in a 1mM solution of **22** in the presence of $CuSO_4$•5 H_2O and sodium ascorbate in DMF, affording stable **22**. The presence of the motor **22** on the surface was confirmed by UV/vis absorption spectroscopy, WCA measurement, attenuated total reflection infrared spectroscopy (ATR-IR), and ellipsometry. After reaction, the UV/vis absorption spectrum of stable **22** showed the characteristic absorption profile of the motors, the WCA decreased from 78º to 65º, the IR spectrum showed the disappearance of the band corresponding to the azide, and the thickness of the organic layer increased by

[†] It should be noted that when motors are assembled too close to the gold surface (Scheme 13b, n=1), quenching of the photoinduced excited state of the motors by the gold substrate may occur, preventing motors from functioning properly.

0.8 nm as determined by ellipsometry. These results all indicate that the ultrafast motor **22** was attached to the azide-functionalized quartz successfully.

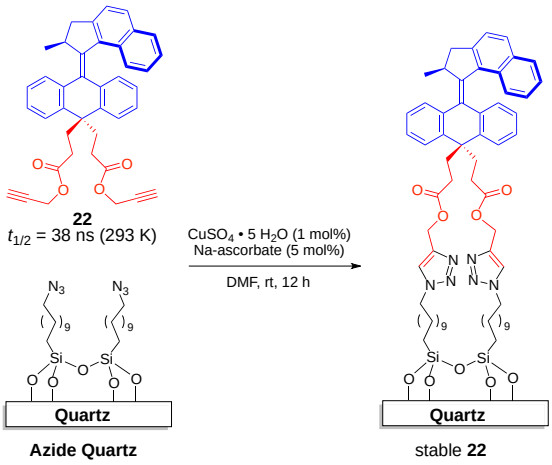

Scheme 14 Grafting of the ultrafast motor **22** to azide-functionalized quartz through a click reaction.

It should be noted that immersion of an unmodified quartz slide in the solution of **22** or immersion of an azide-functionalized quartz in a solution of **22** without $CuSO_4$•5 H_2O did not give the characteristic UV/vis signal of motor **22**, indicating that the Cu(I) catalyst is essential for the interfacial catalytic azide-alkyne cycloaddition. This represents the fastest molecular motor based on overcrowded alkenes that has so far been immobilized on a surface.

1.4.4 Altitudinal molecular motors on surfaces

Although the assembly of azimuthal molecular motors on a variety of surfaces is well-developed over the past decade, molecular motors rotating in an altitudinal orientation relative to the surface are expected to have greater potential for the construction of photo-switchable surfaces. It is easy to envision that the surface accessibility of a functional group on the rotor of the altitudinal motors could be modulated in a cyclic fashion.

The first example of rotary motion on surfaces based on an altitudinal molecular motor was reported by London and Carroll *et al.*[94,95] In this design, a click approach was used to attach dialkyne motor **23** to an azide-functionalized surface by Cu(I)-catalyzed azide-alkyne cycloaddition (Scheme 15). The motor monolayers were characterized by a combination of UV/vis absorption and IR

spectroscopies, ellipsometry, WCA measurement, and XPS as described in the previous section. These measurements indicated that the motors were anchored on the surface successfully and the rotary motion of the surface-bound molecules is preserved. Despite the promise of the current design of altitudinal motors in powering surface-bound nanomachinery, the rotary motion of the surface-bound motors was found to be obstructed by intermolecular interaction when motors **23** are confined in crowded environments compared to solution. This issue was later addressed by designing a tripodal molecular motor with a bulky stator for surface attachment which could provide sufficient free volume for the isomerization steps of the surface-bound motors, as will be discussed in Chapter 3.

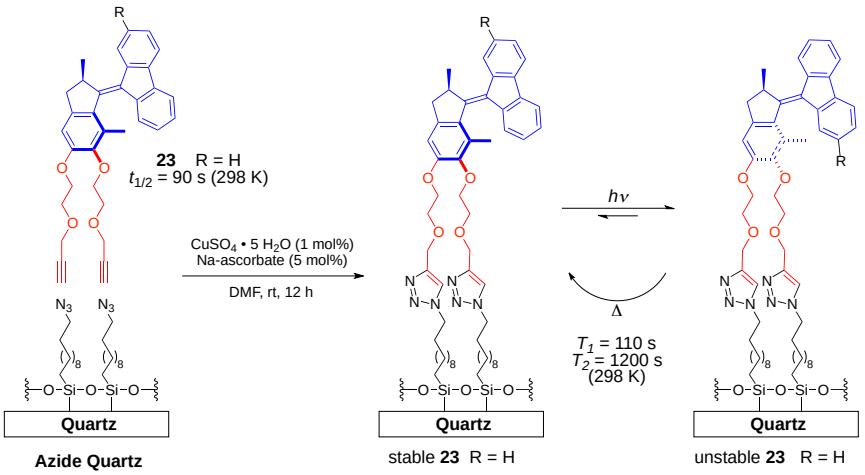

Scheme 15 Attaching dialkyne motor **23** to azide-functionalized quartz through a click approach.

The assembly of stimuli-responsive molecules on silicon-based surfaces is highly desirable because of their relevance to molecular electronic device, relative low price and thermal, chemical, and mechanical stabilities.[96] London *et al.* designed a new approach to assemble molecular motors directly to quartz, silicon wafers, and mica without *prior* activation of these surfaces with amine- or azide-functional groups, as described in section 1.4.3 (Scheme 16).[97]

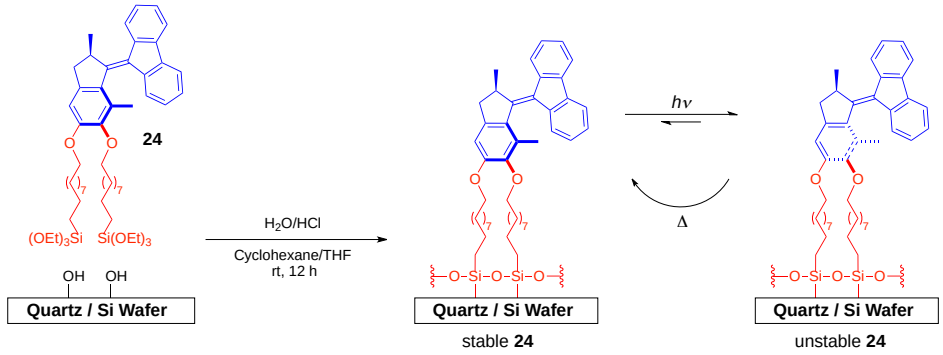

Scheme 16 Attaching disilane motor **24** to quartz and silicon wafer.

In this approach, the molecular motors were functionalized with two triethoxysilane units at their "legs" for attachment to Si-OH terminated surface (quartz and silicon wafer cleaned with piranha solution). The motors attached to these surfaces were found to undergo photochemical and thermal isomerization similar to their solution analogues by UV/vis absorption and CD spectroscopies.

The direct attachment of motor **24** on mica, an atomically flat surface, is of particular interest since it facilitates AFM studies of the photoinduced morphology changes of the motor based films (Figure 10). Such morphological changes have great potential for inducing changes in surface wettability as described in section 1.3.3.

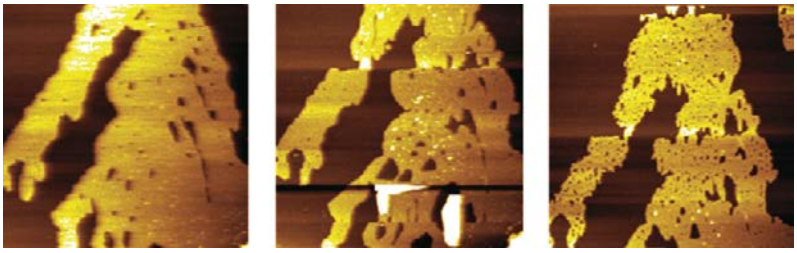

Figure 10 AFM imagines of motor films on mica: (a) Sample before UV irradiation; (b) Sample after irradiation; (c) Sample after standing in dark overnight. Adapted from Ref. [97].

1.4.5 Conclusions

A key challenge in developing surface-bound devices based on molecular motors is to exploit their collective motion for interacting with an external species in a dynamic manner. One way to demonstrate that the collective rotary motion of a surface-bound layer of oriented motors can influence interactions with an overlayer material is to monitor the contact angle of a liquid on top of the motor monolayer. To date, light-driven rotary molecular motor based surfaces that can induce changes in surface wettability upon irradiation have not been reported yet. The unique features that molecular motors are able to undergo controlled unidirectional rotary motion while attached to a surface in either an azimuthal or an altitudinal orientation, a wide range of rates at which they can rotate, a variety of surfaces to which they can be attached, and the potential to induce surface morphological changes make molecular motors attractive candidates for the dynamic modulation of surface properties and inducing macroscopic motion by harnessing collective changes in their molecular structure in surface bound assemblies.

1.5 Aim and outline of this thesis

The proper assembly of light-driven molecular motors on surfaces while retaining their rotary motion is particularly challenging and of great importance for harnessing their collective motion to perform work. To avoid interference effects, orientation with respect to surface, mode of attachment (number of legs), distance from the surface, rigidity of anchoring groups, and packing density of the rotor moieties are all basic issues to be considered and addressed for the successful construction of new surface-bound systems based on molecular motors for dynamic nanoscale applications.

In Chapter 2, the first concept of surface wettability control using light-driven molecular motors is demonstrated. In this design, a surface functionalized with *cis* or *trans* isomers of altitudinal motor with a hydrophobic chain on the rotor (Scheme 15, R= C_4F_9) shows a difference of 12º in WCA between the *cis* and *trans* isomers. However, once the motors are assembled on the surface, the wettability cannot be modulated by UV irradiation.

In Chapter 3, the design, preparation, and characterization of tripodal molecular motors for surface wettability control is described. The design comprises

a molecular motor with a hydrophobic perfluorobutyl chain on the rotor and a tripodal stator containing thiol groups for self-assembly on gold. The bulky stator dictates the orientation and increases the spacing between the rotors of the surface-bound motors sufficiently to facilitate unobstructed rotary motion. This is the first example of dynamic wettability control of solid surfaces using molecular motors decorated with a hydrophobic functional group on the rotor part.

In Chapter 4, the synthesis and photochemistry of novel molecular switches and motors bearing tetrapodal anchoring units are described. The anchoring units consist of anthracene molecules with four "legs" that are terminated with functional groups appropriate for surface assembly. A facile Diels-Alder reaction under mild conditions allows for the attachment of molecular switches and motors to the anthracene anchoring units in high yield. Studies on the photochemical and/or thermal isomerization processes of these tetrapodal molecular switches and motors are included, showing that their dynamic properties are not affected. The tetrapodal system provides an excellent platform for surface assembly of photoresponsive molecules with high control over anchoring at the surfaces.

In Chapter 5, molecular motors containing multivalent carboxylic acid groups on the stator for surface attachment is described. The acids allow for the motors to be attached to amine-coated surface without prior activation of the acid groups. Thermal isomerization of tetravalently attached motors was not inhibited considerably by surface immobilization; however, bivalently attached motors showed a large reduction in the speed of thermal isomerization, demonstrating how subtle differences in molecular structure can considerably impact dynamic processes in nanoscale systems.

With these studies we have made major steps in the design of surface assembled molecular motors and elucidated how dynamic behavior can be fully retained in surface-bound systems. The work described in this thesis sets the stage for the control of various functions using molecular motors including the control of interaction with surface adsorbates while it also provides the stepping stone to detailed studies of single motor rotation.

1.6 References

[1] Coskun, A.; Banaszak, M.; Astumian, R. D.; Stoddart, J. F.; Grzybowski, B. A. *Chem. Soc. Rev.* **2012**, *41*, 19–30.

[2] Bruns, C. J.; Stoddart, J. F. *Acc. Chem. Res.* **2014**, DOI: 10.1021/ar500138u.

[3] *Molecular Devices and Machines: Concepts and Perspectives for the Nanoworld*; Balzani, V., Credi, A., Venturi, M., Eds.; Wiley-VCH: Weinheim, **2008**.

[4] *From Non-Covalent Assemblies to Molecular Machines*; Sauvage, J.-P., Gaspard, P., Eds.; Wiley-VCH: Weinheim, **2010**.

[5] Browne, W. R.; Feringa, B. L. *Nature Nanotech.* **2006**, *1*, 25–35.

[6] Kay, E. R.; Leigh, D. A.; Zerbetto, F. *Angew. Chem. Int. Ed.* **2007**, *46*, 72–191.

[7] *Molecular Switches, 2nd Ed*; Browne, W. R., Feringa, B. L., Eds; Wiley-VCH: Weinheim, **2011**.

[8] Kinbara, K.; Aida, T. *Chem. Rev.* **2005**, *105*, 1377–1400.

[9] Noji, H.; Yasuda, R.; Yoshida, M.; Kinosita, K., Jr. *Nature* **1997**, *386*, 299–302.

[10] Kinosita, K., Jr; Adachi, K.; Itoh, H. *Annu. Rev. Biophys. Biomol. Struct.* **2004**, *33*, 245–268.

[11] Leblond, J.; Petitjean, A. *ChemPhysChem* **2011**, *12*, 1043–1051.

[12] Michl, J.; Sykes, E. C. H. *ACS Nano* **2009**, *3*, 1042–1048.

[13] Yang, J.-S.; Huang, Y.-T.; Ho, J.-H.; Sun, W.-T.; Huang, H.-H.; Lin, Y.-C.; Huang, S.-J.; Huang, S.-L.; Lu, H.-F.; Chao, I. *Org. Lett.* **2008**, *10*, 2279–2282.

[14] Badjic, J. D.; Balzani, V.; Credi, A.; Silvi, S.; Stoddart, J. F. *Science* **2004**, *303*, 1845–1849.

[15] Kudernac, T.; Ruangsupapichat, N.; Parschau, M.; Maciá, B.; Katsonis, N.; Harutyunyan, S. R.; Ernst, K.-H.; Feringa, B. L. *Nature* **2011**, *479*, 208–211.

[16] Chu, P.-L. E.; Wang, L.-Y.; Khatua, S.; Kolomeisky, A. B.; Link, S.; Tour, J. M. *ACS Nano* **2013**, *7*, 35–41.

[17] Kinbara, K.; Aida, T. *Chem. Rev.* **2005**, *105*, 1377–1400.

[18] Szymański, W.; Beierle, J. M.; Kistemaker, H. A. V.; Velema, W. A.; Feringa, B. L. *Chem. Rev.* **2013**, *113*, 6114–6178.

[19] de Jong, J. J.; Lucas, L. N.; Kellogg, R. M.; Van Esch, J. H.; Feringa, B. L. *Science* **2004**, *304*, 278–281.

[20] Lewandowski, B.; De Bo, G.; Ward, J. W.; Papmeyer, M.; Kuschel, S.; Aldegunde, M. J.; Gramlich, P. M. E.; Heckmann, D.; Goldup, S. M.; D'Souza, D. M.; Fernandes, A. E.; Leigh, D. A. *Science* **2013**, *339*, 189–193.

[21] Eelkema, R.; Pollard, M. M.; Vicario, J.; Katsonis, N.; Ramon, B. S.; Bastiaansen, C. W. M.; Broer, D. J.; Feringa, B. L. *Nature* **2006**, *440*, 163–163.

[22] Hou, L.; Zhang, X.; Pijper, T. C.; Browne, W. R.; Feringa, B. L. *J. Am. Chem. Soc.* **2014**, *136*, 910–913.

[23] Tian, D.; Song, Y.; Jiang, L. *Chem. Soc. Rev.* **2013**, *42*, 5184–5209.

[24] Nuzzo, R. G.; Dubois, L. H.; Allara, D. L. *J. Am. Chem. Soc.* **1990**, *112*, 558–569.

[25] Hutchison, J. A.; Uji-i, H.; Deres, A.; Vosch, T.; Rocha, S.; Müller, S.; Bastian, A. A.; Enderlein, J.; Nourouzi, H.; Li, C.; Herrmann, A.; Müllen, K.; De Schryver, F.; Hofkens, J. *Nat. Nanotech.* **2014**, *9*, 131–136.

[26] Velema, W. A.; van der Berg, J. P.; Hansen, M. J.; Szymański, W.; Driessen, A. J. M.; Feringa, B. L. *Nat. Chem.* **2013**, *5*, 924–928.

[27] Katsonis, N.; Kudernac, T.; Walko, M.; van der Molen, S. J.; van Wees, B. J.; Feringa, B. L. *Adv. Mater.* **2006**, *18*, 1397–1400.

[28] Nakanishi, H.; Bishop, K. J. M.; Kowalczyk, B.; Nitzan, A.; Weiss, E. A.; Tretiakov, K. V.; Apodaca, M. M.; Klajn, R.; Stoddart, J. F.; Grzybowski, B. A. *Nature* **2009**, *460*, 371–375.

[29] Lorenzo, M.; Baddeley, C.; Muryn, C.; Raval, R. *Nature* **2000**, *404*, 376–379.

[30] Singh, A.; Myerson, A. S. *J. Pharm. Sci.* **2010**, *99*, 3931–3940.

[31] Fernandes, A.; Hensenne, P.; Mathy, B.; Guo, W.; Nysten, B.; Jonas, A. M.; Riant, O. *Chem. Eur. J.* **2011**, *18*, 788–792.

[32] Coperet, C.; Chabanas, M.; Saint–Arroman, R. P.; Basset,J. M. *Angew. Chem. Int. Ed.* **2003**, *42*, 156–181.

[33] Liu, Y.; Flood, A. H.; Bonvallet, P. A.; Vignon, S. A.; Northrop, B. H.; Tseng, H.-R.; Jeppesen, J. O.; Huang, T. J.; Brough, B.; Baller, M.; Magonov,

S.; Solares, S. D.; Goddard, W. A.; Ho, C.-M.; Stoddart, J. F. *J. Am. Chem. Soc.* **2005**, *127*, 9745–9759.

[34] Ferri, V.; Elbing, M.; Pace, G.; Dickey, M. D.; Zharnikov, M.; Samorì, P.; Mayor, M.; Rampi, M. A. *Angew. Chem. Int. Ed.* **2008**, *47*, 3407–3409.

[35] Hugel, T.; Holland, N. B.; Cattani, A.; Moroder, L.; Seitz, M.; Gaub, H. E. *Science* **2002**, *296*, 1103–1106.

[36] Katsonis, N.; Lubomska, M.; Pollard, M. M.; Feringa, B. L.; Rudolf, P. *Prog. Surf. Sci.* **2007**, 82, 407–434.

[37] Browne, W. R.; Feringa, B. L. *Annu. Rev. Phys. Chem.* **2009**, *60*, 407–428.

[38] Ye, T.; Kumar, A. S.; Saha, S.; Takami, T.; Huang, T. J.; Stoddart, J. F.; Weiss, P. S. *ACS Nano* **2010**, *4*, 3697–3701.

[39] Tatum, L. A.; Su, X.; Aprahamian, I. *Acc. Chem. Res.* **2014**, DOI: 10.1021/ar500111f.

[40] Karan, S.; Gopakumar, T. G.; Jacob, H.; Meyer, S.; Tuczek, F.; Berndt, R. *J. Am. Chem. Soc.* **2014**, *136*, 6163–6166.

[41] Zheng, Y. B.; Pathem, B. K.; Hohman, J. N.; Thomas, J. C.; Kim, M.; Weiss, P. S. *Adv. Mater.* **2013**, *25*, 302–312.

[42] Klajn, R. *Chem. Soc. Rev.* **2014**, *43*, 148–184.

[43] Velema, W. A.; Szymański, W.; Feringa, B. L. *J. Am. Chem. Soc.* **2014**, *136*, 2178–2191.

[44] Klajn, R. *Pure Appl. Chem.* **2010**, *82*, 2247–2279.

[45] Sun, R.; Xue, C.; Ma, X.; Gao, M.; Tian, H.; Li, Q. *J. Am. Chem. Soc.* **2013**, *135*, 5990–5993.

[46] Irie, M.; Mohri, M. *J. Org. Chem.* **1988**, *53*, 803–808.

[47] Irie, M.; Lifka, T.; Uchida, K.; Kobatake, S.; Shindo, Y. *Chem. Commun.* **1999**, 747–750.

[48] Dugave, C.; Demange, L. *Chem. Rev.* **2003**, *103*, 2475–2532.

[49] Waldeck, D. H. *Chem. Rev.* **1991**, *91*, 415–436.

[50] Kessler, D.; Jochum, F. D.; Choi, J.; Char, K.; Theato, P. *ACS Appl. Mater. Interfaces* **2011**, *3*, 124–128.

[51] Xin, B.; Hao, J. *Chem. Soc. Rev.* **2010**, *39*, 769–782.

[52] Rosario, R.; Gust, D.; Hayes, M.; Jahnke, F.; Springer, J.; Garcia, A. A. *Langmuir* **2002**, *18*, 8062–8069.

[53] Samanta, S.; Locklin, J. *Langmuir* **2008**, *24*, 9558–9565.

[54] Feng, L.; Li, S.; Li, Y.; Li, H.; Zhang, L.; Zhai, J.; Song, Y.; Liu, B.; Jiang, L.; Zhu, D. *Adv. Mater.* **2002**, *14*, 1857–1860.

[55] Lafuma, A.; Quéré, D. *Nat. Mater.* **2003**, *2*, 457–460.

[56] Zheng, Y.; Gao, X.; Jiang, L. *Soft Matter* **2007**, *3*, 178–182.

[57] Gao, X.; Jiang, L. *Nature* **2004**, *432*, 36.

[58] Rosario, R.; Gust, D.; Garcia, A. A.; Hayes, M.; Taraci, J. L.; Clement, T.; Dailey, J. W.; Picraux, S. T. *J. Phys. Chem. B* **2004**, *108*, 12640–12642.

[59] Joseph, G.; Pichardo, J.; Chen, G. *Analyst* **2010**, *135*, 2303–2308.

[60] Cassie, A. B. D.; Baxter, S. *Trans. Faraday Soc.* **1944**, *40*, 546–551.

[61] Wenzel, R. N. *Ind. Eng. Chem.* **1936**, *28*, 988–994.

[62] Wang, D.; Jiao, P.; Wang, J.; Zhang, Q.; Feng, L.; Yang, Z. *J. Appl. Polym. Sci.* **2011**, *125*, 870–875.

[63] Kefalas, V. A. *J. Appl. Polym. Sci.* **1995**, *58*, 711–717.

[64] Chen, G.; Soper, S. A.; McCarley, R. L. *Langmuir* **2007**, *23*, 11777–11781.

[65] Akiyama, H.; Tamada, K.; Nagasawa, J.; Abe, K.; Tamaki, T. *J. Phys. Chem. B* **2003**, *107*, 130–135.

[66] Siewierski, L. M.; Brittain, W. J.; Petrash, S.; Foster, M. D. *Langmuir* **1996**, *12*, 5838–5844.

[67] Oh, S.-K.; Nakagawa, M.; Ichimura, K. *J. Mater. Chem.* **2002**, *12*, 2262–2269.

[68] Hamelmann, F.; Heinzmann, U.; Siemeling, U.; Bretthauer, F.; Vor der Brüggen, J. *Appl. Surf. Sci.* **2004**, *222*, 1–5.

[69] Delorme, N.; Bardeau, J. F.; Bulou, A.; Poncin-Epaillard, F. *Langmuir* **2005**, *21*, 12278–12282.

[70] Lim, H. S.; Han, J. T.; Kwak, D.; Jin, M.; Cho, K. *J. Am. Chem. Soc.* **2006**, *128*, 14458–14459.

[71] Lim, H. S.; Lee, W. H.; Lee, S. G.; Lee, D.; Jeon, S.; Cho, K. *Chem. Commum.* **2010**, *46*, 4336–4338.

[72] Jiang, W.; Wang, G.; He, Y.; Wang, X.; An, Y.; Song, Y.; Jiang, L. *Chem. Commum.* **2005**, 3550–3552.

[73] Sun, T.; Wang, G.; Liu, H.; Feng, L.; Jiang, L.; Zhu, D. *J. Am. Chem. Soc.* **2003**, *125*, 14996–14997.

[74] Wan, P.; Jiang, Y.; Wang, Y.; Wang, Z.; Zhang, X. *Chem. Commum.* **2008**, 5710–5712.

[75] Zhang, X.; Zhao, H.; Tian, D.; Deng, H.; Li, H. *Chem. Eur. J.* **2014**, DOI: 10.1002/chem.201402476.

[76] Ichimura, K.; Oh, S. K.; Nakagawa, M. *Science* **2000**, *288*, 1624–1626.

[77] Uchida, K.; Izumi, N.; Sukata, S.; Kojima, Y.; Nakamura, S.; Irie, M. *Angew. Chem. Int. Ed.* **2006**, *45*, 6470–6473.

[78] Uyama, A.; Yamazoe, S.; Shigematsu, S.; Morimoto, M.; Yokojima, S.; Mayama, H.; Kojima, Y.; Nakamura, S.; Uchida, K. *Langmuir* **2011**, *27*, 6395–6400.

[79] Berná, J.; Leigh, D. A.; Lubomska, M.; Mendoza, S. M.; Pérez, E. M.; Rudolf, P.; Teobaldi, G.; Zerbetto, F. *Nat. Mater.* **2005**, *4*, 704–710.

[80] Cecchet, F.; Rudolf, P.; Rapino, S.; Margotti, M.; Paolucci, F.; Baggerman, J.; Brouwer, A. M.; Kay, E. R.; Wong, J. K. Y.; Leigh, D. A. *J. Phys. Chem. B* **2004**, *108*, 15192–15199.

[81] Koumura, N.; Zijlstra, R. W.; van Delden, R. A.; Harada, N.; Feringa, B. L. *Nature* **1999**, *401*, 152–155.

[82] Augulis, R.; Klok, M.; Feringa, B. L.; Loosdrecht, P. H. M. V. *Phys. Stat. Sol. (C)* **2009**, *6*, 181–184.

[83] For the half-lives of the thermal izomerization step of molecular motors, see: (a) **8**, **9**, **10**, **14**, and **15**: Koumura, N.; Geertsema, E. M.; van Gelder, M. B.; Meetsma, A.; Feringa, B. L. *J. Am. Chem. Soc.* **2002**, *124*, 5037–5051. (b) **11**: Vicario, J.; Meetsma, A.; Feringa, B. L. *Chem. Commum.* **2005**, 5910. (c) **12**:

Vicario, J.; Walko, M.; Meetsma, A.; Feringa, B. L. *J. Am. Chem. Soc.* **2006**, *128*, 5127–5135. (d) **13**: Klok, Martin. Motors for use in molecular nanotechnology. Ph.D. Thesis, University of Groningen, **2009**. (e) **16**: Pollard, M. M.; Meetsma, A.; Feringa, B. L. *Org. Biomol. Chem.* **2008**, *6*, 507–512. (f) **17**: Bauer, J.; Hou, L.; Kistemaker, J. C. M.; Feringa, B. L. *J. Org. Chem.* **2014**, *79*, 4446–4455.

[84] Eelkema, R.; Pollard, M. M.; Vicario, J.; Katsonis, N.; Ramon, B. S.; Bastiaansen, C. W. M.; Broer, D. J.; Feringa, B. L. *Nature* **2006**, *440*, 163–163.

[85] (a) Wang, J.; Feringa, B. L. *Science* **2011**, *331*, 1429–1432. (b) Vlatković, M.; Bernardi, L.; Otten, E.; Feringa, B. L. *Chem. Commun.* **2014**, DOI: 10.1039/C4CC00794H.

[86] Balzani, V.; Credi, A.; Venturi, M. *ChemPhysChem* **2008**, *9*, 202–220.

[87] van Delden, R. A.; Wiel, ter, M. K. J.; Pollard, M. M.; Vicario, J.; Koumura, N.; Feringa, B. L. *Nature* **2005**, *437*, 1337–1340.

[88] Pollard, M. M.; Wiel, ter, M. K. J.; van Delden, R. A.; Vicario, J.; Koumura, N.; van den Brom, C. R.; Meetsma, A.; Feringa, B. L. *Chem. Eur. J.* **2008**, *14*, 11610–11622.

[89] Pollard, M. M.; Lubomska, M.; Rudolf, P.; Feringa, B. L. *Angew. Chem.* **2007**, *119*, 1300–1302.

[90] Carroll, G. T.; Pollard, M. M.; van Delden, R.; Feringa, B. L. *Chem. Sci.* **2010**, *1*, 97–101.

[91] Klok, M.; Boyle, N.; Pryce, M. T.; Meetsma, A.; Browne, W. R.; Feringa, B. L. *J. Am. Chem. Soc.* **2008**, *130*, 10484–10485.

[92] Kulago, A. A.; Mes, E. M.; Klok, M.; Meetsma, A.; Brouwer, A. M.; Feringa, B. L. *J. Org. Chem.* **2010**, *75*, 666–679.

[93] Vachon, J.; Carroll, G. T.; Pollard, M. M.; Mes, E. M.; Brouwer, A. M.; Feringa, B. L. *Photochem. Photobiol. Sci.* **2014**, *13*, 241–246.

[94] London, G.; Carroll, G. T.; Fernández Landaluce, T.; Pollard, M. M.; Rudolf, P.; Feringa, B. L. *Chem. Commun.* **2009**, 1712–1714.

[95] Carroll, G. T.; London, G.; Landaluce, T. F.; Rudolf, P.; Feringa, B. L. *ACS Nano* **2011**, *5*, 622–630.

[96] Cerofolini, G. F.; Romano, E. *Appl. Phys. A* **2008**, *91*, 181–210.

[97] London, G; Carroll, G. T.; Feringa, B. L. *Org. Biomol. Chem.* **2013**, *11*, 3477–3483.

Chapter 2

Towards Dynamic Control of Wettability by Using Functionalized Altitudinal Molecular Motors on Solid Surfaces

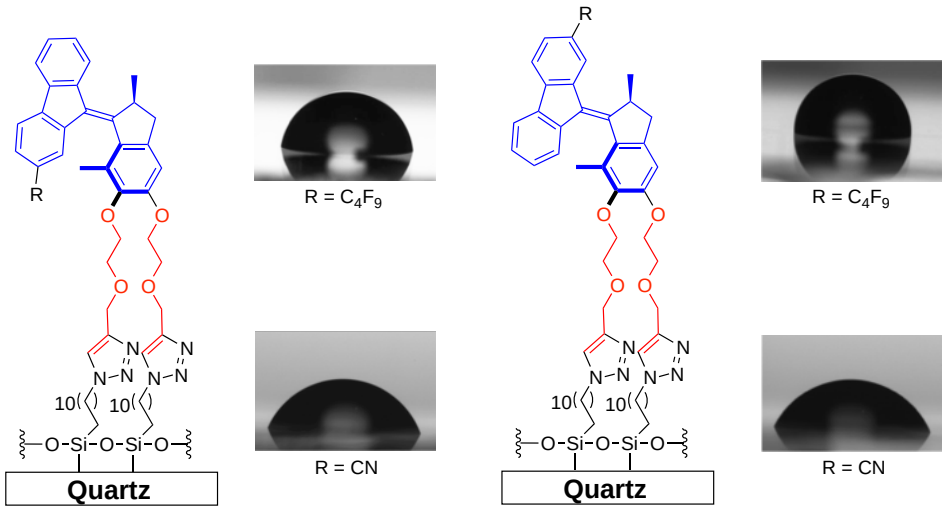

Molecular motors with hydrophobic and hydrophilic functional groups were synthesized and attached to quartz surfaces by interfacial Cu(I)-catalyzed azide-alkyne cycloaddition to achieve dynamic control over the properties of solid surfaces. The functionalized motors preserve their rotary function both in solution and on the surface. The wettability of the surface containing a monolayer of altitudinal motors was shown to depend on whether the motors were assembled in the *cis* or *trans* form.

This chapter has been published:
London, G.†; Chen, K.-Y.†; Carroll, G. T.; Feringa, B. L. *Chem. Eur. J.* **2013**, *19*, 10690–10697.
† equal contribution

2.1 Introduction

Modification of surfaces with self-assembled monolayers[1] (SAMs) provides a convenient, flexible, and simple way to create surfaces with tailored properties, including hydrophobicity/hydrophilicity,[2,3,4] chirality,[5,6] catalytic activity,[7,8] and conductance.[9,10] Amongst SAM-forming molecules, those that can switch reversibly between two or more states in response to external stimuli such as chemicals, an electric field, or light are of particular interest, since stimuli-responsive molecules are important components for molecular materials and devices.[11,12,13] Photoresponsive molecules[14] attract special attention because light hold advantages as a stimulus: it provides a clean and tunable energy input, induce quick responses, enables spatiotemporal control, and can be delivered to a substrate remotely.[15,16]

Photoresponsive surfaces functionalized with azobenzenes have been studied widely and used to tune surface wettability reversibly using light.[17,18,19] The $E \rightarrow Z$ photoisomerization of azobenzenes is accompanied by a change in geometry and dipole moment, which in turn changes the wettability of the monolayers.[20,21] Due to the inherent changes in dipole moment and molecular structure, azobenzenes can affect the wettability of the monolayer assemblies without an additional functional group being required to ensure sufficient surface wettability change.[22,23] Nevertheless, additional functional groups[23,24,25] and surface pretreatment[26] could enhance the effect of photoisomerization.

Molecular motors based on overcrowded alkenes[27] are a unique class of compounds that can use light to power unidirectional rotary motion. When these molecules are anchored to a surface, two types of rotary motion can be distinguished: azimuthal[28,29,30] and altitudinal[31,32] (Figure 2.1). Molecular motors rotating in an altitudinal orientation are expected to allow for the exposure of the functional group on the rotor to be switched in a cyclic fashion.

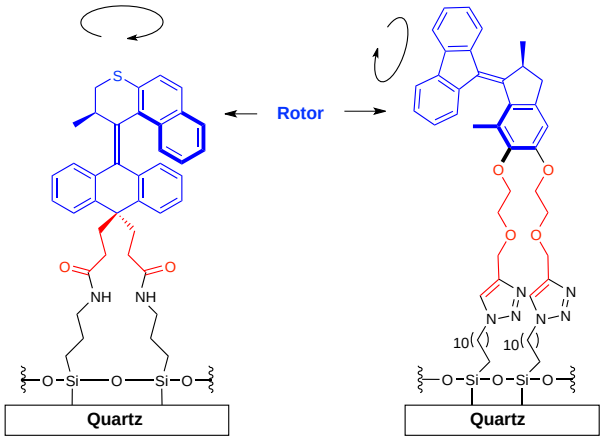

Figure 2.1 Azimuthal (left) and altitudinal (right) rotary motors. The introduction of functional groups on the fluorene-based rotor is required in order to exploit the rotary motion.

Compared to azobenzenes, altitudinal molecular motors with an non-substituted fluorene as rotor (Figure 2.1, right) are not expected to provide an appreciable change in surface wettability upon rotation that could manifest themselves in a change in macroscopic surface properties. Functional groups have to be introduced to the fluorene-based rotors to develop molecular motor-based interfaces that can undergo cyclic changes in surface wettability.

The interfacial Cu(I)-catalyzed azide-alkyne cycloaddition we reported previously was found to be a reliable method to attach bipodal molecular motors to quartz substrates in an altitudinal orientation.[31,32] In this chapter the synthesis of bipodal molecular motors that contain functional groups at the fluorene-based rotors are described. To test the effect of the functional groups on the rotary motion, photochemical and thermal isomerization studies were carried out in solution. Surface attachment in an altitudinal orientation and the isomerization of surface-bound motors are presented, together with data on the influence of the functional groups on surface wettability.

2.2 Synthesis of bipodal molecular motors

The approach toward the synthesis of motor **2.1** and **2.2**, which bears a cyano group and a perfluorobutyl chain on the fluorene-based rotor, is depicted in schemes 2.1, 2.2, and 2.3.

Starting from **2.4**, which was prepared by the oxidation of 2-bromofluorene **2.3**, fluorenone **2.4** was converted to the corresponding hydrazone **2.5** by heating at reflux in CH_3OH in the presence of hydrazine monohydrate followed by oxidation to the diazo derivative **2.6** with MnO_2 in THF (Scheme 2.1). Thioketone **2.7**[31] was reacted with diazo compound **2.6** in a Barton-Kellogg reaction,[33,34] followed by desulfurization, yielding bromo-substituted motor **2.8** in 68% yield over two steps as a mixture of *cis*/*trans* isomers.

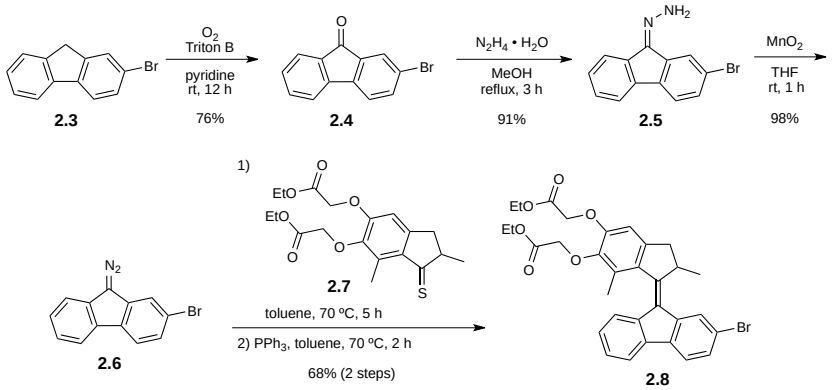

Scheme 2.1. Synthesis of a bromo-substituted molecular motor.

The cyano group is a relatively hydrophilic substituent and was introduced by means of palladium-catalyzed cyanation[35] of bromo motor **2.8** by using the protocol of Jin and Confalone[36] providing cyano motor **2.9** in 87% yield (scheme 2.2).

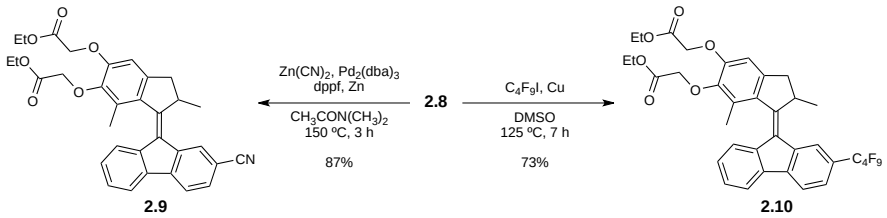

Scheme 2.2. Introduction of the cyano and perfluorobutyl substituents to bromo motor **2.8**.

A possible way to introduce hydrophobicity into the motor is to functionalize the fluorene-based rotor with a perfluoroalkyl chain. Copper-mediated cross-coupling reactions between aryl halides and perfluoroalkyl iodides have been used successfully to synthesize perfluoroalkylated aryl compounds.[37,38] By using this approach, coupling bromo motor **2.8** with perfluorobutyl iodide gave compound **2.10** in 73% yield without the evidence of degradation of the motor (scheme 2.2). The next step is to introduce the terminal alkyne groups to the motors that are necessary for surface attachment by means of Cu(I)-catalyzed azide-alkyne cycloaddition. The ester groups in compounds **2.9** and **2.10** were reduced and the corresponding alcohols **2.11** and **2.12** were alkylated with propargyl bromide (Scheme 2.3). The reduction of the ester groups was carried out with $LiBH_4$ in THF. Separation of the two isomers of compound **2.12** was possible at this stage by column chromatography over silica gel (Et_2O) to provide *cis*-**2.12** and *trans*-**2.12** in 24 and 34% yield, respectively. Next, the *cis*/*trans* mixture of diol **2.11** and the two isomers of diol **2.12** were alkylated with propargyl bromide in the presence of NaH in THF. The *cis* and *trans* isomers of alkene **2.1** were separated by column chromatography over silica by using a toluene/Et_2O (20:1) eluent mixture. The *cis* and *trans* isomers of compounds **2.1** and **2.2** were obtained in 31%, 47%, 64%, and 78% yields, respectively. The structures of dialkyne **2.1** and *cis* and *trans* isomers of diol **2.12** were assigned by comparison of their ^1H NMR spectra with that of previously reported structurally related molecular motors.[39,40,41,42,43,44]

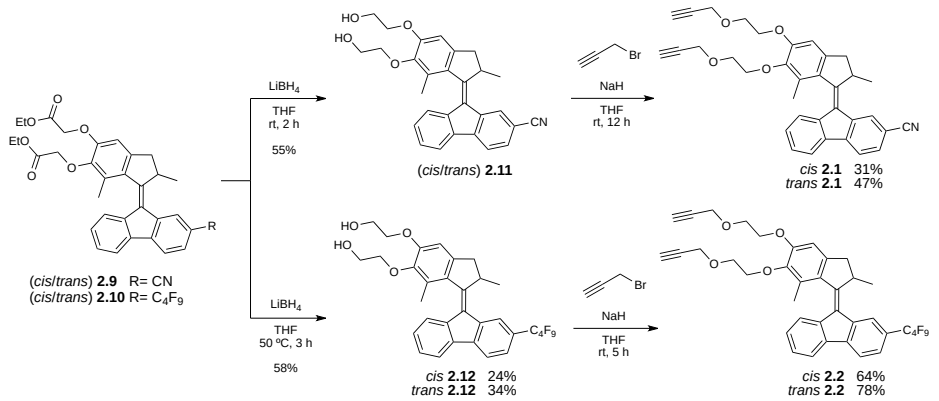

Scheme 2.3 Introduction of terminal alkynes onto substituted motors **2.9** and **2.10**, which enables controlled surface modification by means of interfacial Cu(I)-catalyzed azide-alkyne cycloaddition.[†]

† Dr. Gábor Lodon is acknowledged for the synthesis and characterization of **2.2**, **2.10**, and **2.12**.

2.3 Photochemical and thermal isomerization studies in solution

Verification that **2.1** and **2.2** operate as molecular motors[27] requires photochemical and thermal isomerization studies in solution using low-temperature UV/vis absorption and ^{1}H NMR spectroscopy.

The UV/vis absorption spectra of a sample of the stable-*cis* **2.1** and stable-*trans* **2.1** in CH_3OH at 253 K show absorption bands centered at 395 nm (Figure 2.2a and 2.2b, solid lines), whereas under identical conditions the major absorption band of the stable-*cis* **2.2** and stable-*trans* **2.2** are centered at 388 nm (Figure 2.3a and 2.3b, solid lines).

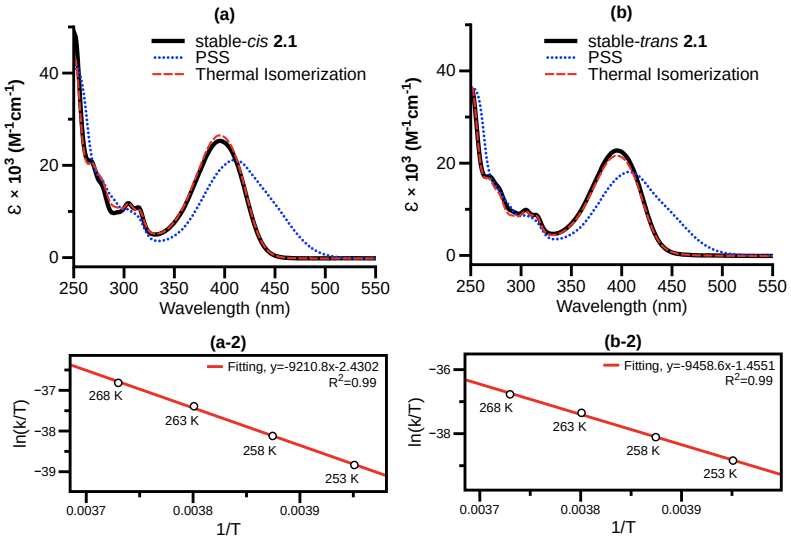

Figure 2.2 UV/vis absorption spectra (CH_3OH, 253 K) of stable-*cis* **2.1** (a) and stable-*trans* **2.1** (b) (solid line). The spectra after UV irradiation (photoisomerization) (dotted line) and heating (thermal isomerization) (dashed line) are also shown; Eyring plot of the conversion of unstable-*trans* **2.1** to stable-*trans* **2.1** (a-2), and unstable-*cis* **2.1** to stable-*cis* **2.1** (b-2) *via* thermal isomerization at different temperatures.

Compared to the parent motor without substituents on the rotor part (main absorption band at 378 nm),[31] introduction of the substituents resulted in a slight red-shift of the UV/vis absorption spectrum. Such shifts have already been observed upon the introduction of electron donating or electron withdrawing groups to molecular motors,[35] azobenzenes and stilbenes.[45,46,47] In the case of the

cyano motors **2.1**, the maxima of the major absorption band of the stable isomers in CH_3OH are more red-shifted compared to that of the perfluorobutyl motors **2.2**. This shift is attributed to the stronger electron-withdrawing character of the cyano group compared to the perfluorobutyl chain.[35]

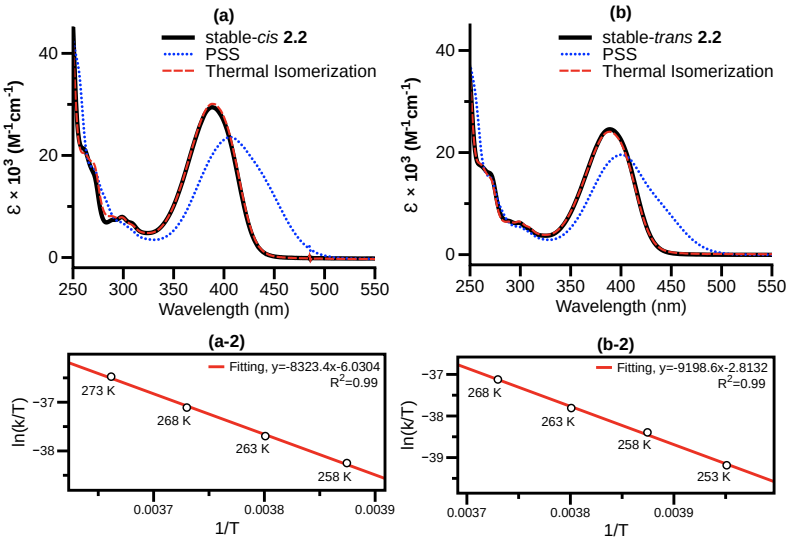

Figure 2.3 UV/vis absorption spectra (CH_3OH, 253 K) of stable-*cis* **2.2** (a) and stable-*trans* **2.2** (b) (solid line). The spectra after photoisomerization (dotted line) and thermal isomerization (dashed line) are also shown; Eyring plot of the conversion of unstable-*trans* **2.2** to stable-*trans* **2.2** (a-2), and unstable-*cis* **2.2** to stable-*cis* **2.2** (b-2) *via* thermal isomerization at different temperatures.

Irradiation of a sample of stable-*cis* **2.1**, stable-*trans* **2.1**, stable-*cis* **2.2**, and stable-*trans* **2.2** in CH_3OH at 253 K with UV light (λ_{max} = 365 nm) led to a red-shift and broadening of their UV/vis absorptions indicating the photochemically induced formation of the unstable isomers (Figure 2.2 and 2.3, dotted lines; Scheme 2.4, steps 1 and 3). The shifted bands are centered at 412 and 407 nm for stable-*cis* **2.1** and stable-*trans* **2.1** and 405 and 400 nm for stable-*cis* **2.2** and stable-*trans* **2.2**, respectively.

During irradiation, clear isosbestic points were maintained in all cases, indicating that the photoisomerization from the stable to unstable form proceeds selectively. Samples were irradiated until no further changes were observed indicating that the photostationary state (PSS) was reached. Allowing the solutions to warm to room temperature (rt) led to reversion to their original absorption

spectra consistent with thermal isomerization to the corresponding stable isomers (Figure 2.2 and 2.3, dashed lines; Scheme 2.4, steps 2 and 4).

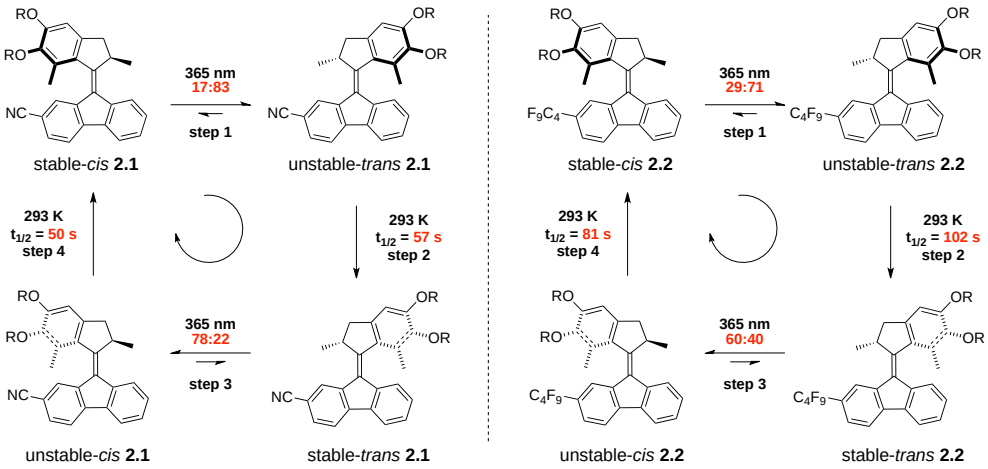

Scheme 2.4 Full 360° rotary cycle for molecular motor **2.1** and **2.2** (R = $CH_2CH_2OCH_2CCH$).

The activation parameters of the thermal isomerization from unstable-*trans* **2.1** to stable-*trans* **2.1** and unstable-*cis* **2.1** to stable-*cis* **2.1** (Scheme 2.4, left, steps 2 and 4) were determined at four temperatures (253, 258, 263 and 268 K) in CH_3OH. The thermal isomerization was followed by monitoring the change in absorbance at 450 nm as a function of time. Using the Eyring equation (Figure 2.2a-2 and b-2), it was determined that the thermal isomerization have a Gibbs free energy of activation ($\Delta^{\ddagger}G^{o}$) of 82.5 kJ/mol (unstable-*trans* **2.1** → stable-*trans* **2.1**) and 82.2 kJ/mol (unstable-*cis* **2.1** → stable-*cis* **2.1**). These values correspond to half-lives ($t_{1/2}$) at rt of 57 and 50 s, respectively.

Using the same procedure, the conversion of unstable-*trans* **2.2** to stable-*trans* **2.2** and unstable-*cis* **2.2** to stable-*cis* **2.2** were monitored at 440 nm as a function of time between 253 K and 273 K (Scheme 2.4, right, steps 2 and 4). The $\Delta^{\ddagger}G^{o}$ was calculated to be 84.0 kJ/mol (unstable-*trans* **2.2** → stable-*trans* **2.2**) and 83.3 kJ/mol (unstable-*cis* **2.2** → stable-*cis* **2.2**) for the thermal isomerization steps. By extrapolation of the plot (Figure 2.3a-2 and b-2), half-lives of 102 s and 81 s at rt were calculated for the unstable-*trans* **2.2** → stable-*trans* **2.2** and unstable-*cis* **2.2** → stable-*cis* **2.2**, respectively.

The values of these half-lives are similar to those obtained for structurally related motors,[41,42,43] indicating that the introduction of the cyano group and

perfluorobutyl chain does not have a significant influence on the thermal isomerization steps.

Further characterization of the unstable isomers and determination of the composition of the PSS was carried out using low-temperature ^{1}H NMR spectroscopy for *cis* and *trans* isomers of **2.1** and **2.2** in their stable forms (Figure 2.4 and 2.5, a and d; see experimental sections for peak assignments). Irradiation (λ_{max} = 365 nm) of a sample of *cis* or *trans* isomers of **2.1** and **2.2**, in their stable forms, in CD_2Cl_2 at 218 K resulted in the appearance of new signals in their ^{1}H NMR spectra.[40] The identity of the unstable isomers was evident from the downfield shifts of proton Ha, Hb, and Hc (Figure 2.4 and 2.5, a → b and d → e). These downfield shifts of the doublet of the stereogenic methyl groups (proton Ha) of the motors in their stable forms are consistent with the conformational change of the stereogenic methyl substituents from the preferred pseudoaxial [$(CHa_3)_{ax}$] to the disfavored pseudoequatorial [$(CHa_3)_{eq}$] orientation upon photoisomerization (Scheme 2.4, steps 1 and 3). The relative integration of the signals of the stable and unstable isomers revealed similar PSS compositions for all compounds, with slightly less favorable values for alkenes **2.2** (Table 2.1).[‡]

Table 2.1 PSS determined by ^{1}H NMR spectroscopy after irradiation at λ_{max} = 365 nm in CD_2Cl_2 at 218 K.

Molecular Motor	$PSS_{365\ nm}$ stable/unstable	^{1}H NMR δ of $(CHa_3)_{ax}$ → $(CHa_3)_{eq}$ [ppm]
cis **2.1**	1:5	1.28 → 1.42
trans **2.1**	1:3.5	1.29 → 1.45
cis **2.2**	1:2.5	1.29 → 1.41
trans **2.2**	1:2	1.29 → 1.46

When the samples that contained the PSS mixtures (Figure 2.4 and 2.5, b and e) were allowed to warm to rt for 30 min, the ^{1}H NMR spectra showed quantitative conversion of the unstable isomers to their corresponding stable isomers (Figure 2.4 and 2.5, b → c and e → f; Scheme 2.4, steps 2 and 4).

‡ A possible explanation for this observation is the sensitivity of the photochemical equilibrium to the combination of the substituent and solvent that has already been observed for similar molecular motors. However, for definitive conclusions on the precise solvent effect further studies on the solvent dependence of the PSS composition of alkenes **2.2** should be performed.

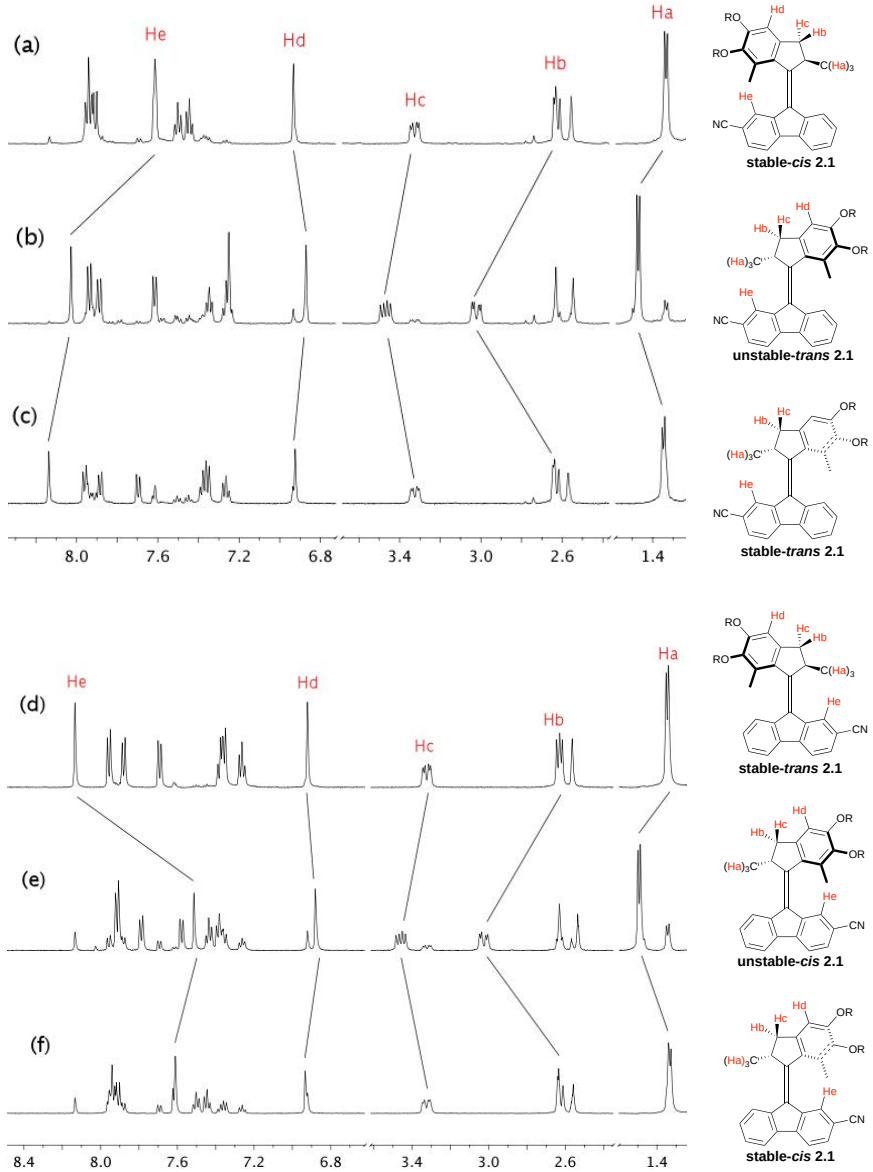

Figure 2.4 Partial ^{1}H NMR spectra (500 MHz, CD_2Cl_2, 218 K) of **2.1** (a) stable-*cis* **2.1** (b) unstable-*trans* **2.1** formed upon UV irradiation to PSS (c) stable-*trans* **2.1** obtained after thermal isomerization of unstable-*trans* **2.1** at rt; (d) stable-*trans* **2.1** (e) unstable-*cis* **2.1** formed upon UV irradiation to PSS (f) stable-*cis* **2.1** obtained after thermal isomerization of unstable-*cis* **2.1** at rt. Signal assignments are given (R = $CH_2CH_2OCH_2CCH$).

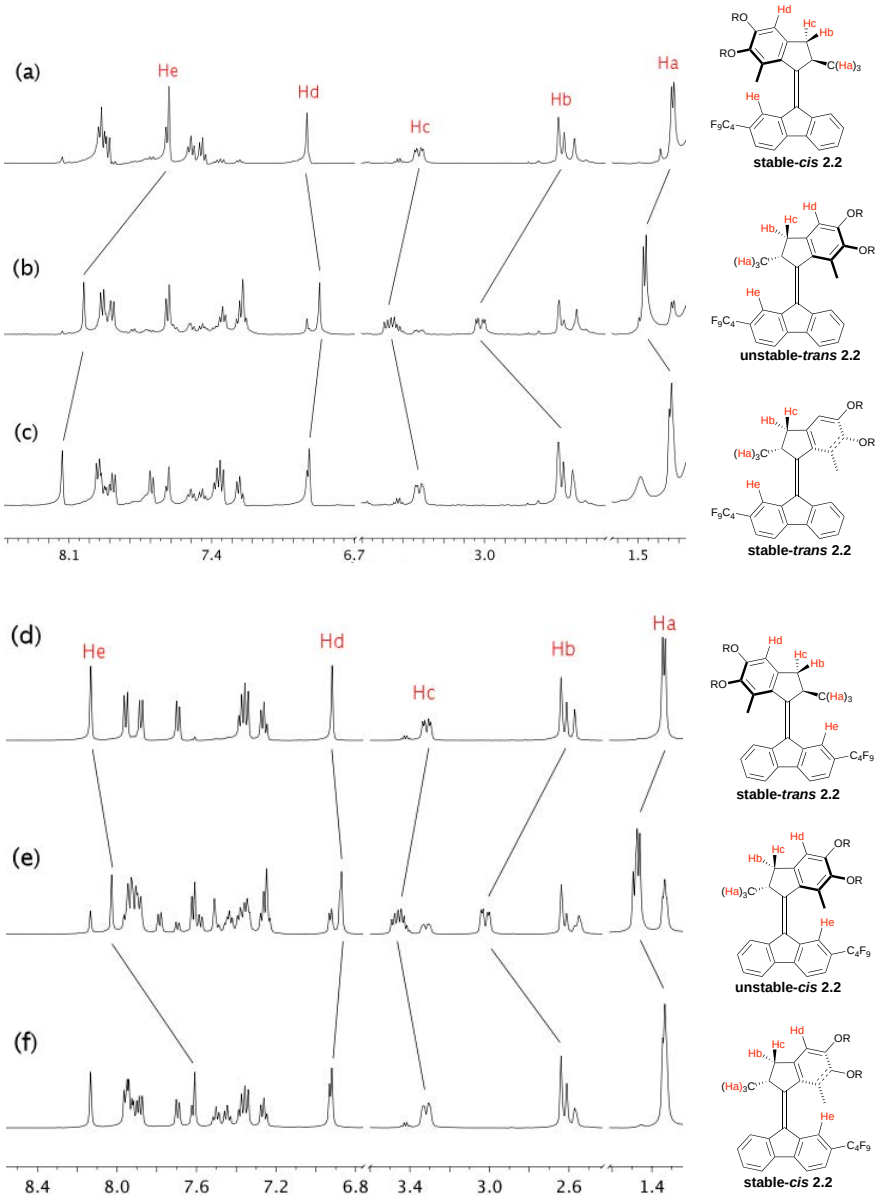

Figure 2.5 Partial ^{1}H NMR spectra (500 MHz, CD_2Cl_2, 218 K) of **2.2** (a) stable-*cis* **2.2** (b) unstable-*trans* **2.2** formed upon UV irradiation to PSS (λ_{max} = 365 nm) (c) stable-*trans* **2.2** obtained after thermal isomerization of unstable-*trans* **2.2** at rt; (d) stable-*trans* **2.2** (e) unstable-*cis* **2.2** formed upon UV irradiation to PSS (f) stable-*cis* **2.2** obtained after thermal isomerization of unstable-*cis* **2.2** at rt. Signal assignments are given (R = $CH_2CH_2OCH_2CCH$).

By studying the photochemical and thermal behavior of **2.1** and **2.2** in solution using a combination of UV/vis absorption and ^{1}H NMR spectroscopy, and by analogy with similar motor systems reported previously, it is concluded that **2.1** and **2.2** function as light-driven rotary motors in solution. In summary, the introduction of the cyano and perfluorobutyl group on the motor moiety does not have a significant influence on the photochemical and thermal behavior of the motors.

2.4 Surface attachment and characterization

Molecular motors **2.1** and **2.2** were attached to quartz surfaces through interfacial Cu(I)-catalyzed azide-alkyne cycloaddition[48,49] as previously developed for molecular motors with a nonfunctionalized rotor part (Figure 2.1, right).[31,32] It was expected that the functional groups would not interfere with the Cu(I)-catalyzed coupling reaction and that the functionalized motors would bind to quartz under identical conditions to those reported previously.[31,32] To attach the alkyne-terminated motors **2.1** and **2.2** to quartz surfaces through interfacial Cu(I)-catalyzed azide-alkyne cycloaddition, an azide-terminated monolayer (**2.13 SAM**) was prepared using azide **2.13** (Scheme 2.5). Piranha-cleaned quartz slides were immersed in a solution of azide **2.13** in cyclohexane/THF that contained a small amount of water and acid to hydrolyze the methoxysilane groups to silanol groups (for further details on surface preparation, see experimental section). Quartz slides were immersed in this hydrolysis solution for 12 h, then rinsed by sonication in toluene, DMF, and CH_3OH, and dried under a stream of argon. The water contact angles (WCA) for **2.13 SAM** prepared by this method were 83 ± 2º, which is in agreement with contact angles reported earlier for azide-functionalized surfaces.[31,32,50,51,52]

To test the effect of the substituents on the photochemical and wetting properties of the modified surface, both isomers of motors **2.1** and **2.2** were attached to quartz substrates functionalized with azide (Scheme 2.5).

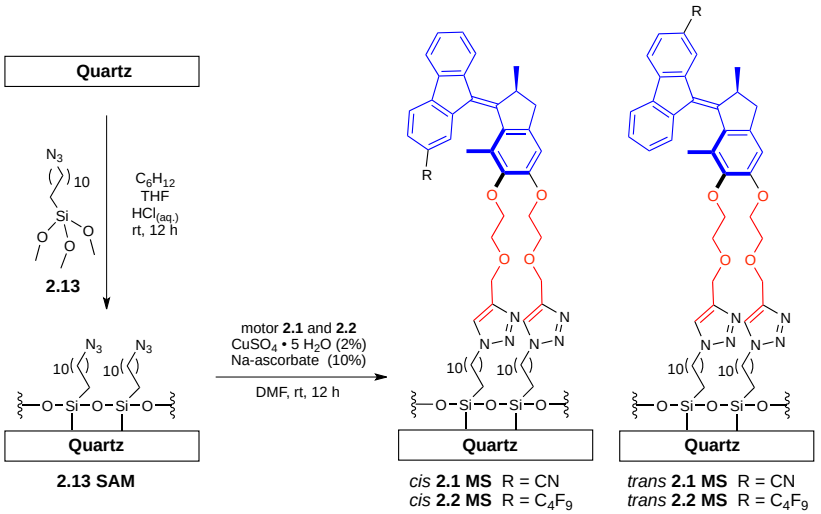

Scheme 2.5 Assembly of an azide-terminated monolayer on quartz surface (left). Attachment of the *cis* and *trans* isomers of motors **2.1** and **2.2** to **2.13 SAM** through a Cu(I)-catalyzed azide-alkyne cycloaddition (right).

The UV/vis spectra of the quartz substrates immersed in a solution of *cis* and *trans* isomers of motors **2.1** and **2.2** in DMF (1 mM) in the presence of Cu(I) catalyst showed the characteristic absorption of the motors, which indicates that the attachment was successful (Figure 2.6, solid line, for further details on surface preparations, see experimental section). The maxima of the major absorption band (centered at 399 nm for **2.1 MS** and 390 nm for **2.2 MS**) and the absorption profile are similar to that observed in CH_3OH solution (Figure 2.2 and 2.3, solid lines).

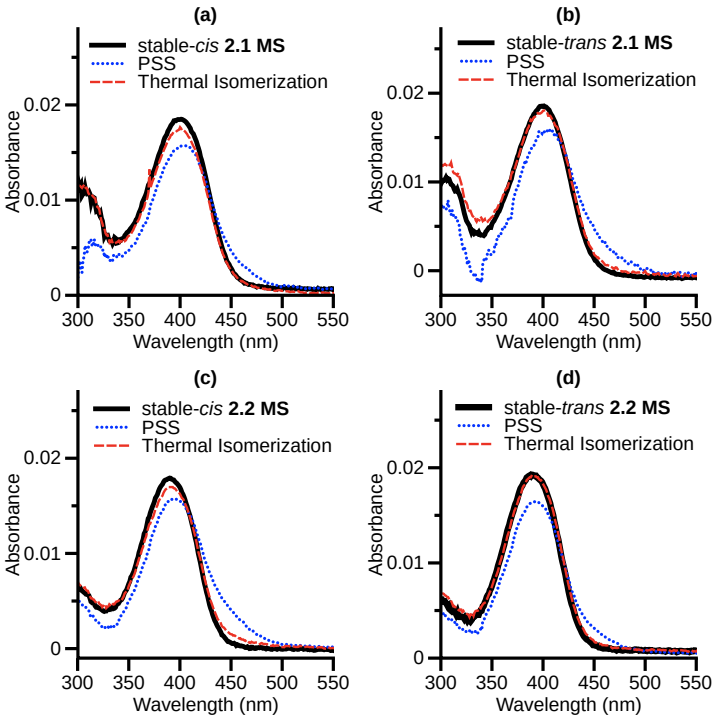

Figure 2.6 UV/vis absorption spectra (268 K) of (a) stable-*cis* **2.1 MS**, (b) stable-*trans* **2.1 MS**, (c) stable-*cis* **2.2 MS**, and (d) stable-*trans* **2.2 MS** on quartz (solid lines). All isomers of the motors undergo photochemical isomerization upon UV irradiation (λ_{max} = 365 nm, dotted lines) and thermal isomerization upon standing at rt overnight (dashed lines).

Based on the assumption that the molar absorptivity (ε) of **2.1** and **2.2** in solution is the same when they are attached to the surface, the surface coverage could be estimated using the Lambert-Beer Law.[53] Considering that both sides of the surfaces are functionalized with molecular motors, the surface coverage is estimated to be 3.7×10^{-10} mol/cm^2 (*cis*-**2.1 MS**), 4.0×10^{-10} mol/cm^2 (*trans*-**2.1 MS**), 3.0×10^{-10} mol/cm^2 (*cis*-**2.2 MS**), and 3.9×10^{-10} mol/cm^2 (*trans*-**2.2 MS**) for a single side. These values are consistent with monolayer formation and are in good agreement with similar overcrowded alkene systems assembled on a variety of surfaces reported previously.[54,55]

Irradiation (λ_{max} = 365 nm) of the functionalized slides at 268 K resulted in a moderate shift of the UV/vis absorption (centered at 403 nm for unstable **2.1 MS** and 394 nm for unstable **2.2 MS**; Figure 2.6, dotted line) similar to that observed in CH_3OH (Figure 2.2 and 2.3, dotted lines), thus indicating the formation of the

unstable form of the surface-bound motors. Upon leaving the sample overnight at rt, the UV/vis absorption reversed, which is consistent with the thermal isomerization process (Figure 2.6, dashed line).

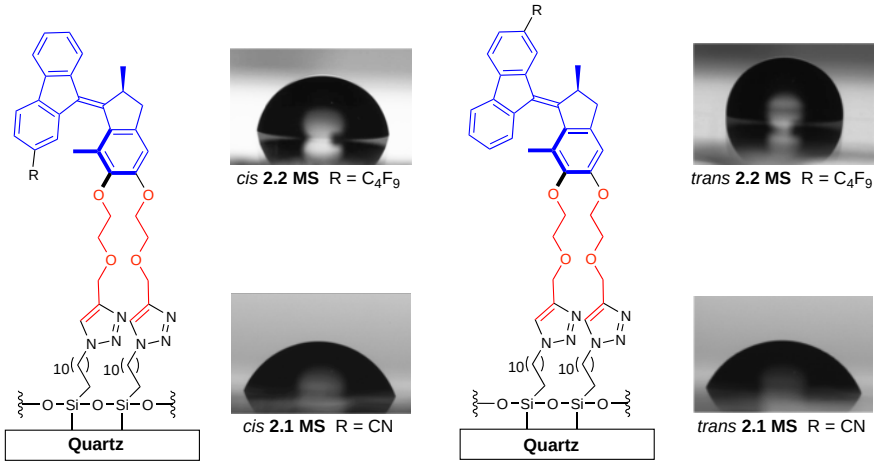

Figure 2.7 Pictures of water droplets on quartz surfaces modified by functionalized altitudinal molecular motors **2.1** and **2.2**.

Contact angle measurements were performed on quartz surfaces modified with *cis* and *trans* isomers of motors **2.1** and **2.2** (Figure 2.7). Motor-modified surfaces *cis*-**2.1 MS** and *trans*-**2.1 MS** showed WCA of 67 ± 1º. and 60 ± 1º, respectively. The contact angle for *cis*-**2.1 MS** is the same as that obtained for the unsubstituted parent motor on quartz, thus indicating that the cyano group does not change the surface wettability considerably, probably due to its small size and comparable polarity to the hydrophilic ethylene glycol units beneath the motor. In the case of *cis*-**2.2 MS**, in which the perfluorobutyl chains are likely hidden from the interface, a WCA of 80 ± 2º was measured. For *trans*-**2.2 MS**, in which the perfluorobutyl chains are exposed to the interface, a contact angle of 92 ± 1º was obtained that is due to the hydrophobic character of the perfluoroalkyl chains. The effect of the substituent on the wettability of the surface is evident when compared to the motor with a symmetric rotor part (Figure 2.1, right), for which a water contact angle of 67 ± 1º was measured.[31] The higher contact angle in the case of *cis*-**2.2 MS** than the unsubstituted symmetric motor analogue is probably due to the shielding of the more polar ethylene glycol units and triazole moieties beneath the chromophore by the perfluoroalkyl chains. The fluorinated chains decrease the free volume in the interface, thereby minimizing the interactions between water and the

hydrophilic components.

Despite the difference in contact angles of water on the different substrates, preliminary attempts to modify the wettability of the surfaces *in situ* did not show substantial effects. This could be due to the observed lower photoconversion in the case of monolayers **2.1 MS** and **2.2 MS** than the motors in solution, as indicated by the smaller redshift of the long-wavelength absorption band in their UV/vis spectra (Figure 2.2 and 2.3 versus Figure 2.6). The lower photoconversion is probably due to the intermolecular interactions between the motors within the monolayer. The increased steric crowding in the interface has already been shown to influence the dynamic behavior of the surface-bound motors by slowing down the thermal isomerization step considerably.[32,54]

2.5 Conclusions

From the experimental data it can be concluded that molecular motors that contain cyano and perfluorobutyl substituents were successfully synthesized and attached in an altitudinal orientation to quartz surfaces by using an interfacial Cu(I)-catalyzed azide-alkyne cycloaddition. Furthermore, it was evident by UV/vis absorption spectroscopy that the rotary function of the motors is preserved while confined at the interface. It has also been shown that the surfaces functionalized with the *cis* and *trans* isomers of the substituted motors **2.1** and **2.2** provided different water contact angles depending on the polarity and orientation of the substituents. In the next chapter efforts towards improved switching efficiency of the surface-bound motors and exploiting the surface wettability change will be described.

2.6 Experimental Section

2.6.1 General remarks

Flash column chromatography was performed as described by Still et al.[56] Chromatography: silica gel, Merck type 9385 230-400 mesh. TLC: silica gel 60, Merck, 0.25 mm, impregnated with a fluorescent indicator (254 nm). Preparative layer chromatography: silica gel, Merck, 1 mm, without a fluorescent indicator. TLC plates were visualized by exposure to ultraviolet light (UV) and/or exposure to ceric ammonium molybdate solution (CAM) or an acidic solution of *p*-anisaldehyde (anisaldehyde) followed by brief heating with a heating gun. Mass spectra (HRMS) were recorded on a Thermo Fisher Scientific Orbitrap XL. ^{1}H and ^{13}C NMR spectra were recorded on a Varian VXR-300, a Varian Mercury Plus, or a Varian Inova 500 operating at 299.97, 399.93, and 499.98 MHz, respectively, for the ^{1}H nucleus, and at 75.43, 100.57 and 124.98 MHz for the ^{13}C nucleus. Chemical shifts for protons are reported in parts per million scale (δ scale) downfield from tetramethylsilane and are referenced to residual protium in the NMR solvents ($CHCl_3$: δ 7.26; CD_2Cl_2: δ 5.32). Chemical shifts for carbon are reported in parts per million (δ scale) downfield from tetramethylsilane and are referenced to the carbon resonances of the solvent ($CDCl_3$: δ 77.0, CD_2Cl_2: δ 54.0). Data are represented as follows: chemical shift, multiplicity (s = singlet, d = doublet, t = triplet, q = quartet, m = multiplet, br = broad), integration, coupling constant in Hz, and assignment. Irradiation experiments were performed using a Spectroline model ENB-280C/FE lamp (λ_{max} = 365 nm, ± 30 nm). NMR samples were placed 2-3 cm from the lamp. UV/vis absorption spectra were obtained using Hewlet-Packard HP 8543 diode array or a Jasco V-630 spectrophotometer in a 1 cm quartz cuvette. Water contact angles were measured under ambient conditions on a SCA20 Dataphysics instrument with software version 3.60.2. Equilibrium contact angles were obtained by applying 1.25 µL water droplets on **2.13 SAM**, **2.1 MS**, and **2.2 MS** using the sessile drop method. The contact angle was measured at three different locations on each surface and the results were averaged.

2.6.2 Synthesis of compounds and intermediates

Compund 2.4

Triton B (5 mL, 40 % in CH_3OH) was added to a stirred solution of 2-bromo-9*H*-fluorene **2.3** (10 g, 40 mmol) in pyridine (50 mL), upon which the reaction mixture turned red. Air was bubbled through the reaction mixture *via* a needle for 10 h. The green solution was poured into 10 % aq. HCl (100 mL) and the precipitate was filtered and recrystallized twice from EtOH yielding **2.4** (7.9 g, 76%) as yellow needles. M.p. 146 – 147 ºC; ^{1}H-NMR (400 MHz, $CDCl_3$) δ 7.70 (s, 1H), 7.61 (d, *J* = 7.4 Hz, 1H), 7.56 (d, *J* = 7.9 Hz, 1H), 7.47 (m, 2H), 7.33 (d, *J* = 7.9 Hz, 1H), 7.31–7.25 (m, 1H); ^{13}C NMR (APT, 50 MHz, $CDCl_3$) δ 192.6, 143.6, 142.9, 137.0, 135.7, 135.0, 133.6, 129.4, 127.5, 124.6, 122.9, 121.7, 120.4; HRMS (APCI-ion trap) *m/z*: $[M + H]^+$ Calcd for $C_{13}H_7OBr$ 258.9753, found 258.9751.

Compund 2.5

To a stirred suspension of 2-bromo-9*H*-fluoren-9-one **2.4** (3.0 g, 11.0 mmol) in CH_3OH (30 mL), hydrazine monohydrate (4 mL) was added and the reaction mixture was heated to reflux for 2 h, turning from yellow to orange. The reaction mixture was poured into water (50 mL) and extracted with CH_2Cl_2 (2×50 mL). The organic phase was dried ($MgSO_4$) and the solvent was evaporated under reduced pressure to give a pale brown solid. Recrystallization from cyclohexane yielded **2.5** as a mixture of *E* and *Z* isomers (2.73 g, 91%) as pale brown needles. M.p. 139 ºC; ^{1}H-NMR (400 MHz, $CDCl_3$) δ 8.09 – 8.00 (d, *J*= 1.6 Hz, 1H), 7.86 (m, 2H), 7.78–7.66 (m, 2H), 7.65–7.57 (m, 2H), 7.56 (d, *J* = 1.7 Hz, 1H), 7.54–7.47 (m, 1H), 7.47–7.40 (m, 2H), 7.40–7.28 (m, 3H), 6.50 (s, 2H), 6.42 (s, 2H); ^{13}C NMR (50 MHz, $CDCl_3$) δ 144.2, 143.7, 140.2, 140.0, 137.5, 137.1, 132.3, 131.6, 131.1, 129.9, 129.7, 128.6, 128.4 , 128.2, 128.0, 125.3, 123.9, 121.7, 121.6, 121.0, 120.83, 120.80, 120.6, 119.6; HRMS (ESI-ion trap) *m/z*: $[M + H]^+$ Calcd for $C_{13}H_9BrN_2$ 273.0017, found 273.0022.

Compund 2.6

MnO_2 (3.8 g, 44 mmol) was added to a stirred solution of **2.5** (3 g, 11 mmol) in THF (100 mL) upon which the color changed from yellow to red. The resulting suspension was stirred for 5 min and filtered over a plug of SiO_2. The solvent was removed under reduced pressure yielding **2.6** as a light red solid (2.9 g, 98%). The product was used in the next reaction step without further purification. M.p.

121 ºC; ^{1}H NMR (400 MHz, $CDCl_3$) δ 7.89 (d, *J* = 7.6 Hz, 1H), 7.75 (d, *J* = 8.2 Hz, 1H), 7.60 (s, 1H), 7.52–7.35 (m, 3H), 7.32 (t, *J* = 7.4 Hz, 1H); ^{13}C NMR (50 MHz, $CDCl_3$) δ 134.7, 132.7, 130.5, 130.2, 127.6, 126.7, 124.8, 122.0, 121.0, 120.1, 119.2; HRMS (APCI-ion trap) *m/z*: $[M - N_2 + H]^+$ Calcd for $C_{13}H_7BrN_2$ 242.9851, found 242.9803.

Compund 2.8

2-bromodiazofluorenone **2.6** (1.23 g, 4.7 mmol) was added to a solution of thioketone **2.7** (1.64 g, 4.3 mmol) in toluene (30 mL). The mixture was heated up to 55 ºC for 3 h. The formation of the episulfide was monitored by ^{1}H NMR spectroscopy by following the shift of the aromatic proton of the thioketone from 6.66 ppm to 6.35 and 6.37 ppm (*E*/*Z* isomers of the episulfide). After the conversion of the thioketone was complete, PPh_3 (1.2 g, 4.7 mmol) was added to the episulfide solution and the mixture was heated for an additional 2 h at 75 ºC. The reaction mixture was cooled to rt and concentrated *in vacuo*. EtOAc (60 mL) was added to the mixture, which resulted in the precipitation of PPh_3S as yellow crystals. The precipitate was filtered and the procedure was repeated once more. The solvent was removed under reduced pressure. The product was obtained as a mixture of *E* and *Z* isomers (42 : 58) after column chromatography (SiO_2, *n*-hexane : EtOAc = 4 : 1) as a yellow solid (1.6 g, 2.93 mmol, 68 %). ^{1}H NMR (400 MHz, $CDCl_3$) δ 1.30-1.34 (m, 9H major, 9H minor), 2.23 (s, 3H, major), 2.24 (s, 3H, minor), 2.54 (d, *J*= 14.7 Hz, 1H major, 1H minor), 3.29 (dd, *J* = 5.8, 14.76 Hz, 1H major, 1H minor), 4.04-4.15 (m, 1H major, 1H minor), 4.26-4.33 (m, 4H major, 4H minor), 4.67 (d, *J* = 15.8 Hz, 1H major), 4.70 (d, *J* = 15.7 Hz, 1H minor), 4.74 (s, 2H, major), 4.75 (s, 2H, minor), 4.83 (d, *J* = 15.7 Hz, 1H, minor), 4.90 (d, *J* = 15.8 Hz, 1H, major), 6.75 (s, 1H, major), 6.77 (s, 1H, minor), 7.17 (t, *J* = 7.6 Hz, 1H, major), 7.29 (t, *J* = 7.5 Hz, 1H, major), 7.32-7.41 (m, 1H major, 3H minor), 7.45-7.48 (m, 1H major, 1H minor), 7.61 (d, *J* = 8.1 Hz, 1H, minor), 7.66 (d, *J* = 8.1 Hz, 1H, major), 7.71 (d, *J* = 7.3 Hz, 1H, major), 7.76-7.79 (m, 1H, minor), 7.82-7.85 (m, 1H, minor), 7.95 (s, 1H, major); ^{13}C NMR (100 MHz, $CDCl_3$) δ 14.1, 14.2, 16.2, 18.8, 18.9, 41.3, 41.4, 44.7, 44.8, 60.9, 61.0, 61.4, 65.8, 65.9, 68.1, 69.3, 69.7, 108.2, 108.4, 119.1, 119.6, 120.2, 120.3, 120.4, 120.7, 123.6, 123.7, 126.4, 126.7, 126.8, 126.9, 127.0, 127.1, 128.1, 128.4, 129.3, 129.4, 131.9, 132.1, 134.0, 134.2, 137.4, 137.9, 138.4, 138.7, 139.2, 139.3, 141.3, 143.5, 143.7, 145.1, 145.6, 151.2, 151.7, 152.8, 152.9, 168.4, 168.5, 169.3, 169.5; HRMS (ESI-ion trap) *m/z*: $[M + H]^+$ Calcd for $C_{32}H_{32}O_6Br$ 591.1377, found 591.1379.

Compund 2.9

A solution of (*cis/trans*)-**2.8** (546 mg, 1.00 mmol) in N,N-dimethylacetamide (22 mL) was added to a mixture of $Pd_2(dba)_3$ (18.5 mg, 0.02 mmol, 2 mol%), dppf (22.3 mg, 0.04 mmol, 4 mol%), Zn powder (13.1 mg, 0.20 mmol, 20 mol%) and $Zn(CN)_2$ (235.0 mg, 2.00 mmol, 200 mol%) purged with argon and the mixture was heated at 150 ºC for 5 h. The reaction mixture was cooled to rt, diluted with EtOAc (50 mL), and washed with saturated aq Na_2CO_3 (60 mL), brine (20 mL), dried (Na_2SO_4) and concentrated *in vacuo*. Purification by column chromatography (SiO_2, n-hexane : EtOAc = 4 : 1) afforded the product as a mixture of *trans* and *cis* isomers (~ 2 : 1) as a yellow solid (479 mg, 0.89 mmol, 89%). *Cis/trans* mixture: ^{1}H NMR (400 MHz, $CDCl_3$) δ 1.29-1.36 (m, 9H major, 9H minor), 2.23 (s, 3H, major), 2.25 (s, 3H, minor), 2.57 (d, *J* = 14.8 Hz, 1H, minor), 2.58 (d, *J* = 14.8 Hz, 1H, major), 3.31 (dd, *J* = 5.7, 14.6 Hz, 1H major, 1H minor), 4.04-4.16 (m, 1H major, 1H minor), 4.26-4.34 (m, 4H major, 4H minor), 4.68 (d, *J* = 15.9 Hz, 1H, major), 4.75 (s, 2H, major), 4.76 (s, 2H, minor), 4.84 (d, *J* = 3.6 Hz, 2H, minor), 4.92 (d, *J* = 15.9 Hz, 1H, major), 6.76 (s, 1H, major), 6.79 (s, 1H, minor), 7.26 (m, 1H, major), 7.35 (dt, *J* = 1.0, 7.5 Hz, 1H, major), 7.40 (d, *J* = 7.7 Hz, 1H, major), 7.43-7.47 (m, 2H, minor) 7.57 (dd, *J* = 1.4, 7.9 Hz, 1H minor), 7.63 (dd, *J* = 1.3, 7.9 Hz, 1H, major), 7.65 (br s, 1H, minor), 7.80 (d, *J* = 7.3 Hz, 1H, major) 7.83 (d, *J* = 7.4 Hz, 1H, minor), 7.85-7.91 (m, 2H, minor) 7.88 (d, *J* = 7.9 Hz, 1H, major), 8.09 (s, 1H, major); ^{13}C NMR (125 MHz, $CDCl_3$) δ 14.1, 14.2, 16.2, 18.9, 19.2, 41.4, 44.9, 45.2, 60.9, 61.0, 61.5, 65.7, 65.9, 69.2, 69.3, 108.2, 108.5, 109.4, 109.5, 119.6, 119.8, 120.0, 120.1, 120.2, 120.6, 123.8, 123.82, 127.0, 127.1, 127.2, 127.3, 127.5, 127.6, 128.4, 128.5, 130.1, 130.4, 132.1, 132.3, 133.6, 133.9, 137.3, 137.7, 137.8, 138.3, 139.5, 140.1, 142.6, 143.3, 143.8, 143.9, 145.1, 145.4, 151.6, 151.8, 154.5, 154.7, 168.4, 169.5, 169.6; HRMS (ESI-ion trap) *m/z*: $[M + Na]^+$ Calcd for $C_{33}H_{31}NO_6Na$ 560.2044, found 560.2022.

Compund 2.11

A solution of (*E*/*Z*)-**2.9** (339 mg, 0.63 mmol) in THF (22 mL) was added to a suspension of $LiBH_4$ (14.4 mg, 0.66 mmol) in THF (3 mL) and the mixture was stirred at rt for 90 min. The mixture was diluted with EtOAc (25 mL) and washed with H_2O (20 mL), brine (10 mL), dried (Na_2SO_4) and concentrated *in vacuo*. Purification by flash column chromatography (SiO_2, EtOAc) afforded **2.11** as a mixture of isomers (1 : 1.7) as a yellow solid (152 mg, 0.34 mmol, 55%). ^{1}H NMR (500 MHz, $CDCl_3$) δ 1.36 (d, *J* = 6.6 Hz, 3H, minor), 1.37 (d, *J* = 6.7 Hz, 3H, major), 2.18 (s, 3H, minor), 2.19 (s, 3H, major), 2.61 (d, *J* = 14.9 Hz, 1H, minor),

2.62 (d, *J* = 14.8 Hz, 1H, major), 3.34 (dd, *J* = 5.70, 14.8 Hz, 1H major, 1H minor), 3.92-4.23 (m, 9H major, 8H minor), 4.28-4.32 (m, 1H, minor) 6.90 (s, 1H, major) 6.91 (s, 1H, minor), 7.22 (t, *J* = 7.6 Hz, 1H, major), 7.33-7.38 (m, 2H, major), 7.41-7.49 (m, 2H, minor), 7.56 (dd, *J* = 1.3, 7.9 Hz, 1H, minor), 7.63-7.65 (m, 1H major, 1H minor), 7.81-7.85 (m, 1H major, 1H minor), 7.87-7.89 (m, 1H, minor) 7.89 (d, *J* = 7.9 Hz, 1H, major), 7.91 (d, *J* = 7.8 Hz, 1H, minor), 8.10 (s, 1H, major); ^{13}C NMR (125 MHz, $CDCl_3$) δ 155.0, 154.8, 153.4, 153.0, 145.6, 144.6, 144.5, 143.2, 142.8, 140.2, 139.6, 138.5, 137.8, 137.4, 133.3, 133.0, 132.2, 131.9, 130.1, 129.985, 128.6, 128.1, 127.3, 127.3, 127.2, 127.1, 127.0, 123.8, 123.4, 120.7, 120.3, 120.2, 120.1, 119.9, 119.8, 109. 6, 109.1, 108.3, 108.1, 74.4, 74.3, 70.6, 70.6, 64.4, 62.2, 62.0, 61.0, 45.0, 44.8, 41.6, 41.5, 19.2, 18.9, 16.1, 15.9; HRMS (ESI-ion trap) *m/z*: $[M + Na]^+$ Calcd for $C_{29}H_{27}NO_4Na$ 476.1832, found 476.1843.

Compund 2.1

A solution of (*E*/*Z*)-**2.11** (160 mg, 0.35 mmol) in THF (14 mL) was added dropwise to the suspension of NaH (95%, 34.45 mg, 1.36 mmol) in THF (6 mL) and the mixture was stirred at rt for 30 min. To this mixture propargyl bromide (80 % in toluene, 170 µL, 1.53 mmol,) was added. The solution was stirred at rt for 12 h. The mixture was diluted with EtOAc (25 mL) and washed with H_2O (20 mL), brine (10 mL), dried (Na_2SO_4) and concentrated *in vacuo*. Purification by column chromatography (SiO_2, *n*-hexane : EtOAc = 4 : 1) afforded the product as a mixture of *E* and *Z* isomers as a yellow solid (118 mg, 0.22 mmol, 63%). 85 mg (0.16 mmol) of the *E*/*Z* mixture was separated by column chromatography (SiO_2, toluene : Et_2O 20 : 1). Stable-*cis* **2.1** **(**26 mg, 0.05 mmol, 31%, R_f= 0.45) was obtained as a yellow solid: ^{1}H NMR (400 MHz, $CDCl_3$) δ 1.34 (d, *J* = 6.7 Hz, 3H), 2.16 (s, 3H), 2.41 (t, *J* = 2.4 Hz, 1H), 2.49 (t, *J* = 2.4 Hz, 1H), 2.58 (d, *J* = 14.8 Hz, 1H), 3.32 (dd, *J* = 5.7, 14.7 Hz, 1H), 3.92-3.94 (m, 2H), 4.00 (t, *J* = 4.77 Hz, 2H), 4.12 (quin, *J* = 8.0 Hz, 1H), 4.23-4.30 (m, 4H), 4.31-4.32 (m, 4H), 6.88 (s, 1H), 7.40 (dt, *J* = 1.1, 7.4 Hz, 1H), 7.45 (dt, *J* = 1.5, 7.6 Hz, 1H), 7.55 (dd, *J* = 1.4, 7.9 Hz, 1H), 7.65 (d, *J* = 0.8 Hz, 1H), 7.83 (dd, *J* = 0.5, 7.9 Hz, 1H), 7.87 (dd, *J* = 0.9, 7.3 Hz, 1Hz), 7.90 (d, *J* = 7.6 Hz, 1H); ^{13}C NMR (100 MHz, $CDCl_3$) δ 16.1, 19.0, 41.5, 45.0, 58.4, 58.6, 68.1, 68.2, 69.3, 72.0, 74.4, 74.8, 108.5, 109.2, 119.7, 119.9, 120.7, 123.8, 126.8, 127.2, 128.5, 130.0, 131.8, 132.8, 137.7, 137.9, 140.2, 142.6, 144.0, 146.2, 153.7, 155.5; UV/vis (CH_3OH, 253 K): λ_{max} (ε) = 395 nm (25299 $M^{-1}cm^{-1}$). Stable-*trans* **2.1** (40 mg, 0.075 mmol, 47%, R_f=0.55) was obtained as a yellow solid: ^{1}H NMR (400 MHz, $CDCl_3$) δ 1.36 (d, *J* = 6.7 Hz, 3H),

2.18 (s, 3H), 2.43 (t, *J* = 2.3 Hz, 1H), 2.49 (t, *J* = 2.3 Hz, 1H), 2.59 (d, *J* = 14.8 Hz, 1H), 3.32 (dd, *J* = 5.9, 14.8 Hz, 1H), 3.89-3.93 (m, 2H), 3.99 (t, *J* = 4.7 Hz, 2H), 4.03-4.16 (m, 2H), 4.22-4.38 (m, 3H), 4.30 (d, *J* = 2.3 Hz, 2H), 4.32 (d, *J* = 2.4 Hz, 2H), 6.87 (s, 1H), 7.22 (t, *J* = 7.3 Hz, 1H), 7.33 (t, *J* = 7.3 Hz, 1H), 7.38 (d, *J* = 7.9 Hz, 1H), 7.63 (dd, *J* = 0.8, 7.9 Hz, 1H), 7.81 (d, *J* = 7.6 Hz, 1H), 7.88 (d, *J* = 7.9 Hz, 1H), 8.09 (s, 1H); ^{13}C NMR (125 MHz, $CDCl_3$) δ 16.0, 19.3, 41.5, 45.0, 58.3, 58.6, 68.0, 68.2, 69.3, 71.6, 74.6, 74.8, 108.3, 109.5, 120.0, 120.1, 120.3, 123.6, 127.1, 127.1, 127.2, 128.2, 130.0, 132.1, 133.0, 137.3, 138.6, 139.6, 143.2, 143.9, 145.8, 153.3, 155.3. 2.1; UV/vis (CH_3OH, 253 K): λ_{max} (ε) = 395 nm (22743 $M^{-1}cm^{-1}$). Stable **2.1**: HRMS (ACPI-ion trap) *m/z*: $[M + H]^+$ Calcd for $C_{35}H_{31}NO_4$ 529.2253, found 530.2324.

2.6.3 Low temperature ^{1}H NMR spectroscopic characterization of the unstable isomers of 2.1 and 2.2 and procedure to determine the composition of the photostationary state

Irradiation experiment to generate unstable-*trans* 2.1

Stable-*cis* **2.1** (2 mg) was dissolved in CD_2Cl_2 (1 mL). This sample was placed in an NMR tube and irradiated (λ_{max} = 365 nm) at 218 K at a distance of 3 cm from the center of the lamp. ^{1}H NMR spectra of the sample were taken before, during and after irradiation at 218 K. No further changes were observed after 7 h of irradiation. The relative integration of the absorptions from the two isomers revealed a PSS ratio 1/5 for stable-*cis* **2.1**/unstable-*trans* **2.1** (Figure 2.4b). After warming the sample to rt, only the stable isomers were observed by (Figure 2.4c). Stable-*cis* **2.1** (Figure 2.4a): ^{1}H NMR (500 MHz, CD_2Cl_2, 218 K) δ 1.28 (d, *J* = 6.5 Hz, 3H), 2.08 (s, 3H), 2.51 (s, 1H), 2.56-2.60 (m, 2H), 3.28 (dd, *J* = 5.4, 14.7 Hz, 1H), 3.80-3.88 (m, 2H), 3.95 (t, *J* = 3.6 Hz, 2H), 4.06-4.13 (m, 2H), 4.16-4.24 (m, 3H), 4.27 (s, 2H), 4.29 (d, *J* = 1.4 Hz, 2H), 6.89 (s, 1H), 7.40 (t, *J* = 7.3 Hz, 1H), 7.46 (t, *J* = 7.4 Hz, 1H), 7.57 (s, 2H), 7.85-7.91 (m, 3H); Unstable-*trans* **2.1** (Figure 2.4b): ^{1}H NMR (500 MHz, CD_2Cl_2, 218 K) δ 1.42 (d, *J* = 6.4 Hz, 3H), 1.93 (s, 3H), 2.50-2.60 (absorptions in this region could not be resolved due to overlap with remaining stable-*cis* **2.1**), 2.98 (dd, *J* = 5.30, 16.4 Hz, 1H), 3.42 (dd, *J* = 8.2, 16.3 Hz, 1H), 3.72-4.13 (absorptions in this region could not be resolved due to overlap with remaining stable-*cis* **2.1**), 4.20 (d, *J* = 2.2 Hz, 2H), 4.21-4.25 (absorptions in this region could not be resolved due to overlap with remaining stable-*cis* **2.1**), 4.28 (d, *J* = 2.2 Hz, 2H), 6.83 (s, 1H), 7.19-7.23 (m, 2H), 7.30 (t, *J*

= 7.7 Hz, 1H), 7.57 (d, *J* = 7.6 Hz, 1H), 7.84 (d, *J* = 7.7 Hz, 1H), 7.89 (d, *J* = 7.8 Hz, 1H), 7.98 (s, 1H).

Irradiation experiment to generate unstable-*cis* 2.1:
Using the same procedure, no further changes were observed after 7 h of irradiation. The PSS ratio for stable-*trans* **2.1**/unstable-*cis* **2.1** was determined to be 1/3.5 (Figure 2.4e). After warming the sample to rt, only the stable isomers were observed (Figure 2.4f). Stable-*trans* **2.1** (Figure 2.4d): ^{1}H NMR (500 MHz, CD_2Cl_2, 218 K) δ 1.29 (d, *J* = 6.5 Hz, 3H), 2.09 (s, 3H), 2.52 (s, 1H), 2.57-2.60 (m, 2H), 3.28 (dd, *J* = 5.5, 14.7 Hz, 1H), 3.77-3.86 (m, 2H), 3.92-3.95 (m, 2H), 3.99-4.06 (m, 2H), 4.18-4.32 (m, 3H), 4.24 (s, 2H), 4.29 (s, 2H), 6.88 (s, 1H), 7.22 (t, *J* = 7.5 Hz, 1H), 7.3-7.34 (m, 2H), 7.65 (d, *J* = 7.9 Hz, 1H), 7.83 (d, *J* = 7.6 Hz, 1H), 7.91 (d, *J* = 7.9 Hz, 1H), 8.09 (s, 1H); Unstable-*cis* **2.1** (Figure 2.4e): ^{1}H NMR (500 MHz, CD_2Cl_2, 218 K) δ 1.45 (d, *J* = 6.4 Hz, 3H), 1.92 (s, 3H), 2.48-2.50 (m, 1H), 2.55-2.60 (absorptions in this region could not be resolved due to overlap with remaining stable-*trans* **2.1**), 2.98 (dd, *J* = 5.3, 16.0 Hz, 1H), 3.41 (dd, *J* = 8.2, 16.3 Hz, 1H), 3.74-4.31 (absorptions in this region could not be resolved due to overlap with remaining stable-*trans* **2.1**), 4.22 (d, *J* = 2.2 Hz, 2H), 6.83 (s, 1H), 7.30-7.35 (absorptions in this region could not be resolved due to overlap with remaining stable-*trans* **2.1**), 7.39 (t, *J* = 7.7 Hz, 1H), 7.47 (s, 1H), 7.53 (dd, *J* = 0.7, 7.9 Hz, 1H), 7.74 (d, *J* = 7.8 Hz, 1H), 7.87 (d, *J* = 7.8 Hz, 2H)

Irradiation experiment to generate unstable-*trans* 2.2:
Using the same procedure, no further changes were observed after 7 h of irradiation. The PSS ratio for stable-*cis* **2.2**/unstable-*trans* **2.2** was determined to be 1/3.5 (Figure 2.5b). After warming the sample to rt, only the stable isomers were observed (Figure 2.5c). Stable-*cis* **2.2** (Figure 2.5a): ^{1}H NMR (500 MHz, CD_2Cl_2, 218 K) δ 1.29 (d, *J* = 6.6 Hz, 3H), 2.06 (s, 3H), 2.52 (t, *J* = 2.3 Hz, 1H), 2.55-2.58 (m, 2H), 3.28 (dd, *J* = 5.3, 14.6 Hz, 1H) 3.79-3.85 (m, 2H), 3.9-4.0 (m, 4H), 4.10 (quin, *J* = 6.0 Hz, 1H), 4.14-4.25 (m, 2H), 4.26 (t, *J* = 2.4 Hz, 2H), 4.29 (d, *J* = 2.3 Hz, 2H), 6.88 (s, 1H), 7.39 (t, *J* = 7.3 Hz, 1H), 7.44 (t, *J* = 8.0 Hz, 1H), 7.48 (d, *J* = 8.5 Hz, 1H), 7.51 (s, 1H), 7.89-7.92 (m, 3H); Unstable-*trans* **2.2** (Figure 2.5b): ^{1}H NMR (500 MHz, CD_2Cl_2, 218 K) δ 1.41 (d, *J* = 6.3 Hz, 3H), 1.95 (s, 3H), 2.50-2.51 (m, 1H), 2.55-2.59 (absorptions in this region could not be resolved due to overlap with remaining stable-*cis* **2.2**), 3.40 (dd, *J* = 8.4, 16.1 Hz, 1H), 3.72-4.29 (absorptions in this region could not be resolved due to overlap with remaining stable-*cis* **2.2**), 6.82 (s, 1H), 7.19-7.22 (m, 2H), 7.28-7.31 (m, 1H),

7.32-7.51 (absorptions in this region could not be resolved due to overlap with remaining stable-*cis* **2.2**), 7.82 (s, 1H), 7.85 (d, *J* = 7.8 Hz, 1H), 7.89-7.94 (absorptions in this region could not be resolved due to overlap with remaining stable-*cis* **2.2**).

Irradiation experiment to generate unstable-*cis* 2.2:

Using the same procedure, no further changes were observed after 7 h of irradiation. The PSS ratio for stable-*trans* **2.2**/unstable-*cis* **2.2** was determined to be 1/2 (Figure 2.5e). After warming the sample to rt, only the stable isomers were observed (Figure 2.5f). Stable-*trans* **2.2** (Figure 2.5d): ^{1}H NMR (500 MHz, CD_2Cl_2, 218 K) δ 1.29 (d, *J* = 6.6 Hz, 3H), 2.09 (s, 3H), 2.52 (t, *J* = 2.3 Hz, 1H), 2.58 (d, *J* = 14.7 Hz, 1H), 2.59 (t, *J* = 2.5 Hz, 1H), 3.28 (dd, *J* = 5.6, 14.7 Hz, 1H), 3.77-3.86 (m, 3H), 3.94 (t, *J* = 3.9 Hz, 2H), 3.98-4.02 (m, 1H), 4.06 (t, *J* = 6.5 Hz, 1H), 4.17-4.32 (m, 2H) 4.24 (d, *J* = 2.0 Hz, 2H), 4.28 (d, *J* = 2.3 Hz, 2H), 6.87 (s, 1H), 7.20 (t, *J* = 7.6 Hz, 1H), 7.30-7.34 (m, 2H), 7.55 (d, *J* = 8.1 Hz, 1H), 7.84 (d, *J* = 7.4 Hz, 1H), 7.95 (d, *J* = 8.0 Hz, 1H), 8.00 (s, 1H); Unstable-*cis* **2.2** (Figure 2.5e): ^{1}H NMR (500 MHz, CD_2Cl_2, 218 K) δ 1.46 (d, *J* = 6.2 Hz, 3H), 1.89 (s, 3H), 2.49-2.51 (m, 1H), 2.55-2.60 (absorptions in this region could not be resolved due to overlap with remaining stable-*trans* **2.2**), 3.00 (dd, *J* = 5.7, 16.4 Hz, 1H), 3.41 (dd, *J* = 8.4, 16.3 Hz, 1H), 3.74-4.32 (absorptions in this region could not be resolved due to overlap with remaining stable-*trans* **2.2**), 4.22 (s, 2H), 6.83 (s, 1H), 7.19-7.39 (absorptions in this region could not be resolved due to overlap with remaining stable-*trans* **2.2**), 7.37 (s, 2H), 7.44 (d, *J* = 7.9 Hz, 1H), 7.74 (d, *J* = 7.7 Hz, 1H), 7.87 (d, *J* = 7.4 Hz, 1H), 7.92 (d, *J* = 7.8 Hz, 1H).

2.6.4 Preparation of the surface

Preparation of azide terminated monolayer 2.13 SAM

1.25 mL of the hydrolysis solution containing 11-azidoundecyltrimethoxy silane **2.13** (0.04 g), THF (6 ml), double-distilled H_2O (31 µl), and 37% $HCl_{(aq.)}$ (4 µl) was added to cyclohexane (25 mL) to give a slighty hazy solution. The piranha-cleaned quartz slides were immersed into this solution overnight. After the assembly the slides were sonicated in DMF, toluene and CH_3OH for 2 min each and dried under a stream of argon.

Preparation of the 2.1 MS and 2.2 MS

Compounds **2.1** and **2.2** were grafted to the **2.13 SAM** by immersing this slide into a 1 mM solution of *cis* and *trans* isomers of **2.1** and **2.2** in DMF containing 1 mol% $CuSO_4 \cdot 5H_2O$ and 5 mol% sodium-ascorbate relative to the alkyne moieties. The azide functionalized slides were immersed for 12 h at rt. The modified quartz substrates (**2.1 MS** and **2.2 MS**) were sonicated in DMF, water and CH_3OH for 2 min each and then dried under a stream of argon.

2.7 References

[1] Love, J. C.; Estroff, L. A.; Kriebel, J. K.; Nuzzo, R. G.; Whitesides, G. M. *Chem. Rev.* **2005**, *105*, 1103–1169.

[2] Bain, C. D.; Whitesides, G. M. *J. Am. Chem. Soc.* **1988**, *110*, 5897–5898.

[3] Nuzzo, R. G.; Dubois, L. H.; Allara, D. L. *J. Am. Chem. Soc.* **1990**, *112*, 558–569.

[4] Janssen, D.; De Palma, R.; Verlaak, S.; Heremans, P.; Dehaen, W. *Thin Solid Films* **2006**, 515, 1433–1438.

[5] Ariga, K.; Richards, G. J.; Ishihara, S.; Izawa, H.; Hill, J. P. *Sensors* **2010**, *10*, 6796–6820.

[6] Singh, A.; Myerson, A. S. *J. Pharm. Sci.* **2010**, *99*, 3931–3940.

[7] Coperet, C.; Chabanas, M.; Saint–Arroman, R. P.; Basset,J. M. *Angew. Chem. Int. Ed.* **2003**, *42*, 156–181.

[8] Kakkar, A. K. *Chem. Rev.* **2002**, *102*, 3579–3587.

[9] Katsonis, N.; Kudernac, T.; Walko, M.; van der Molen, S. J.; van Wees, B. J.; Feringa, B. L. *Adv. Mater.* **2006**, *18*, 1397–1400.

[10] Nakanishi, H.; Bishop, K. J. M.; Kowalczyk, B.; Nitzan, A.; Weiss, E. A.; Tretiakov, K. V.; Apodaca, M. M.; Klajn, R.; Stoddart, J. F.; Grzybowski, B. A. *Nature* **2009**, *460*, 371–375.

[11] Browne, W. R.; Feringa, B. L. *Annu. Rev. Phys. Chem.* **2009**, *60*, 407–428.

[12] Katsonis, N.; Lubomska, M.; Pollard, M.; Feringa, B.; Rudolf, P. *Prog. Surf. Sci.* **2007**, *82*, 407–434.

[13] Wang, S. T.; Song, Y. L.; Jiang, L. *J. Photochem. Photobiol. C* **2007**, *8*, 18–29.

[14] *Molecular Switches, 2nd Ed*; Browne, W. R., Feringa, B. L., Eds; Wiley–VCH: Weinheim, **2011**.

[15] Velema, W. A.; van der Berg, J. P.; Hansen, M. J.; Szymański, W.; Driessen, A. J. M.; Feringa, B. L. *Nat. Chem.* **2013**, *5*, 924–928.

[16] Zheng, Y. B.; Pathem, B. K.; Hohman, J. N.; Thomas, J. C.; Kim, M.; Weiss, P. S. *Adv. Mater.* **2013**, *25*, 302–312.

[17] Browne, W. R.; Feringa, B. L. *Annu. Rev. Phys. Chem.* **2009**, *60*, 407–428.

[18] Katsonis, N.; Lubomska, M.; Pollard, M.; Feringa, B.; Rudolf, P. *Prog. Surf. Sci.* **2007**, *82*, 407–434.

[19] Wang, S. T.; Song, Y. L.; Jiang, L. *J. Photochem. Photobiol. C* **2007**, *8*, 18–29.

[20] *Photoisomerization of azobenzenes*; Rau, H.*;* CRC Press, Boca Raton, **1990**.

[21] Klajn, R. *Pure Appl. Chem.* **2010**, *82*, 2247–2279.

[22] Rosario, R.; Gust, D.; Hayes, M.; Jahnke, F.; Springer, J.; Garcia, A. A. *Langmuir* **2002**, *18*, 8062–8069.

[23] Siewierski, L. M.; Brittain, W. J.; Petrash, S.; Foster, M. D. *Langmuir* **1996**, *12*, 5838–5844.

[24] Demirel, G. B.; Dilsiz, N.; Cakmak, M.; Caykara, T. *J. Mater. Chem.* **2011**, *21*, 3189–3196.

[25] Min, M.; Bang, G. S.; Lee, H.; Yu, B. C. *Chem. Commun.* **2010**, *46*, 5232–5234.

[26] Lim, H. S.; Han, J. T.; Kwak,D.; Jin, M. H,; Cho, K. *J. Am. Chem. Soc.* **2006**, *128*, 14458–14459.

[27] Koumura, N.; Zijlstra, R. W.; van Delden, R. A.; Harada, N.; Feringa, B. L. *Nature* **1999**, *401*, 152–155.

[28] van Delden, R. A.; Wiel, ter, M. K. J.; Pollard, M. M.; Vicario, J.; Koumura, N.; Feringa, B. L. *Nature* **2005**, *437*, 1337–1340.

[29] Pollard, M. M.; Lubomska, M.; Rudolf, P.; Feringa, B. L. *Angew. Chem.* **2007**, *119*, 1300–1302.

[30] Carroll, G. T.; Pollard, M. M.; van Delden, R.; Feringa, B. L. *Chem. Sci.* **2010**, *1*, 97.

[31] London, G.; Carroll, G. T.; Fernández Landaluce, T.; Pollard, M. M.; Rudolf, P.; Feringa, B. L. *Chem. Commum.* **2009**, 1712–1714.

[32] Carroll, G. T.; London, G.; Landaluce, T. F.; Rudolf, P.; Feringa, B. L. *ACS Nano* **2011**, *5*, 622–630.

[33] Barton, D. H. R.; Willis, B. J. *J. Chem. Soc. –Perkin Trans. 1* **1972**, 305–310.

[34] Buter, J.; Wassenaar, S.; Kellogg, R. M. *J. Org. Chem.* **1972**, *37*, 4045–4060.

[35] Pollard, M. M.; Wesenhagen, von, P.; Pijper, D.; Ben L Feringa. *Org. Biomol. Chem.* **2008**, *6*, 1605–1612.

[36] Jin, F.; Confalone, P. N. *Tetrahedron Lett.* **2000**, *41*, 3271–3273.

[37] Facchetti, A.; Deng, Y.; Wang, A. C.; Koide, Y.; Sirringhaus, H.; Marks, T. J.; Friend, R. H. *Angew. Chem. Int. Ed.* **2000**, *39*, 4547–4551.

[38] Li, Y.; Tan, L.; Wang, Z.; Qian, H.; Shi, Y.; Hu, W. *Org. Lett.* **2008**, *10*, 529–532.

[39] Bauer, J.; Hou, L.; Kistemaker, J. C. M.; Feringa, B. L. *J. Org. Chem.* **2014**, DOI: 10.1021/jo500411z.

[40] Pollard, M. M.; Meetsma, A.; Feringa, B. L. *Org. Biomol. Chem.* **2008**, *6*, 507–512.

[41] Cnossen, A.; Pijper, D.; Kudernac, T.; Pollard, M. M.; Katsonis, N.; Feringa, B. L. *Chem. Eur. J.* **2009**, *15*, 2768–2772.

[42] Pijper, D.; Feringa, B. L. *Angew. Chem. Int. Ed.* **2007**, *46*, 3693–3696.

[43] Vicario, J.; Meetsma, A.; Feringa, B. L. *Chem. Commum.* **2005**, 5910.

[44] Vicario, J.; Walko, M.; Meetsma, A.; Feringa, B. L. *J. Am. Chem. Soc.* **2006**, *128*, 5127–5135.

[45] Schulte–Frohlinde, D.; Gorner, H. *Pure Appl. Chem.* **1979**, *51*, 279–297.

[46] King, N. R.; Whale, E. A.; Davis, F. J.; Gilbert, A.; Mitchell, G. R. *J. Mater.*

Chem. **1997**, *7*, 625–630.

[47] Lummerstorfer, T.; Hoffmann, H. *J. Phys. Chem. B* **2004**, *108*, 3963–3966.

[48] Chelmowski, R.; Kafer, D.; Koster, S. D.; Klasen, T.; Winkler, T.; Terfort, A.; Metzler–Nolte, N.; Woll, C. *Langmuir* **2009**, *25*, 11480–11485.

[49] Collman, J. P.; Devaraj, N. K.; Chidsey, C. E. D. *Langmuir* **2004**, *20*, 1051–1053.

[50] Prakash, S.; Long, T. M.; Selby, J. C.; Moore, J. S.; Shannon, M. A. *Anal. Chem.* **2007**, *79*, 1661–1667.

[51] Fryxell, G. E.; Rieke, P. C.; Wood, L. L.; Engelhard, M. H.; Williford, R. E.; Campbell, G. L. Graff, A. A.; Wiacek, R. J.; Lee, L.; Halverson, A.; *Langmuir* **1996**, *12*, 5064–5075.

[52] Heise, A.; Stamm, M.; Rauscher, M.; Duschner, H.; Menzel, H. *Thin Solid Films* **1998**, *327*, 199–203.

[53] Durfor, C. N.; Turner, D. C.; Georger, J. H.; Peek, B. M.; Stenger, D. A. *Langmuir* **1994**, *10*, 148–152.

[54] Ivashenko, O.; Logtenberg, H.; Areephong, J.; Coleman, A. C.; Wesenhagen, P. V.; Geertsema, E. M.; Heureux, N.; Feringa, B. L.; Rudolf, P.; Browne, W. R. *J. Phys. Chem. C* **2011**, *115*, 22965–22975.

[55] Coleman, A. C.; Areephong, J.; Vicario, J.; Meetsma, A.; Browne, W. R.; Feringa, B. L. *Angew. Chem. Int. Ed.* **2010**, *49*, 6580–6584.

[56] Still, W. C.; Kahn, M.; Mitra, A. *J. Org. Chem.* **1978**, *43*, 2923–2925.

Chapter 3

Control of Surface Wettability Using Tripodal Light-Activated Molecular Motors

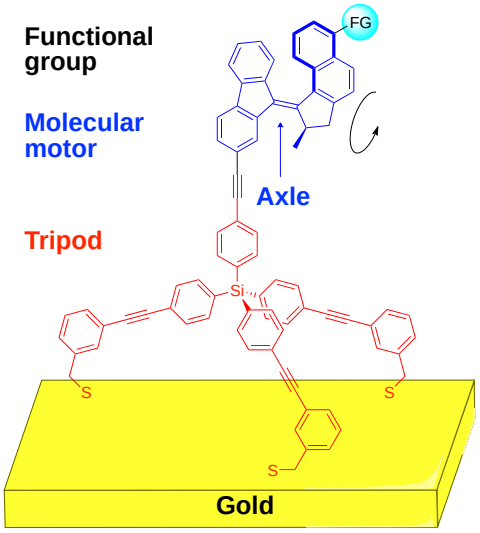

Fluorinated light-driven molecular motors were synthesized and immobilized on gold in an altitudinal orientation *via* tripodal stators. In this design the functionalized molecular motors are not interfering and preserve their rotary function on gold. The wettability of the self-assembled monolayers can be switched by UV irradiation.

This chapter has been published:
Chen, K.-Y.; Ivashenko, O.; Carroll, G. T.; Robertus, J.; Kistemaker, J. C. M.; London, G.; Browne, W. R.; Rudolf, P.; Feringa, B. L. *J. Am. Chem. Soc.* **2014**, *136*, 3219–3224.

3.1 Introduction

One of the major challenges in nanotechnology is to demonstrate that molecular machines can be harnessed to perform useful work.[1] Inspired by the machines of the macroscopic world, molecular tweezers, propellers, gears, brakes, elevators, valves, rotors, switches and nanocars have been developed.[2] Additionally, it has been shown that molecular switches and motors can be used to perform various tasks in solution, such as reversible change in supramolecular organization,[3] host-guest interactions,[4] controlling the chiral space in which a catalytic reaction takes place,[5] and synthesizing a peptide in a sequence-specific manner.[6]

Confining molecules at an interface inhibits Brownian motion and allows for the modification of the surface properties of a material or even the possibility to perform work at the molecular level through externally induced reversible structural changes.[7] In recent years, increasing attention has focused on surface-immobilized systems containing molecules that are capable of undergoing reversible structural changes upon the application of external stimuli.[8] Various types of external stimuli, i.e. chemical,[9] electric,[10] or light[8a], can be applied to address molecules on surfaces. Among these stimuli the use of light, which allows spatiotemporal control,[11] is of particular interest due to the potential fast response times of photochemical processes and because light provides a clean, noninvasive and tunable energy input.[12]

Surfaces functionalized with photoresponsive azobenzene or spiropyran derivatives have been studied widely due to the propensity for these interfaces to undergo reversible light-induced wettability changes.[13] Azobenzenes exhibit a change in conformation and dipole moment upon $E \rightarrow Z$ photoisomerization, resulting in changes to their polarity and accordingly the wettability of the surface.[14] Spiropyrans can also be switched photochemically between a relatively hydrophobic spirocyclic and a hydrophilic merocyanine form, which induces a large change in molecular dipole moment.[15] A number of approaches have been developed in order to enhance the wettability contrast between the two states of the azobenzene- and spiropyran-functionalized surfaces by using mixed layers,[16] increasing surface roughness,[13a] and using polymer-based surfaces.[17] However, controlling the water contact angle (WCA) on flat and smooth surfaces functionalized with photoresponsive organic monolayers remains challenging. The change of the WCA of azobenzene monolayers is typically of the order of 2–14°,[18] and 5–14°[19] for spiropyran monolayers. Such modest changes encourage efforts to

design and study new responsive surfaces *via* the assembly of photochromic organic monolayers on flat substrates.

Light-driven molecular motors based on overcrowded alkenes[20] are a unique class of organic molecules that are able to use light to power unidirectional rotation. When such molecules are attached to a surface, two types of orientation can be distinguished: azimuthal[21] and altitudinal[22] (Figure 3.1). Motors rotating in an altitudinal orientation relative to the surface have great potential for the construction of photoswitchable surfaces because the exposure of a functional group on the rotor can be switched in a cyclic fashion.[22d] Despite the promise of altitudinal motors in powering surface-mounted nanomachinery, the speed of rotation has been shown to be affected by intermolecular interactions.[22b] Although dilution (mixed monolayers) can minimize molecular interactions (but with the consequence of fewer molecular motors on the surface), the anticipated dynamic change in properties of these systems is reduced.

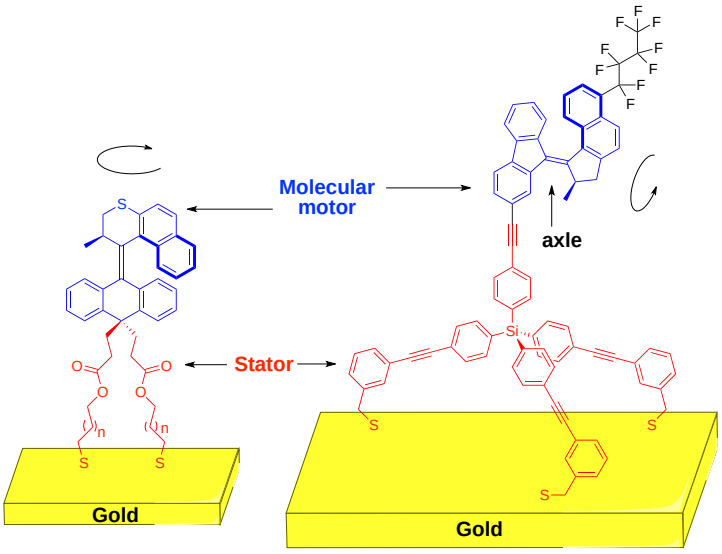

Figure 3.1 Azimuthal (left) and altitudinal (right) rotary motors on surfaces.

A key challenge in developing surface-bound devices based on molecular motors is to exploit the collective motion of the motor to interact with an external species in a dynamic manner. One way to demonstrate that the rotary motion of a surface-bound layer of oriented motors can collectively influence interactions with an overlayer material is to monitor the contact angle of a liquid on top of the motor monolayer. Changes in the contact angle of a liquid droplet at the surface of the

motor layer can be correlated to collective changes in the orientation of the rotor moieties with respect to the surface. Disruptive interactions between motors are expected to be minimized by designing motors with bulky stators that minimize the interaction between the rotor parts.

Light-driven, rotary, molecular-motor-based surfaces that undergo changes in wettability upon irradiation have not been reported to date. The wettability of a recently reported surface containing a monolayer of altitudinal motors was shown to depend on whether the motors were assembled in the *cis* or *trans* form.[22d] However, once the motors were assembled, the wettability could not be modified, which was attributed to a lower photoconversion when motors are confined to a crowded monolayer compared to when in solution.

In this chapter we report a novel altitudinal light-driven molecular motor design comprising of a rotor with a hydrophobic perfluorobutyl group and a tripodal stator containing thiol groups for self-assembly on gold is described (Figure 3.1, right). The bulky stator increases the spacing between the rotors of the surface-bound motors sufficiently to facilitate unobstructed rotary motion. Water droplets placed on the motor-modified surfaces undergo changes in the contact angle upon irradiation of the surfaces with UV light. This is the first example showing that the wetting properties of surfaces functionalized with molecular motors based on overcrowded alkenes can be switched with light.

3.2 Design of tripodal molecular motors

The motor **3.8** (Scheme 3.1) was selected, as it exhibits a substantial barrier toward thermal isomerization,[23] making this step slow at room temperature (rt) and thus facilitating characterization of the separate states during the rotary cycle in solution and on the surface. In addition, a hydrophobic perfluorobutyl group was incorporated onto the rotor part of the altitudinal motor in order to enhance the surface wettability changes upon switching.

A tripod[24] was chosen as the surface anchoring group for the following reasons: (1) The rigid tripod is a promising stator to anchor the motor in a fixed and altitudinal orientation with respect to the surface; (2) as we reported previously, when the motor-embedded chromophores are assembled too close to the gold substrate (Figure 3.1, left, n=1), energy transfer from the excited state of the motor to the gold substrate may occur,[21a] preventing the motor from rotating. Mounting the motor onto tripodal legs allows binding to gold in a rigid manner that is

expected to sufficiently isolate the motor from the surface, allowing efficient photoinduced isomerization (Figure 3.1, right); (3) it was previously shown that the attachment of overcrowded alkenes to surfaces *via* two-legs results in a high density of packing.[22b] The increase of the half-life of the thermal isomerization step indicates intermolecular interactions between the surface-bound overcrowded alkenes, resulting in a decrease in the overall speed of the rotary cycle.[22b, 25]

The bulky tripodal structure presented in this report is an ideal candidate to create free volume between the rotors, limiting interactions between the surface-bound motors and also enforcing altitudinal orientation. Calculations show that the area occupied by the tripod is expected to exceed the theoretical dimensions of the motor unit (Figure 3.2).

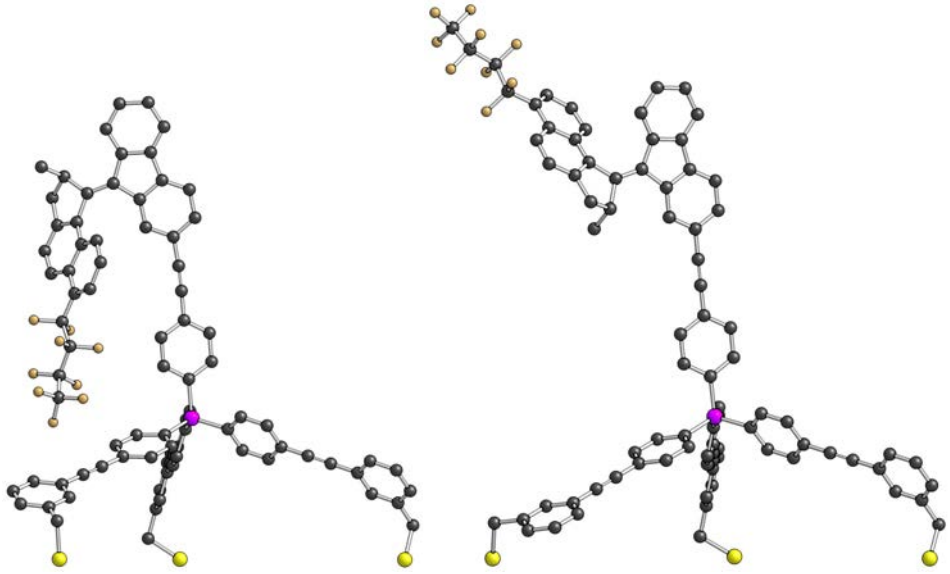

Figure 3.2 B3LYP/6-31G(d,p) optimized structure for stable-*cis* **3.1** (left) and stable-*trans* **3.1** (right). H-atoms are all omitted.[†]

[†] Jos C. M. Kistemaker is acknowledged for the computational chemistry.

3.3 Synthesis of tripodal molecular motors

The approach toward the synthesis of motor **3.1**, which bears a perfluorobutyl chain at the rotor and a tripod at the stator to allow surface attachment, is depicted in scheme 3.1.

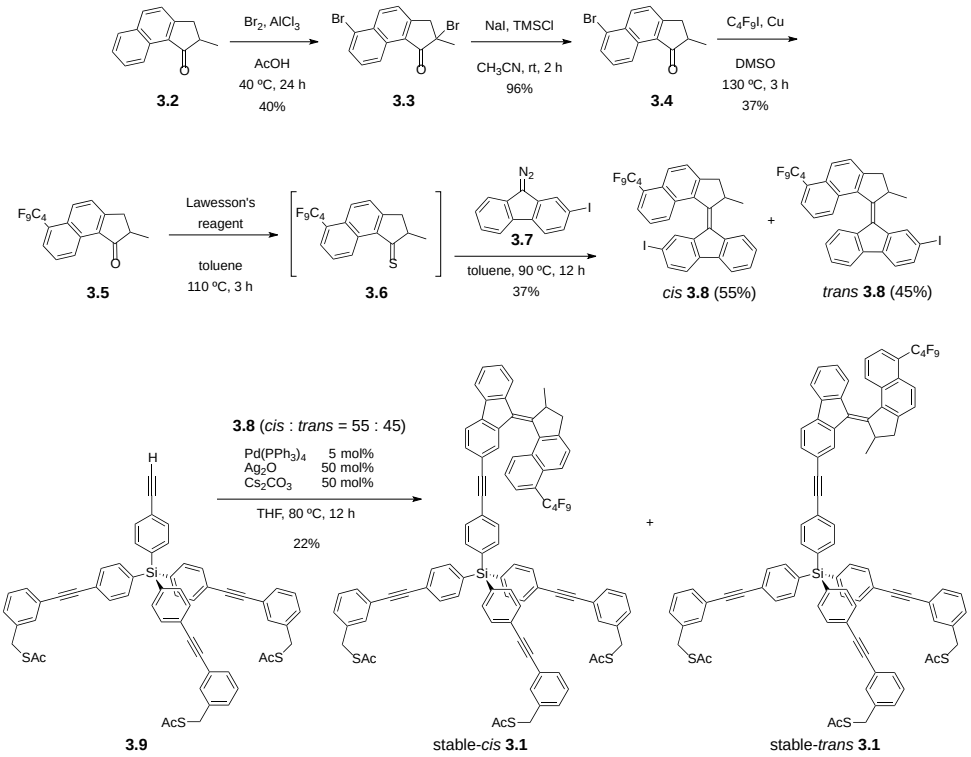

Scheme 3.1 Synthesis of molecular motor **3.1**.

Starting from **3.2**, which was synthesized by a one pot Friedel-Crafts acylation / Nazarov cyclization, ketone **3.2** was subsequently brominated by treating it with four equiv of bromine in the presence of $AlCl_3$ in AcOH to form dibromosubstituted **3.3**. The α-bromo substituent in **3.3** was removed by treatment with NaI and TMSCl in CH_3CN to form **3.4**. The perfluorobutyl chain was introduced by treating **3.4** with nonafluoro-1-iodobutane and copper/bronze in DMSO, affording **3.5**.

Ketone **3.5** was treated with Lawesson's reagent in toluene to give the reactive thioketone **3.6**. The key step in the synthesis of **3.8**, which has a highly

sterically hindered double bond, is the Barton-Kellogg diazo-thioketone coupling. [26] This coupling was performed by heating thioketone **3.6** and diazo compound **3.7** in toluene at reflux to afford overcrowded alkene **3.8** as a mixture of *cis* and *trans* isomers.

Motor **3.8** and tripod **3.9** were connected by a Sonogashira[27] coupling reaction in the presence of $Pd(PPh_3)_4$ providing **3.1** in 22% yield as a mixture of *cis* and *trans* isomers. Preparative thin layer chromatography provided pure stable-*cis* **3.1** and stable-*trans* **3.1**. Their configuration was assigned by comparison of their ^{1}H NMR spectra with those of previously reported structurally related motors.[28]

3.4 Photochemical and thermal isomerization studies

Photochemical and thermal isomerization studies were carried out in solution using both low-temperature UV/vis absorption and ^{1}H NMR spectroscopy to demonstrate that stable-*cis* **3.1** and stable-*trans* **3.1** operate as molecular motors. [20]

The UV/vis absorption spectra of stable-*cis* **3.1** and stable-*trans* **3.1** in CH_2Cl_2 at 253 K both show absorption bands centered at 395 nm (Figure 3.3, solid lines).

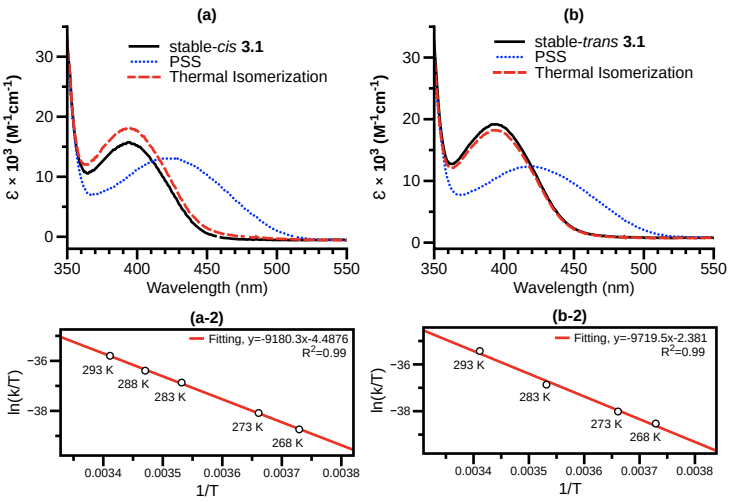

Figure 3.3 UV/vis absorption spectra (CH_2Cl_2, 253 K) of stable-*cis* **3.1** (a) and stable-*trans* **3.1** (b) (solid line). The spectra after UV irradiation (photoisomerization) (dotted line) and heating (thermal isomerization) (dashed line) are also shown; Eyring plot of the conversion of unstable-*trans* **3.1** to stable-*trans* **3.1** (a-2), and unstable-*cis* **3.1** to stable-*cis* **3.1** (b-2) *via* thermal isomerization at different temperatures.

Irradiation of the same sample with UV light (λ_{max} = 365 nm) resulted in a red-shift of the band at 395 nm to an absorption centered at 450 nm, indicating the photochemically induced formation of the unstable isomers (Figure 3.3, dotted lines; Scheme 3.2, steps 1 or 3). This red-shift is consistent with increased strain at the central double bond, and hence the generation of a higher energy isomer.[29] During the irradiation of each compound, isosbestic points were maintained indicating that the photoisomerization was a selective process.

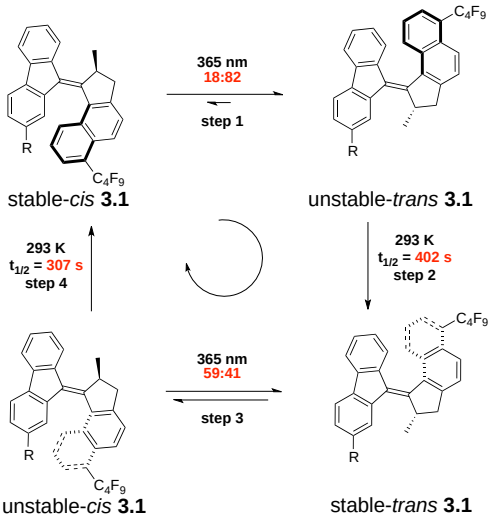

Scheme 3.2 Full 360º rotary cycle for molecular motor **3.1** (R= **3.9**, Scheme 3.1).

Samples were irradiated until no further changes were observed, indicating that the photostationary state (PSS) was reached (Figure 3.3, dotted lines). Allowing the solutions to warm to rt resulted in a blue-shift of the band at 450 to 395 nm, which is consistent with thermal isomerization to the corresponding stable isomers (Figure 3.3, dashed lines; Scheme 3.2, step 2 or 4).

The activation parameters of the thermal isomerization from unstable-*trans* **3.1** to stable-*trans* **3.1** (Scheme 3.2, step 2) were determined at five temperatures (268, 273, 283, 288 and 293 K) in CH_2Cl_2. The thermal isomerization was followed by monitoring the change in absorption at 450 nm. Using the Eyring equation (Figure 3.3a-2), it was determined that this isomerization has a Gibbs free energy of activation ($\Delta^{\ddagger}G^{o}$) of 87.3 kJ/mol (unstable-*trans* **3.1** → stable-*trans* **3.1**). This value corresponds to a half-life at rt of 402 s. Using the same procedure, the activation parameters of the thermal isomerization from unstable-*cis* **3.1** to

stable-*cis* **3.1** (Scheme 3.2, step 4) were determined at four temperatures (268, 273, 283 and 293 K) in CH_2Cl_2. The thermal isomerization was followed by monitoring the change in absorbance at 450 nm. Using the Eyring equation (Figure 3.3b-2), it was determined that this isomerization has a Gibbs free energy of activation ($\Delta^{\ddagger}G^{o}$) of 86.6 kJ/mol (unstable-*cis* **3.1** → stable-*cis* **3.1**). This value corresponds to a half-life at rt of 307 s. These half-lives are similar to those obtained for structurally related motors.[28]

The PSS ratio for stable-*cis* **3.1**/unstable-*trans* **3.1** and stable-*trans* **3.1**/unstable-*cis* **3.1** were determined by low temperature ^{1}H NMR spectroscopy (Figure 2.4). 2 mg of stable-*cis* **3.1** was dissolved in 1 mL CD_2Cl_2 in an NMR tube and the ^{1}H NMR spectra were recorded before, during and after UV irradiation (λ_{max} = 365) at 233 K. No further changes were observed after 6 h of irradiation. By comparing the integrals of the absorption of stable-*cis* **3.1** and unstable-*trans* **3.1** in the aliphatic and aromatic regions (Figure 3.4a and b; proton Ha, Hb, He, Hf and Hg; a photostationary ratio 18/82 for stable-*cis* **3.1**/unstable-*trans* **3.1** (Scheme 3.2, step 1) was determined. Using the same procedure, the PSS ratio for stable-*trans* **3.1**/unstable-*cis* **3.1** was determined to be 41/59 (Figure 3.4d and e; proton Ha, Hb, He, Hf and Hg; Scheme 3.2, step 3). After the samples containing the PSS mixtures were warmed to rt and kept at this temperature for 30 min, the samples were measured again at 233 K, the ^{1}H NMR spectra showed quantitative conversion of the unstable isomers to the corresponding stable isomers (Figure 3.4c, b → c and e → f; scheme 3.2, step 2 and 4).

By studying the photochemical and thermal behavior of **3.1** in solution using a combination of UV/vis absorption and ^{1}H NMR spectroscopy, and by analogy with similar motor systems reported previously,[28] it is concluded that **3.1** functions as a light-driven rotary motor in solution. In summary, the introduction of the tripod and a perfluorobutyl group on the motor moiety does not have a significant influence on the photochemical and thermal behavior of the motor.

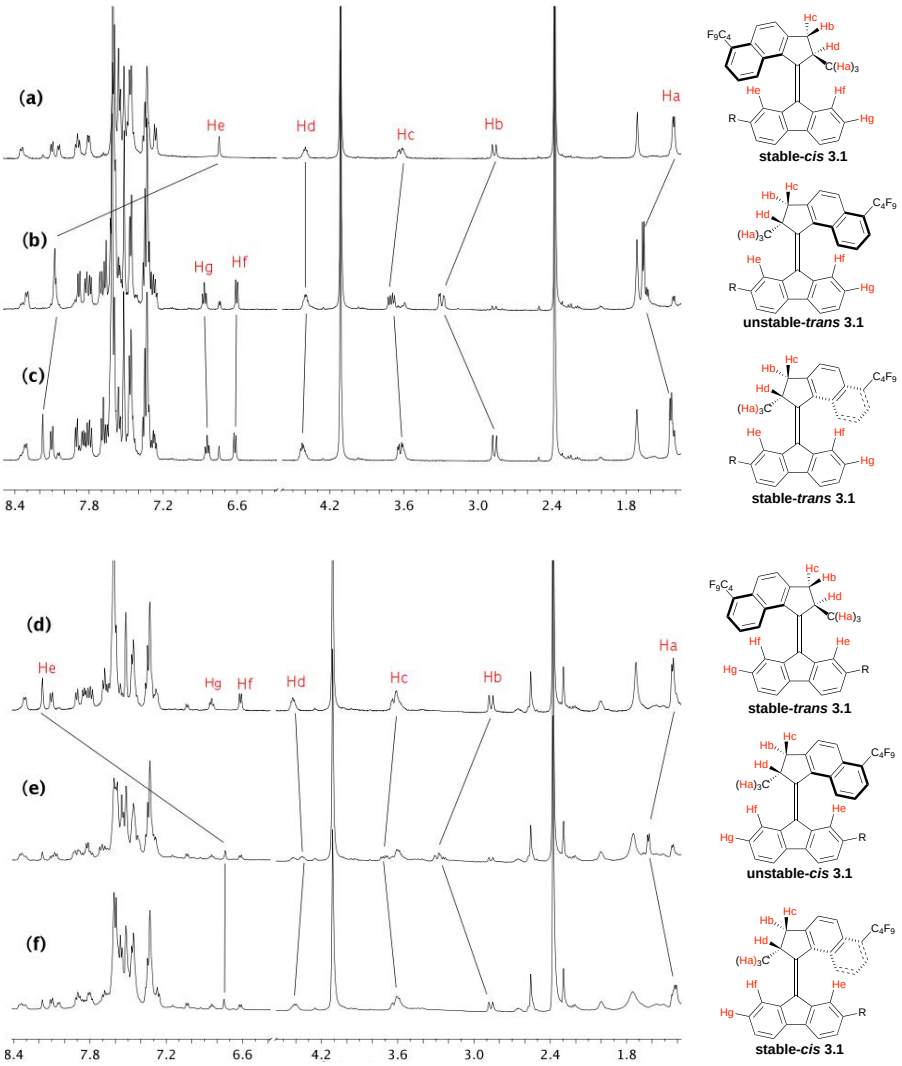

Figure 3.4 Partial ^{1}H NMR spectra (500 MHz, CD_2Cl_2, 233 K) of **3.1** (a) stable-*cis* **3.1** (b) unstable-*trans* **3.1** formed upon UV irradiation to PSS (c) stable-*trans* **3.1** obtained after thermal isomerization of unstable-*trans* **3.1** at rt; (d) stable-*trans* **3.1** (e) unstable-*cis* **3.1** formed upon UV irradiation to PSS (f) stable-*cis* **3.1** obtained after thermal isomerization of unstable-*cis* **3.1** at rt. Signal assignments are given (R = 3.9, scheme 3.1).

3.5 Surface attachment and characterization

Immobilization of motor **3.1** on surfaces was achieved by immersion of a gold substrate in a solution of stable-*cis* **3.1** or stable-*trans* **3.1** with hydrazine as a deprotecting reagent. (Scheme 3.3, for further details on surface preparations, see experimental section) The mean monolayer thickness values of 16.9 ± 0.3 Å for stable-*cis* **3.1 SAM** and 18.4 ± 0.1 Å for stable-*trans* **3.1 SAM** were determined by XPS[30] (see experimental section) and are in good agreement with similar overcrowded alkene systems assembled on a variety of surfaces previously reported by our group.[22a,25,31] The surface coverage on gold (2.2×10^{-11} mol cm^{-2} for stable-*cis* **3.1 SAM** and 2.4×10^{-11} mol cm^{-2} for stable-*trans* **3.1 SAM**, as determined by UV/vis absorption spectroscopy, Figure 3.3 and 3.5) are consistent with monolayer formation.

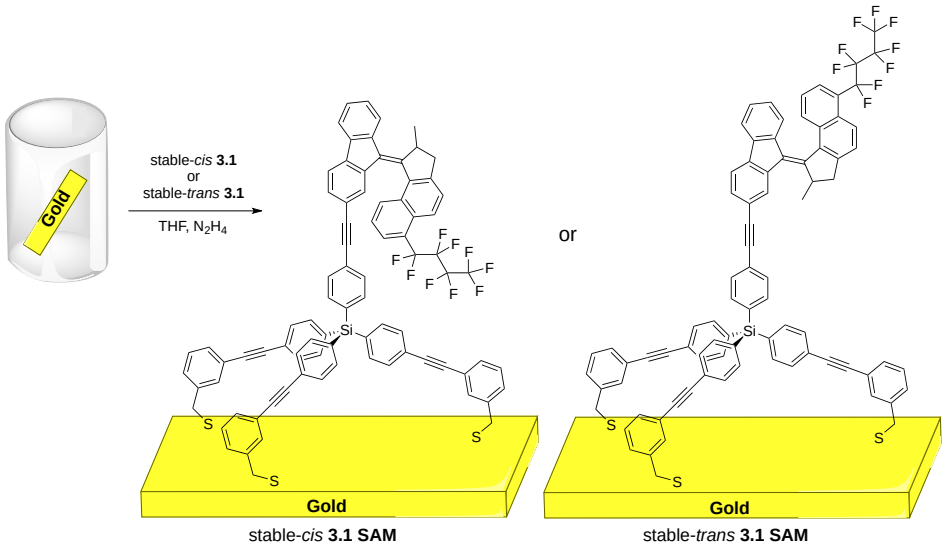

Scheme 3.3 Immobilization of molecular motor **3.1** onto a gold film.

The UV/vis absorption spectra of stable-*cis* and stable-*trans* **3.1 SAM**s showed the characteristic absorption of the motors after rinsing the substrates copiously with THF and CH_3OH, indicating that the attachment of motor **3.1** on the gold substrate was successful. (Figure 3.5, solid line). The major absorption bands (centered at 395 nm for stable **3.1 SAM**s) are similar to those observed for **3.1** in CH_2Cl_2 solution (Figure 3.3).

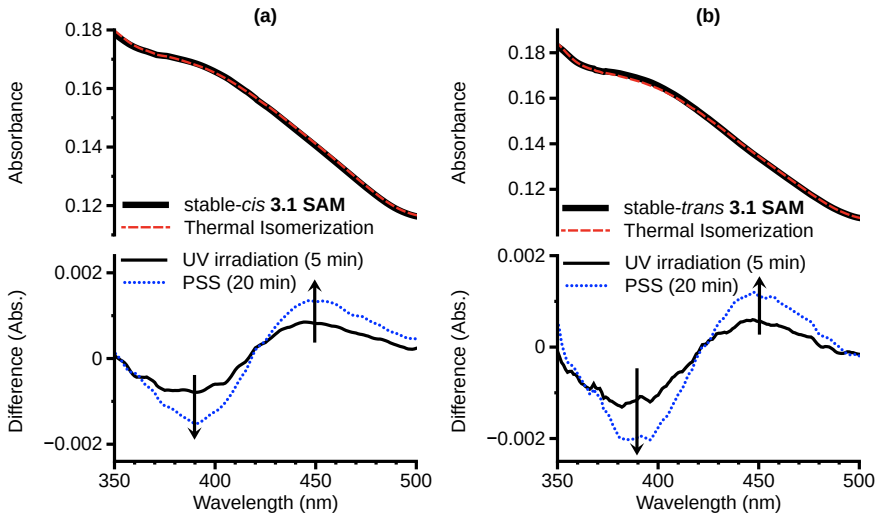

Figure 3.5 UV/vis absorption spectra of (a) stable-*cis* **3.1 SAM** and (b) stable-*trans* **3.1 SAM** (solid lines, upper panel). Both isomers undergo photoisomerization upon UV irradiation and the difference between the spectra of the initial state and irradiated samples are shown (solid and dotted lines at lower panel). The spectra after thermal isomerization are also shown (dashed lines).

Irradiation of stable **3.1 SAM**s with UV light (λ_{max} = 365 nm) resulted in a red-shift in the UV/vis absorption to 450 nm (Figure 3.5, lower panel) similar to that observed in CH_2Cl_2 solution (Figure 3.3), indicating the formation of the unstable form of the surface-bound motors (Scheme 3.2, steps 1 and 3). After keeping the surfaces in the dark at rt for 12 h, the original UV/vis absorption spectra recovered, which is consistent with the thermal isomerization of the motors (Figure 3.5, dashed line; Scheme 3.2, step 2 or 4).

In order to compare the surface-bound system with the solution analogue, we followed the thermal isomerization by monitoring the change in the UV/vis absorption spectra at 450 nm as a function of time. (Figure 3.6) The thermal decay of the signals were fitted with monoexponential decay, and the half-life for unstable-*trans* **3.1 SAM** → stable-*trans* **3.1 SAM** ($t_{1/2}$ = 530 s at rt) and unstable-*cis* **3.1 SAM** → stable-*cis* **3.1 SAM** ($t_{1/2}$ = 351 s at rt) were extracted. These values are similar to those observed in CH_2Cl_2 solution (Scheme 3.2, steps 2 and 4) showing that the thermal isomerization steps were not inhibited using the tripod as a surface attachment group and spacer between the motor and gold film. The bulky structure of the tripod increases the distance between motor chromophores in the surface-bound monolayer, minimizing inter-rotor interactions.

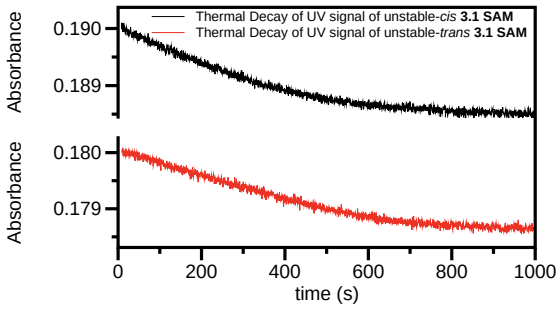

Figure 3.6 Thermal decay of UV/vis signals at 450 nm at rt during thermal isomerization of the motors as a function of time. (The black line is shown with an offset of +0.01)

The overview X-ray photoelectron (XPS) scans of the monolayers stable-*cis* **3.1 SAM** and stable-*trans* **3.1 SAM** before and after UV irradiation for 2 h are also shown in Figure 3.7. The spectra obtained after UV irradiation qualitatively resemble those collected on the pristine **3.1 SAM**s, indicating the stability of the motor and tripod moieties on the gold surface under exposure to UV light for a considerable amount of time.

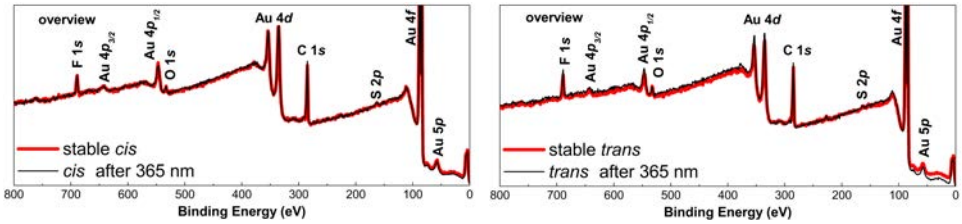

Figure 3.7 Overview XPS spectra of stable-*cis* **3.1 SAM** (left) and stable-*trans* **3.1 SAM** (right) before (red line) and after (black line) UV irradiation for 2 h, showing core level contributions of F 1*s*, O 1*s*, C 1*s*, S 2*p* and Au substrate 4*p*, 4*d*, 4*f* and 5*p* peaks. Au 4*f* doublet was truncated to facilitate observation of weaker lines.[‡]

‡ Dr. Oleksii Ivashenko is acknowledged for the characterization of **3.1 SAM**s by XPS.

Water contact angle (WCA) measurements were performed on motor **3.1 SAM** on flat gold (150 nm Au/mica) in order to determine the wettability of the monolayers. In the case of stable-*cis* **3.1 SAM**, where the hydrophobic perfluorobutyl group is likely to be hidden from the interface, a contact angle of 60 ± 1º was measured; however, stable-*trans* **3.1 SAM**, where the perfluorobutyl groups are exposed to the interface, shows a contact angle of 82 ± 1º (Figure 3.8), which is attributed to the hydrophobic nature of the perfluorobutyl chain.

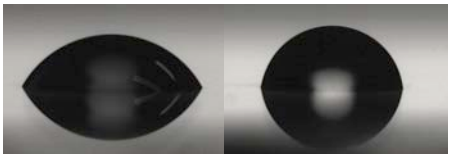

Figure 3.8 Water droplet on stable-*cis* **3.1 SAM** (left) and stable-*trans* **3.1 SAM** (right).

In the present system using an altitudinal molecular motor, control of surface wettability was achieved by irradiating both **3.1 SAM**s with UV light (λ_{max} = 365 nm), which resulted in WCA changes of the stable-*cis* **3.1 SAM** from 60 ± 1º to 76 ± 1º and for the stable-*trans* **3.1 SAM**, 82 ± 1º to 68 ± 1º. (Table 3.1). The changes in WCA after UV irradiation are a manifestation of the photoinduced switching of the motors on gold and are consistent with UV/vis spectroscopic data (Figure 3.6).

Table 3.1 Water contact angle for stable-*cis* 3.1 SAM and stable-*trans* 3.1 SAM before and after UV irradiation on flat surface.

	Contact Angle (º)	
	before irradiation	after irradiation
Stable-*cis* **3.1 SAM**	60 ± 1	76 ± 1
Stable-*trans* **3.1 SAM**	82 ± 1	68 ± 1

The ratios between stable-*cis* **3.1** and unstable-*trans* **3.1** or stable-*trans* **3.1** and unstable-*cis* **3.1** are 18:82 or 41:59 in solution, respectively, at the photostationary state ($PSS_{365\ nm}$, Scheme 3.2, steps 1 or 3). The separation between the molecular motors and the surface as well as each other achieved with the present immobilization approach means that it would be reasonable to expect that the PSS achieved in solution is retained in the **SAM**s also. Indeed, on the first cycle the changes observed are consistent with the PSS observed in solution. Hence, upon irradiation of the molecular motors anchored on the surface, the

changes in wettability are not expected to show full reversibility over several cycles but instead reach an intermediate situation between purely *cis*- and *trans*-states, as is observed experimentally (Figure 3.9). These data demonstrate that the design employed in anchoring the molecular motor to the surface allows light to be used to change molecular state and thereby achieve the highly challenging task of changing wettability with an external stimulus.

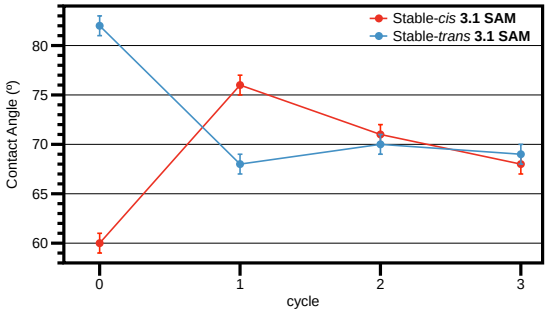

Figure 3.9 Water contact angle of stable-*cis* **3.1 SAM** and stable-*trans* **3.1 SAM** as a function of UV irradiation cycle.

Modifying the wettability of a substrate with a monolayer of rotary motors upon irradiation is unprecedented. Previously, surfaces functionalized with *cis* or *trans* isomers of altitudinal motors with the same perfluorobutyl chain on the rotor as reported here showed only a difference of 12 º in WCA between the *cis* and *trans* surfaces, and the surface wettability could not be modified by UV irradiation.[22d] Presumably, without the bulky tripod spacer the motor chromophores are too crowded to allow for a sufficient yield of photoisomerization to detect an appreciable change in macroscopic properties.[22d]

Incorporating three phenyl-acetylene-based “legs” into the structure of the motor increases the space between the rotors, allowing for facile rotary motion and hence modification of the surface properties.

3.6 Conclusions

Motors bearing a hydrophobic perfluorobutyl group on the rotor and rigid phenyl-acetylene-based tripod on the stator were successfully synthesized and attached to a gold surface.

The spacing between the motor and the gold surface is sufficient to effectively compete with quenching of the excited state by the gold surface and to allow for photoisomerization of the central alkene. Confinement of altitudinal motors at surfaces *via* flexible long chains was reported to reduce the rate of the thermal isomerization process,[22b] however, the system described herein has overcome this issue. In the present system the thermal isomerization is not inhibited, showing that the tripod is an ideal surface anchoring group to prevent the motors from interacting with each other and from interacting directly with the underlying gold substrate.

Additionally, although previously reported nonsymmetric altitudinal motors bearing fluoro groups were unable to change the water contact angle by irradiation post-assembly, the current system can change the contact angle of a water drop by up to 16º upon irradiation of the motor-water interface. This is the first example of controlling the surface wettability of a monolayer of motors by irradiation. The tripod structure minimizes obstruction of the rotary cycle and enhances the ability to modulate collective interactions at the motor–water interface. The current design features will be key to fabricating future nanoscale systems that can be used to exploit the rotary cycle to perform work at the molecular level, to control interactions with surface adsorbates and to apply single molecule techniques to measure the rotation of a single motor on a surface.

3.7 Experimental Section

3.7.1 General remarks

For general remarks on the synthesis and characterization of compunds and intermediates, see Chapter 2. All UV/Vis absorption spectra in solution were recorded by Hewlet-Packard HP 8543 diode array. To generate the unstable form of the motor, samples were irradiated with UV light (Spectroline model ENB-280C/FE lamp, λ_{max} = 365 nm) at a distance of 3 cm from the centre of the lamp.

3.7.2 Synthesis of compounds and intermediates

Compound 3.3

To a solution of **3.2** (7.2 g, 36.7 mmol) in acetic acid (100 mL) $AlCl_3$ was added (0.5 g, 3.6 mmol), the solution was stirred vigorously at 40 ºC for 1 h until most of the $AlCl_3$ was dissolved. Then Br_2 (23.5 g, 146.9 mmol) was added dropwise to the mixture and stirred at 40 ºC for 1 d. The mixture was cooled to rt, diluted with EtOAc (200 mL) washed with aqueous $Na_2S_2O_{3(sat.)}$ (2×50 mL), water (100 mL), brine (50 mL) and then dried (Na_2SO_4) before being concentrated *in vacuo*. Recrystallization from dichloromethane and pentane afforded **3.3** as a light orange solid. (5.2 g, 14.7 mmol, 40%). M.p. 70 – 72 ºC; ^{1}H NMR (400 MHz, $CDCl_3$) δ 2.02 (s, 1H), 3.62 (d, *J* = 18.6 Hz, 1H), 3.92 (d, *J* = 18.6 Hz, 1H), 7.52-7.59 (m, 2H), 7.88 (d, *J* = 7.5 Hz, 1H), 8.58 (d, *J* = 8.7 Hz, 1H), 9.14 (d, *J* = 8.4 Hz, 1H); ^{13}C NMR (100 MHz, $CDCl_3$) δ 27.4, 46.6, 59.9, 123.5, 124.0, 124.9, 127.2, 130.1, 131.5, 131.6, 131.9, 136.4, 153.0, 200.6; HRMS (EI-ion trap) *m/z*: $[M]^+$ Calcd for $C_{14}H_{10}Br_2O$ 351.9098, found 351.9110.

Compound 3.4

A solution of **3.3** (4.08 g, 11.5 mmol) in acetonitrile (130 mL) was added to a stirred solution of sodium iodide (5.1 g, 34.3 mmol) in acetonitrile (30 mL). The mixture was stirred at rt for 30 min, chlorotrimethylsilane (3.1 g, 28.9 mmol) was added and the mixture was further stirred for 2 h at rt. The mixture was diluted with EtOAc (200 mL) washed with aqueous $Na_2S_2O_{3(sat.)}$ (2×50 mL), water (100 mL), brine (50 mL), dried (Na_2SO_4) and then concentrated *in vacuo* affording **3.4** as a white solid (3.2 g, 11.5 mmol, 96%). M.p. 72 – 74 ºC; ^{1}H NMR (300 MHz, $CDCl_3$) δ 1.38 (d, *J* = 7.3 Hz, 3H), 2.73-2.92 (m, 2H), 3.50 (dd, *J* = 18.3, 8.2 Hz, 1H), 7.46-7.53 (m, 1H), 7.60 (d, *J* = 8.7 Hz, 1H), 7.84 (dd, *J* = 7.5, 0.8 Hz, 1H),

8.49 (d, J = 8.7 Hz, 1H), 9.19 (d, J = 8.4 Hz, 1H); ^{13}C NMR (100 MHz, $CDCl_3$) δ 16.7, 35.1, 42.7, 123.0, 123.7, 125.3, 129.3, 130.3, 130.7, 131.0, 131.2, 134.6, 157.1, 209.5; HRMS (EI-ion trap) *m/z*: $[M]^+$ Calcd for $C_{14}H_{11}BrO$ 273.9993, found 273.9982.

Compound 3.5

A suspension of activated copper-bronze (2.8 g, 44.1 mmol) in dry DMSO (80 mL) was heated to 130 ºC for 15 min. Nonafluoro-1-iodobutane (7.6 g, 21.9 mmol) was added dropwise and the mixture was stirred at 130 ºC for 45 min. Ketone **3.4** (1.2 g, 4.7 mmol) in DMSO (80 mL) was added dropwise and the mixture was stirred for an additional 3 h at the same temperature. The mixture was diluted with diethyl ether (100 mL) and filtered over celite to remove copper-bronze. The organic phase was washed with water (2×100 mL), brine, dried (Na_2SO_4) and concentrated *in vacuo*. The crude product was purified by column chromatography (SiO_2, 7:3 pentane:CH_2Cl_2) to give **3.5** (670 mg, 1.6 mmol, 37%) as a dark oil. ^{1}H NMR (500 MHz, $CDCl_3$) δ 1.39 (d, J = 7.3 Hz, 3H), 2.89-2.79 (m, 2H), 3.50 (dd, J = 18.2, 8.1 Hz, 1H), 7.64 (d, J = 9.0 Hz, 1H), 7.75 (t, J = 7.9 Hz, 1H), 7.88 (d, J = 7.4 Hz, 1H), 8.43 (d, J = 8.9 Hz, 1H), 9.54 (d, J = 8.4 Hz, 1H); ^{13}C NMR (75 MHz, $CDCl_3$) δ 209.6, 156.5, 131.9, 131.9, 131.8, 131.8, 130.7, 130.4, 129.4, 128.9, 128.4, 128.2, 128.1, 127.3, 125.8, 42.5, 34.9, 16.5; HRMS (ESI-ion trap) *m/z*: $[M]^+$ Calcd for $C_{18}H_{11}F_9O$ 415.0739, found 415.0733.

Compound 3.8

To a solution of **3.5** (287 mg, 0.7 mmol) in toluene (10 mL) was added Lawesson's reagent (476.3 mg, 1.2 mmol). The mixture was heated at 90 ºC for 3 h. The toluene was distilled off *in vacuo* and the residue was purified by column chromatography (pentane:CH_2Cl_2, 1:1). The first wine-red band was collected (92 mg, 0.2 mmol), concentrated and added immediately to a solution of **3.7** (123.6 mg, 0.4 mmol) in toluene (30 mL). The mixture was heated at 90 ºC for 12 h then cooled down to rt and concentrated *in vacuo*. The crude product was purified by flash column chromatography (SiO_2, 1:4 pentane:CH_2Cl_2) affording **3.8** (52 mg, 0.076 mmol, 37%, mixture of *cis* and *trans* isomers) as yellow sticky oil. The *trans* and *cis* isomers can be separated by column chromatography (SiO_2, 10:1 pentane:ether). Stable-*trans* **3.8**: ^{1}H NMR (400 MHz, CD_2Cl_2) δ 1.40 (d, J = 6.7 Hz, 3H), 2.84 (d, J = 15.4 Hz, 1H), 3.62 (dd, J = 15.3, 5.4 Hz, 1H), 4.36-4.27 (m, 1H), 6.58 (d, J = 7.9 Hz, 1H), 6.82 (t, J = 7.5 Hz, 1H), 7.24 (t, J = 7.4 Hz, 1H),

7.40 (t, *J* = 7.9 Hz, 1H), 7.63 (d, *J* = 7.9 Hz, 1H), 7.76 (d, *J* = 8.2 Hz, 3H), 7.85 (d, *J* = 7.2 Hz, 1H), 8.07 (d, *J* = 8.4 Hz, 1H), 8.42-8.28 (m, 2H); ^{13}C NMR (100 MHz, CD_2Cl_2) δ 19.4, 42.4, 46.1, 92.6, 119.8, 121.9, 125.6, 125.8, 126.4, 127.1, 127.9, 128.0, 128.0, 128.1, 128.2, 129.8, 130.6, 131.1, 132.8, 133.8, 135.29, 136.1, 136.4, 137.1, 137.5, 139.4, 139.9, 142.2, 148.7, 152.6; ^{19}F NMR (376 MHz, CD_2Cl_2) -81.33, -103.90, -121.09, -125.72. Stable-*cis* **3.8**: ^{1}H NMR (400 MHz, CD_2Cl_2) δ 1.36 (d, *J* = 6.2 Hz, 3H), 2.80 (d, *J* = 15.5 Hz, 1H), 3.56 (dd, *J* = 15.5, 5.7 Hz, 1H), 4.39-4.25 (m, 1H), 6.78 (s, 1H), 7.53-7.34 (m, 5H), 7.71 (d, *J* = 8.8 Hz, 1H), 7.81-7.77 (m, 1H), 7.85 (d, *J* = 7.4 Hz, 1H), 7.96 (d, *J* = 8.1 Hz, 2H), 8.31 (d, *J* = 8.9 Hz, 1H); ^{13}C NMR (100 MHz, CD_2Cl_2) δ 19.4, 42.3, 45.8, 91.3, 120.4, 121.2, 124.8, 125.5, 125.6, 125.7, 125.7, 126.3, 127.9, 128.0, 128.1, 128.2, 128.3, 129.7, 130.3, 131.0, 132.7, 133.8, 135.3, 136.1, 137.3, 139.2, 139.6, 139.7, 148.6, 152.7; ^{19}F NMR (376 MHz, CD_2Cl_2) δ -81.23, -104.10, -121.11, -125.65. Stable-**3.8**: HRMS (ESI-ion trap) *m/z*: $[M + H]^+$ Calcd for $C_{31}H_{19}F_9I$ 689.0382, found 689.0382.

Compound 3.1

A mixture of stable-*cis* **3.8** and stable-*trans* **3.8** (53.7 mg, 58.1 mmol), **3.9** (40 mg, 58.1 mmol), Ag_2O (8.1 mg, 34.8 mmol), Cs_2CO_3 (11.4 mg, 34.8 mmol) and $Pd(PPh_3)_4$ (3.4 mg, 2.9 mmol) was stirred in dry THF (6 mL) at 90 ºC for 12 h. After the mixture was cooled to rt, it was diluted with diethyl ether (6 mL) and filtered over a plug of celite. After removal of all volatiles *in vacuo*, the product was purified by column chromatography (SiO_2, 1:5 pentane:CH_2Cl_2), yielding a yellow oil (19 mg, 12.8 mmol, 22%, mixture of *cis* and *trans* isomers). The *cis and trans* isomers were separated by preparative thin layer chromatography (Silica gel, 1:1 hexane:*tert*-butyl methyl ether). Stable-*trans* **3.1**: ^{1}H NMR (500 MHz, CD_2Cl_2) δ 1.49 (d, *J* = 6.7 Hz, 2H), 2.40 (s, 9H), 2.89 (d, *J* = 15.2 Hz, 1H), 3.68 (dd, *J* = 15.2, 5.4 Hz, 1H), 4.15 (s, 6H), 4.49-4.43 (m, 1H), 6.64 (d, *J* = 7.9 Hz, 1H), 6.85 (t, *J* = 7.7 Hz, 1H), δ 7.89 (dd, *J* = 13.8, 7.6 Hz, 2H), 7.81 (dd, *J* = 15.6, 8.3 Hz, 15H), 7.72-7.65 (m, 5H), 7.65-7.57 (m, 6H), 7.55-7.50 (m, 4H), 7.50-7.41 (m, 6H), 7.38-7.27 (m, 10H), 8.14 (d, *J* = 8.4 Hz, 1H), 8.22 (s, 1H), 8.37 (d, *J* = 8.6 Hz, 1H); ^{19}F NMR (376 MHz, CD_2Cl_2) δ -81.15, -103.83, -120.92, -125.76; UV/vis (CH_2Cl_2, 253 K): λ_{max} (ε) = 395 nm (19166 $M^{-1}cm^{-1}$). Stable-*cis* **3.1**: ^{1}H NMR (500 MHz, CD_2Cl_2) δ 1.46 (d, *J* = 6.7 Hz, 3H), 2.40 (s, 10H), 2.89 (d, *J* = 15.4 Hz, 1H), 3.67 (dd, *J* = 15.6, 5.7 Hz, 1H), 4.16 (s, 8H), 4.47-4.41 (m, 1H), 6.77 (s, 1H), 7.39-7.28 (m, 10H), 7.56-7.41 (m, 14H), 7.69-7.56 (m, 17H), 7.81 (d, *J* = 8.2 Hz, 2H),

7.91 (d, *J* = 7.1 Hz, 2H), 8.07 (d, *J* = 7.3 Hz, 1H), 8.14 (d, *J* = 8.4 Hz, 1H), 8.39 (d, *J* = 8.8 Hz, 1H); ^{19}F NMR (376 MHz, CD_2Cl_2) δ -81.15, -103.83, -120.92, -125.76; UV/vis (CH_2Cl_2, 253 K): λ_{max} (ε) = 395 nm (15724 $M^{-1}cm^{-1}$). Stable-**3.1**: ^{13}C NMR (101 MHz, $CDCl_3$) δ 19.1, 19.3, 22.7, 29.7, 30.3, 33.1, 41.8, 41.9, 45.2, 45.5, 88.8, 89.1, 89.4, 89.4, 90.3, 90.4, 91.3, 92.1, 119.1, 119.5, 119.7, 120.1, 120.3, 120.4, 121.2, 121.4, 123.4, 123.5, 124.2, 124.7, 124.8, 125.0, 125.1, 125.4, 125.6, 127.4, 127.6, 128.4, 128.7, 128.9, 129.0, 129.2, 130.3, 130.5, 130.6, 130.7, 130.8, 131.0, 131.1, 131.7, 132.0, 132.2, 133.0, 133.4, 133.6, 133.7, 135.1, 135.9, 136.1, 136.2, 136.6, 136.9, 137.1, 137.3, 138.0, 138.0, 139.1, 139.5, 139.7, 139.9, 140.2, 147.6, 147.7, 151.4, 151.4, 194.9; HRMS (APCI-ion trap) *m/z*: $[M + Na]^+$ Calcd for $C_{90}H_{61}F_9O_3S_3SiNa$ 1507.3300, found 1508.3337.

3.7.3 Preparation of the 3.1 SAMs

Method A: Quartz microscope slides (Ted Pella, Inc.) were cut into 1×2.5 cm^2 pieces, cleaned by immersing in a piranha solution at 90 ºC for 1 h and rinsed copiously first with doubly distilled water (3 times), then with CH_3OH and dried under a stream of N_2 before surface modification. (*Caution! Piranha solution is highly corrosive and reactive toward organics*)

Before gold deposition the piranha-cleaned quartz slides were silanized rather than using chromium as the adhesive coating in order to increase the optical transparency of the substrate. For this, the slides were immersed in 1 mM solution of 3-aminopropyl(diethoxy)methylsilane in freshly distilled toluene for 12 h, then copiously rinsed with toluene and methanol, sonicated first in toluene, then in methanol and dried under a stream of N_2.

Au films were prepared by vapour deposition of a 5 nm thick layer of gold (purity 99.99%, *Schöne Edelmetaal* B.V.) on the 3-aminopropyl(diethoxy)methylsilyl functionalized slides in a custom-built high-vacuum evaporator (base pressure 10^{-7} mbar). The UV/Vis absorption spectrum of this semi-transparent gold film is shown (Figure 3.11). 20 mL solution of THF containing stable-*cis* **3.1** or stable-*trans* **3.1** (5 mM) was purged with argon for 1 h and then hydrazine monohydrate (20 µL) was added. The gold film was immersed in this solution at rt for 16 h. The slides were removed, washed with THF, CH_3OH and dried under a stream of argon. The **SAM**s prepared this way were used for UV/Vis absorption spectroscopic studies.

Method B: Au films on mica were prepared by vapour deposition of 150 nm thick films of Au in a custom-built high-vacuum evaporator (base pressure 10^{-7} mbar). Prior to vapour deposition, mica sheets were freshly cleaved and annealed at 375 °C for 16 h in order to remove impurities. 20 mL solution of THF containing stable-*cis* **3.1** or stable-*trans* **3.1** (5 mM) was purged with argon for 1 h and then hydrazine monohydrate (20 µL) was added. The clean substrate was immersed immediately after gold deposition in this solution at rt for 16 h. Subsequently, the slides were removed, washed with THF, CH_3OH, and dried under a stream of argon. The **SAM**s prepared this way were used for XPS studies and contact angle measurements.

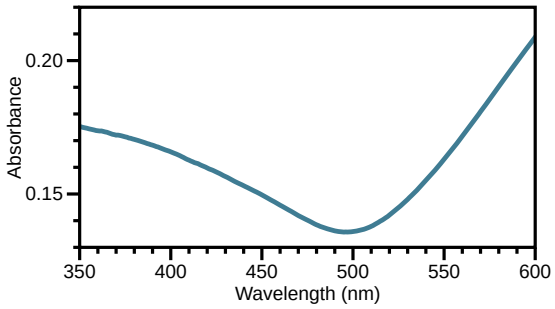

Figure 3.10 UV/Vis absorption spectrum of the semi-transparent gold film on glass which displays a plasmon band around 600 nm in accordance with a gold film of this thickness prepared on silanated quartz.

3.7.4 Characterization of the 3.1 SAMs

UV/Vis absorption spectroscopy of the 3.1 SAMs on a gold surface

UV/Vis absorption spectra were recorded using a Jasco V-630 spectrophotometer under N_2 atmosphere. (Scan rate 100 nm/min; Band Width 1.0 nm, N_2 atmosphere was used for baseline correction). The samples were irradiated with UV light (spectroline model ENB-280C/FE lamp, λ_{max} = 365 nm) at a distance of 3 cm.

Determining the thickness of the 3.1 SAMs from XPS results

The thickness of the self-assembled monolayers were calculated from the attenuation of the Au 4*f* XPS signal of the substrate. A clean substrate shows integrated intensity I_{Au0}. Due to grafting of the tripod molecules which form a film of thickness *d*, the integrated intensity I_{Au} of substrate decreases according to Equation **3.1**, where θ is the angle of the detector with respect to the normal to the surface (37º) and λ is the attenuation length of photoelectrons in hydrocarbon **SAM**s (42 Å).

$$I_{Au} = I_{AuO}\exp(-d/\lambda \sin\theta) \qquad (\mathbf{Eq.\,3.\,1})$$

We found film thicknesses of 16.9 ± 0.3 Å for the stable-*cis* **3.1 SAM** and of 18.4 ± 0.1 Å for stable-*trans* **3.1 SAM**, respectively. These thicknesses agree with single layers of tripod molecules present on the surface.

Contact angles measurements

Water contact angles were measured under ambient conditions on a SCA20 Dataphysics instrument with software version 3.60.2. Equilibrium contact angles were obtained by applying 1 µL water droplets on stable-*cis* **3.1 SAM** or stable-*trans* **3.1 SAM** using the sessile drop method. The contact angle was measured at two different locations on each surface and the results were averaged. For the irradiation experiment, a molecular motor **3.1** functionalized slides were transferred into a vial capped with a septum purged with argon and irradiated with UV light (Spectroline model ENB-280C/FE lamp, λ_{max} = 365 nm) at a distance of 3 cm for 20 min. After measuring the WCA of the irradiated surface, the slide was incubated in the dark for 12 h. The slide was then irradiated again prior to taking the CA, which was measured in the same manner as described above. The procedure was repeated once more.

3.8 References

[1] (a) Saha, S.; Stoddart, J. F. *Chem. Soc. Rev.* **2006**, *36*, 77–92. (b) Browne, W. R.; Feringa, B. L. *Nat. Nanotechnol.* **2006**, *1*, 25–35. (c) Kay, E. R.; Leigh, D. A.; Zerbetto, F. *Angew. Chem. Int. Ed.* **2007**, *46*, 72–191. (d) *Molecular Devices and Machines: Concepts and Perspectives for the Nanoworld*; Balzani, V., Credi, A., Venturi, M., Eds.; Wiley-VCH: Weinheim, **2008**. (e) *From Non-Covalent Assemblies to Molecular Machines*; Sauvage, J.-P., Gaspard, P., Eds.; Wiley-VCH: Weinheim, **2010**. (f) Coskun, A.; Banaszak, M.; Astumian, R. D.; Stoddart, J. F.; Grzybowski, B. A. *Chem. Soc. Rev.* **2012**, *41*, 19–30.

[2] (a) Kinbara, K.; Aida, T. *Chem. Rev.* **2005**, *105*, 1377–1400. (b) Kottas, G. S.; Clarke, L. I.; Horinek, D.; Michl, J. *Chem. Rev.* **2005**, *105*, 1281–1376. (c) Michl, J.; Sykes, E. C. H. *ACS Nano* **2009**, *3*, 1042–1048. (d) Kudernac, T.; Ruangsupapichat, N.; Parschau, M.; Maciá, B.; Katsonis, N.; Harutyunyan, S. R.; Ernst, K.-H.; Feringa, B. L. *Nature* **2011**, *479*, 208–211. (e) *Molecular Switches, 2nd Ed*; Browne, W. R., Feringa, B. L., Eds; Wiley-VCH: Weinheim, **2011**. (f) Szymański, W.; Beierle, J. M.; Kistemaker, H. A. V.; Velema, W. A.; Feringa, B. L. *Chem. Rev.* **2013**, *113*, 6114–6178.

[3] de Jong, J. J.; Lucas, L. N.; Kellogg, R. M.; Van Esch, J. H.; Feringa, B. L. *Science* **2004**, *304*, 278–281.

[4] Thomas, C. R.; Ferris, D. P.; Lee, J.-H.; Choi, E.; Cho, M. H.; Kim, E. S.; Stoddart, J. F.; Shin, J.-S.; Cheon, J.; Zink, J. I. *J. Am. Chem. Soc.* **2010**, *132*, 10623–10625.

[5] Wang, J.; Feringa, B. L. *Science* **2011**, *331*, 1429–1432.

[6] Lewandowski, B.; De Bo, G.; Ward, J. W.; Papmeyer, M.; Kuschel, S.; Aldegunde, M. J.; Gramlich, P. M. E.; Heckmann, D.; Goldup, S. M.; D'Souza, D. M.; Fernandes, A. E.; Leigh, D. A. *Science* **2013**, *339*, 189–193.

[7] (a) Hugel, T.; Holland, N. B.; Cattani, A.; Moroder, L.; Seitz, M.; Gaub, H. E. *Science* **2002**, *296*, 1103–1106. (b) Liu, Y.; Flood, A. H.; Bonvallet, P. A.; Vignon, S. A.; Northrop, B. H.; Tseng, H.-R.; Jeppesen, J. O.; Huang, T. J.; Brough, B.; Baller, M.; Magonov, S.; Solares, S. D.; Goddard, W. A.; Ho, C.-M.; Stoddart, J. F. *J. Am. Chem. Soc.* **2005**, *127*, 9745–9759. (c) Ferri, V.; Elbing, M.; Pace, G.; Dickey, M. D.; Zharnikov, M.; Samorì, P.; Mayor, M.;

Rampi, M. A. *Angew. Chem. Int. Ed.* **2008**, *47*, 3407–3409. (d) Robertus, J.; Browne, W. R.; Feringa, B. L. *Chem. Soc. Rev.* **2010**, *39*, 354–378. (e) Nakanishi, H.; Bishop, K. J. M.; Kowalczyk, B.; Nitzan, A.; Weiss, E. A.; Tretiakov, K. V.; Apodaca, M. M.; Klajn, R.; Stoddart, J. F.; Grzybowski, B. A. *Nature* **2009**, 460, 371–375.

[8] (a) Katsonis, N.; Lubomska, M.; Pollard, M. M.; Feringa, B. L.; Rudolf, P. *Prog. Surf. Sci.*, **2007**, 82, 407–434. (b) Browne, W. R.; Feringa, B. L. *Annu. Rev. Phys. Chem.* **2009**, *60*, 407–428.

[9] Ye, T.; Kumar, A. S.; Saha, S.; Takami, T.; Huang, T. J.; Stoddart, J. F.; Weiss, P. S. *ACS Nano* **2010**, *4*, 3697–3701.

[10] Alemani, M.; Peters, M. V.; Hecht, S.; Rieder, K.-H.; Moresco, F.; Grill, L. *J. Am. Chem. Soc.* **2006**, *128*, 14446–14447.

[11] Velema, W. A.; van der Berg, J. P.; Hansen, M. J.; Szymański, W.; Driessen, A. J. M.; Feringa, B. L. *Nat. Chem.* **2013**, *5*, 924–928.

[12] Zheng, Y. B.; Pathem, B. K.; Hohman, J. N.; Thomas, J. C.; Kim, M.; Weiss, P. S. *Adv. Mater.* **2013**, *25*, 302–312.

[13] (a) Ichimura, K.; Oh, S. K.; Nakagawa, M. *Science* **2000**, *288*, 1624–1626. (b) Berná, J.; Leigh, D. A.; Lubomska, M.; Mendoza, S. M.; Pérez, E. M.; Rudolf, P.; Teobaldi, G.; Zerbetto, F. *Nat. Mater.* **2005**, *4*, 704–710. (c) Yang, D.; Piech, M.; Bell, N. S.; Gust, D.; Vail, S.; Garcia, A. A.; Schneider, J.; Park, C.-D.; Hayes, M. A.; Picraux, S. T. *Langmuir* **2007**, *23*, 10864–10872. (d) Xin, B.; Hao, J. *Chem. Soc. Rev.* **2010**, *39*, 769–782.

[14] Klajn, R. *Pure Appl. Chem.* **2010**, *82*, 2247–2279.

[15] Berkovic, G.; Krongauz, V.; Weiss, V. *Chem. Rev.* **2000**, *100*, 1741–1754.

[16] Lim, H. S.; Han, J. T.; Kwak, D.; Jin, M.; Cho, K. *J. Am. Chem. Soc.* **2006**, *128*, 14458–14459.

[17] (a) Feng, C. L.; Zhang, Y. J.; Jin, J.; Song, Y. L.; Xie, L. Y.; Qu, G. R.; Jiang, L.; Zhu, D. B. *Langmuir* **2001**, *17*, 4593–4597. (b) Groten, J.; Bunte, C.; Rühe, J. *Langmuir* **2012**, *28*, 15038–15046.

[18] (a) Siewierski, L. M.; Brittain, W. J.; Petrash, S.; Foster, M. D. *Langmuir* **1996**, *12*, 5838–5844. (b) Oh, S.-K.; Nakagawa, M.; Ichimura, K. *J. Mater. Chem.* **2002**, *12*, 2262–2269. (c) Hamelmann, F.; Heinzmann, U.; Siemeling,

U.; Bretthauer, F.; Vor der Brüggen, J. *Appl. Surf. Sci.* **2004**, *222*, 1–5. (d) Delorme, N.; Bardeau, J. F.; Bulou, A.; Poncin-Epaillard, F. *Langmuir* **2005**, *21*, 12278–12282.

[19] (a) Rosario, R.; Gust, D.; Hayes, M.; Jahnke, F.; Springer, J.; Garcia, A. A. *Langmuir* **2002**, *18*, 8062–8069. (b) Rosario, R.; Gust, D.; Garcia, A. A.; Hayes, M.; Taraci, J. L.; Clement, T.; Dailey, J. W.; Picraux, S. T. *J. Phys. Chem. B* **2004**, *108*, 12640–12642. (c) Dattilo, D.; Armelao, L.; Fois, G.; Mistura, G.; Maggini, M. *Langmuir* **2007**, *23*, 12945–12950.

[20] (a) Koumura, N.; Zijlstra, R. W.; van Delden, R. A.; Harada, N.; Feringa, B. L. *Nature* **1999**, *401*, 152–155. (b) *Molecular Motors*; Schliwa, M., Ed.; Wiley-VCH: Weinheim, 2003.

[21] (a) Carroll, G. T.; Pollard, M. M.; van Delden, R.; Feringa, B. L. *Chem. Sci.* **2010**, *1*, 97–101. (b) Perera, U. G. E.; Ample, F.; Kersell, H.; Zhang, Y.; Vives, G.; Echeverria, J.; Grisolia, M.; Rapenne, G.; Joachim, C.; Hla, S.-W. *Nat. Nanotech.* **2012**, *8*, 46–51.

[22] (a) London, G.; Carroll, G. T.; Fernández Landaluce, T.; Pollard, M. M.; Rudolf, P.; Feringa, B. L. *Chem. Commun.* **2009**, 1712–1714. (b) Carroll, G. T.; London, G.; Landaluce, T. F.; Rudolf, P.; Feringa, B. L. *ACS Nano* **2011**, *5*, 622–630. (c) London, G.; Carroll, G. T.; Feringa, B. L. *Org. Biomol. Chem.* **2013**, *11*, 3477–3483. (d) London, G.; Chen, K.-Y.; Carroll, G. T.; Feringa, B. L. *Chem. Eur. J.* **2013**, *19*, 10690–10697.

[23] Pollard, M. M.; Von Wesenhagen, P.; Pijper, D.; Feringa, B. L. *Org. Biomol. Chem.* **2008**, *6*, 1605–1612.

[24] (a) Shirai, Y.; Cheng, L.; Chen, B.; Tour, J. M. *J. Am. Chem. Soc.* **2006**, *128*, 13479–13489. (b) Shirai, Y.; Guerrero, J. M.; Sasaki, T.; He, T.; Ding, H.; Vives, G.; Yu, B.-C.; Cheng, L.; Flatt, A. K.; Taylor, P. G.; Gao, Y.; Tour, J. M. *J. Org. Chem.* **2009**, *74*, 7885–7897. (c) Wagner, S.; Leyssner, F.; Kördel, C.; Zarwell, S.; Schmidt, R.; Weinelt, M.; Rück-Braun, K.; Wolf, M.; Tegeder, P. *Phys. Chem. Chem. Phys.* **2009**, *11*, 6242–6248.

[25] Ivashenko, O.; Logtenberg, H.; Areephong, J.; Coleman, A. C.; Wesenhagen, P. V.; Geertsema, E. M.; Heureux, N.; Feringa, B. L.; Rudolf, P.; Browne, W. R. *J. Phys. Chem. C* **2011**, *115*, 22965–22975.

[26] Buter, J.; Wassenaar, S.; Kellogg, R. M. *J. Org. Chem.* **1972**, *37*, 4045–4060.

[27] Mori, A.; Kawashima, J.; Shimada, T.; Suguro, M.; Hirabayashi, K.; Nishihara, Y. *Org. Lett.* **2000**, *2*, 2935–2937.

[28] (a) Vicario, J.; Walko, M.; Meetsma, A.; Feringa, B. L. *J. Am. Chem. Soc.* **2006**, *128*, 5127–5135. (b) Pijper, D.; Feringa, B. L. *Angew. Chem. Int. Ed.* **2007**, *46*, 3693–3696.

[29] ter Wiel, M. K. J.; van Delden, R. A.; Meetsma, A.; Feringa, B. L. *J. Am. Chem. Soc.* **2005**, *127*, 14208–14222.

[30] Bain, C. D.; Whitesides, G. M. *J. Phys. Chem.* **1989**, *93*, 1670–1673.

[31] (a) van Delden, R. A.; ter Wiel, M. K. J.; Pollard, M. M.; Vicario, J.; Koumura, N.; Feringa, B. L. *Nature* **2005**, *437*, 1337–1340. (b) Coleman, A. C.; Areephong, J.; Vicario, J.; Meetsma, A.; Browne, W. R.; Feringa, B. L. *Angew. Chem. Int. Ed.* **2010**, *49*, 6580–6584.

Chapter 4

Tetrapodal Molecular Switches and Motors: Synthesis and Photochemistry

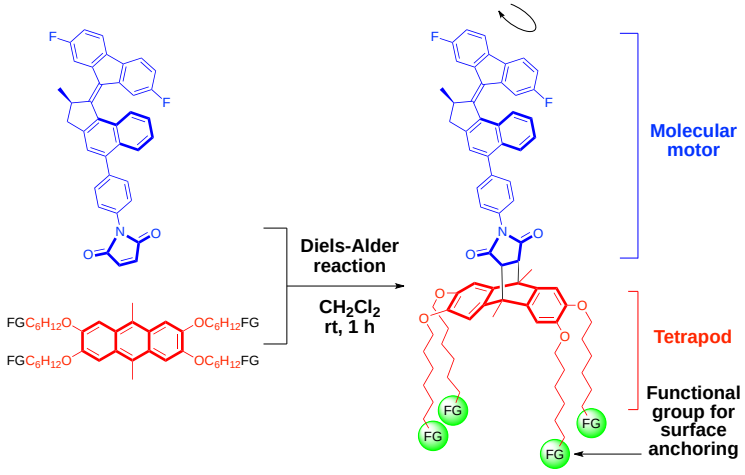

The design, synthesis, and dynamic behavior of a series of novel tetrapodal molecular switches and motors containing common functional groups for attachment to various inorganic and organic surfaces are presented. Using a Diels-Alder reaction, an anthracene unit with four functionalized alkyl substituents ("legs") was coupled to maleimide-functionalized molecular switches or motors under ambient conditions. Terminal functional groups at the "legs" include thioacetates and azides, making these switches and motors ideal candidates for attachment to metallic or alkyne-functionalized surfaces. UV/vis absorption spectroscopy shows that the molecular switches and motors retain their ability to undergo reversible photochemical and/or thermally-induced isomerization processes after attachment to the tetrapodal anthracene moieties.

This chapter has been published:
Chen, K.-Y.; Wezenberg, S. J.; Carroll, G. T.; London, G.; Kistemaker, J. C. M.; London, G.; Pijper, T. C; Feringa, B. L. *J. Org. Chem.* **2014**, *79*, 7032-7040.

4.1 Introduction

Achieving molecular-level control over macroscopic phenomena is a key challenge in nanotechnology.[1-6] Tuning the surface properties of a material, including wettability,[7,8] optical properties,[9,10] and conductance[11-14] without modifying the bulk properties is of particular interest. One approach towards this goal is to attach photochromic molecules,[4, 15 , 16] which are capable of undergoing reversible structural changes upon application of external stimuli, *e.g.* light, to the interfaces. Azobenzenes,[15,17] dithienylethenes,[15,18,19] and molecular motors[20,21] based on overcrowded alkenes have proven to be particularly versatile photochromic molecules in surface-immobilized systems.[14,22-27]

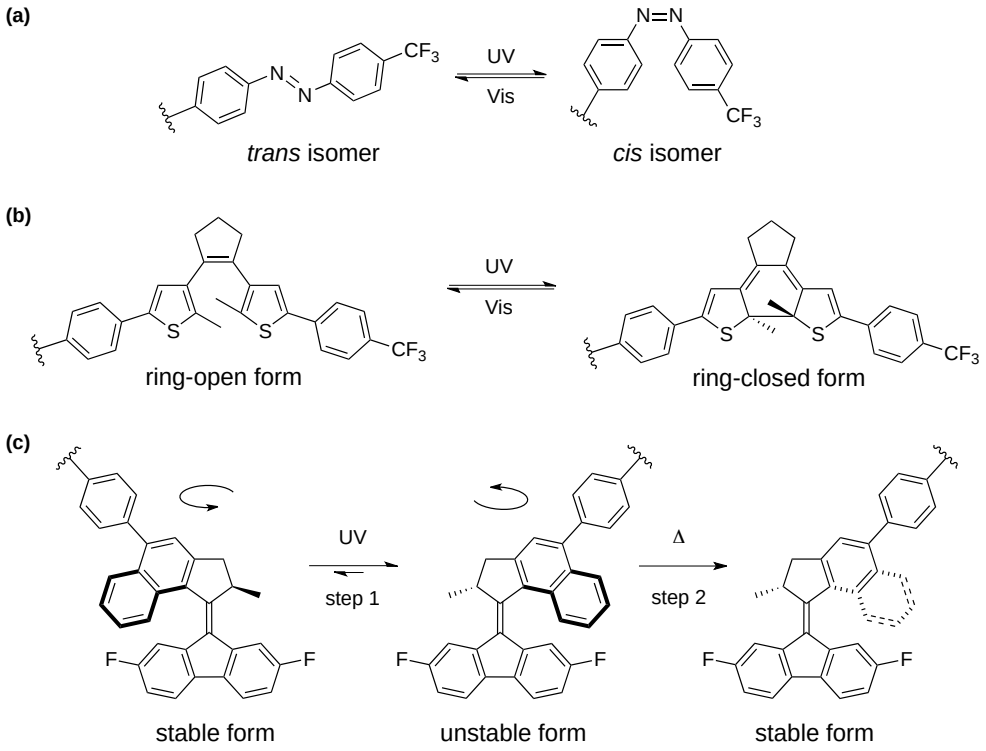

Scheme 4.1 Photoisomerization of (a) azobenzenes and (b) dithienylethenes. (c) Photochemical and thermal isomerization of molecular motors.

The origin of the popularity of azobenzene in these applications is their relatively facile synthesis and fatigue resistant *trans*→*cis* photoisomerization

(Scheme 4.1a) which is accompanied by large changes in geometry and dipole moment.[17,28] Dithienylethenes can undergo a reversible photocyclization between a ring-open and ring-closed form by irradiation with UV and visible light (Scheme 4.1b). Compared to other photochromic compounds, dithienylethenes display excellent thermal stability for both isomers as well as high fatigue resistance.[18,19] Molecular motors based on overcrowded alkenes are a unique group of photoresponsive organic molecules that are capable of converting light energy into repetitive unidirectional rotation and are promising candidates in photochemically-driven systems and as multistage switches (Scheme 4.1c).[20,21,27]

Although the key components of surface-bound systems are the photochromic moieties that undergo structural changes upon the absorption of light, in most cases, the anchoring strategy can have a considerable impact on their switching efficiencies and performances. Their proper assembly on the surface is essential for the dynamic control of surface properties by light. The two foremost reasons for inefficient switching of monolayers of photoisomerizable chromophores are steric crowding (often observed with azobenzenes[29,30-35] and molecular motors[36,37]) and electronic effects (most often observed with dithienylethenes[38,39]).

A general approach to deal with the disadvantages of tight packing is to provide the photochromic units with sufficient free volume to undergo the desired conformational changes. Photoresponsive azobenzene-based monolayers have been prepared using bulky anchoring groups[29,31] or substituents[32,34] as well as in mixed monolayer environments[30,35] applying alkyl thiols or silanes as diluents to ensure efficient performance. Previous studies in our group have shown that the photochemical and thermal isomerization behavior of altitudinal bipodal molecular motors (Figure 4.1, left, R = H) are obstructed by intermolecular interactions when they were confined to a crowded monolayer compared to the motor molecules in solution.[36]

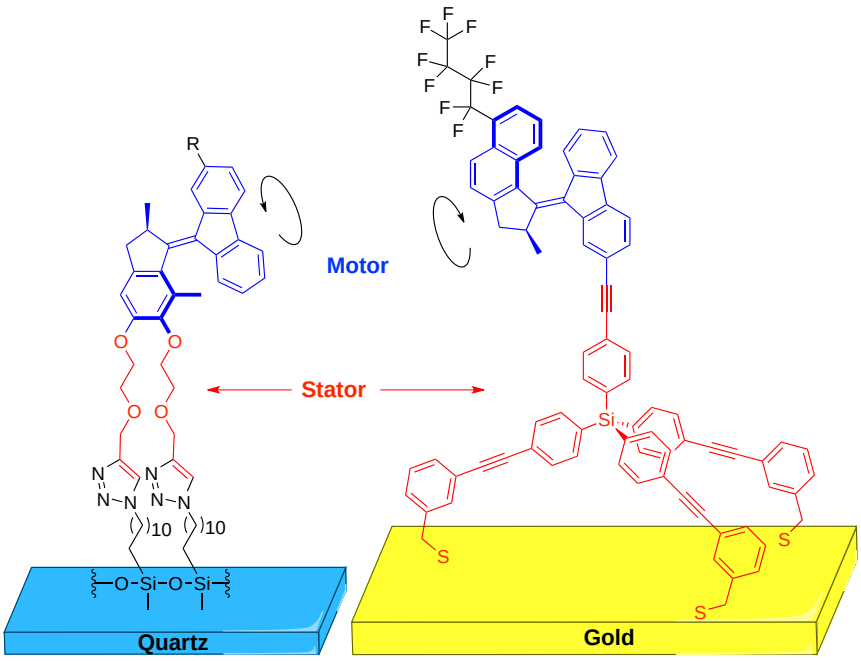

Figure 4.1 Bipodal (left, R = H or C_4F_9) and tripodal (right) molecular motors.

To address this problem, we recently developed a tripodal surface-attached altitudinal, rotary molecular motor system (Figure 4.1, right) that is able to undergo photoisomerization, which is accompanied by changes in surface wettability, when irradiated with UV light.[27] In comparison, a related bipodal system was unable to alter surface wettability upon UV irradiation (Figure 4.1, left, R = C_4F_9).[37] The extra free volume between the surface-bound motors in the tripodal system resulted in enhanced switching behavior,[27] whereas intermolecular interactions in the bipodal system interfered with isomerization,[37] resulting in negligible changes in surface wettability upon UV irradiation.

Driven by our interest in surface-bound dynamic molecular systems for nanoscale applications and control over assembly and dynamic functions, we envisioned novel anchoring strategies for molecular switches and motors as is shown in Scheme 4.2.

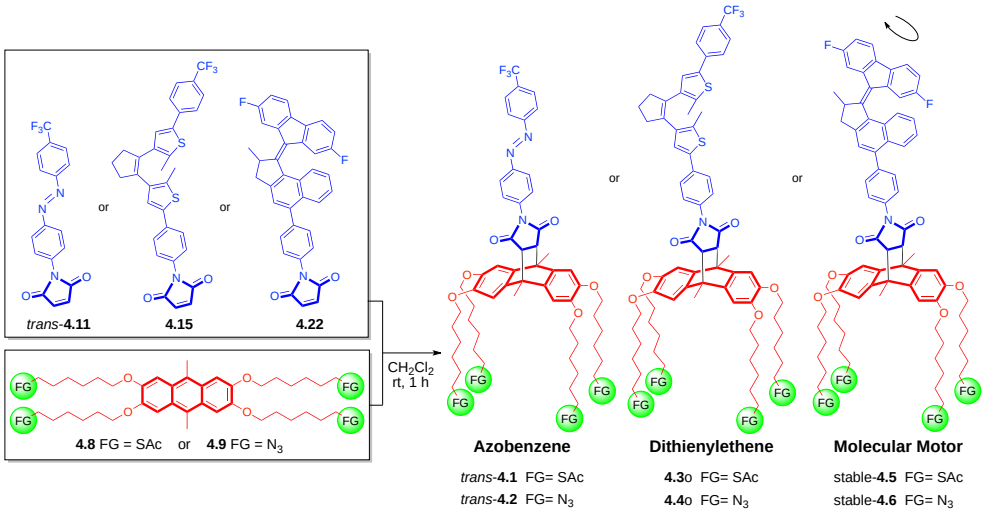

Scheme 4.2 Synthetic route toward tetrapodal molecular switches and motors *via* a Diels-Alder approach. For the calculated energy-minimized geometries of the Diels-Alder adducts, see section 4.5.3..

The tetrapodal portion of the molecules **4.1**-**4.6** consist of an anthracene derived core with four pendant alkyl chains terminated with surface-reactive groups for attachment to metallic or organic interfaces (Scheme 4.2). Terminal thioacetate (SAc) functional groups at the "legs" allow for the attachment to metallic surfaces such as copper, silver, and gold[40,41] while terminal azide (N_3) functional groups were incorporated for attachment to organic surfaces containing alkynes[36] *via* a Cu(I)-catalyzed azide-alkyne cycloaddition (1,3-dipolar cycloaddition).[42] Note that although the latter reaction requires that alkynes are introduced at the interfaces, it has shown to be a very versatile approach for modifying the surface of a variety of materials including Si wafers,[36] quartz,[43] polymer films,[44] and nanoparticles.[45] The anthracene core in **4.8** and **4.9** provides a stable diene moiety[46] which can react with molecular switches or motors containing dienophiles.

Here, we report a new synthetic route to produce six unique photoresponsive tetrapodal molecules suitable for surface attachment by reacting three different maleimide-functionalized molecular switches or motors with two different anthracene-based tetrapods *via* a Diels-Alder cycloaddition (Scheme 4.2). Construction of these tetrapodal photochromes is more versatile than that of our recently reported tripodal molecular motors (Figure 4.1, right),[27] and after surface assembly it is expected to maintain sufficient free volume, allowing for

photochemical and/or thermal isomerization to occur with minimal, if any, interference from neighboring molecules.

4.2 Synthesis of the tetrapodal molecular switches and motors

The synthetic approach toward tetrapod scaffolds **4.8** and **4.9** is shown in Scheme 4.3. The tetrapod contains four functionalized alkyl chains suitable for surface attachment and an anthracene moiety that provides a diene to react with maleimide-functionalized photochromes *via* a Diels-Alder reaction. The four bromide substituents of compound **4.7**[47] were replaced with either thioacetate groups *via* reaction with potassium thioacetate in DMF, or with azide groups using sodium azide in DMF to afford tetrapod **4.8** and **4.9** in 95% and 92% yield, respectively.

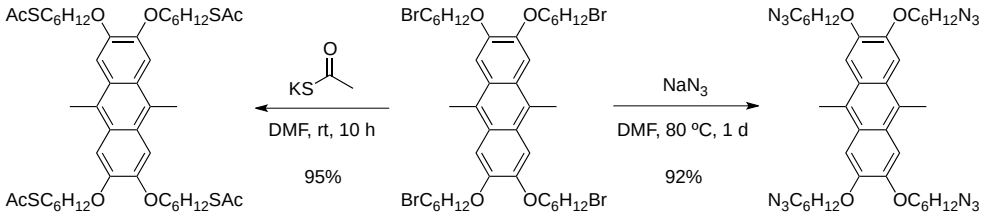

4.8 **4.7** **4.9**

Scheme 4.3 Synthesis of tetrapods **4.8** and **4.9**.

The molecular switches and motor used in this study (*i.e. trans*-**4.11**, **4.15** and **4.22**, Scheme 4.2) were modified with a maleimide group allowing them to react with anthracene **4.8** or **4.9** *via* a Diels-Alder reaction. Note that the synthetic procedure includes the introduction of fluorine atoms into each photochromic moiety in order to facilitate the future characterization of the surface when water contact angle[48] and X-ray photoelectron spectroscopy (XPS)[†] measurements are performed.

[†] Fluorine atom(s) will be an important marker for monitoring the progress of the interfacial Diels-Alder reactions between the molecular switches/motors and an anthracene functionalized surface by using XPS, a surface sensitive technique.

Maleimide-functionalized azobenzene *trans*-**4.11** was synthesized by treating aniline **4.10**[49] with maleic anhydride in chloroform followed by cyclization using a solution of sodium acetate in acetic anhydride (Scheme 4.4).

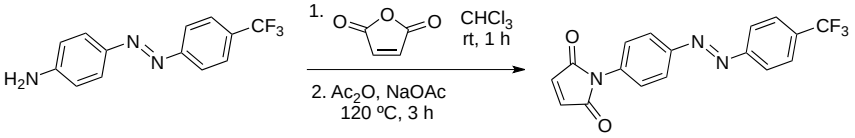

Scheme 4.4 Synthesis of a maleimide-functionalized azobenzene *trans*-**4.11**.

Dithienylethene **4.15** was synthesized as depicted in Scheme 4.5. The dichloro compound **4.12**[50] was first mono-functionalized with a trifluoromethylbenzene group through a Suzuki cross-coupling affording the monochloro compound **4.13**. A second Suzuki cross-coupling with commercially available *p*-$IC_6H_4NH_2$ yielded intermediate **4.14**. The maleimide-functionalized dithienylethene **4.15** was then obtained using a similar procedure as described above for the synthesis of *trans*-**4.11**.

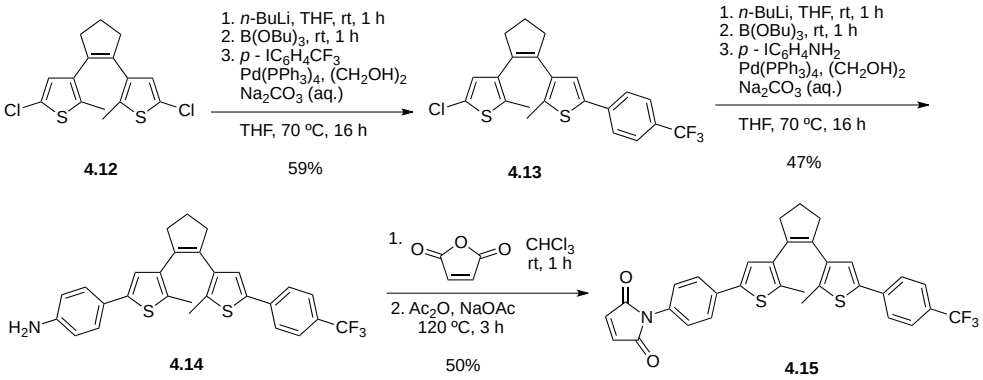

Scheme 4.5 Synthesis of a maleimide-functionalized dithienylethene **4.15**.

Molecular motor **4.22** was synthesized according to the route depicted in Scheme 4.6. Ketone **4.16**[51] was treated with Lawesson's reagent in chloroform to give the thioketone intermediate **4.17**. The highly sterically hindered olefin in **4.19** was formed using a Barton-Kellogg diazo-thioketone coupling by heating thioketone **4.17** and the known diazo compound **4.18**[52] at 100 ºC in toluene. A subsequent palladium catalyzed cross-coupling was used to attach the aniline

group in **4.21**, followed by the introduction of the maleimide group to afford molecular motor **4.22**.

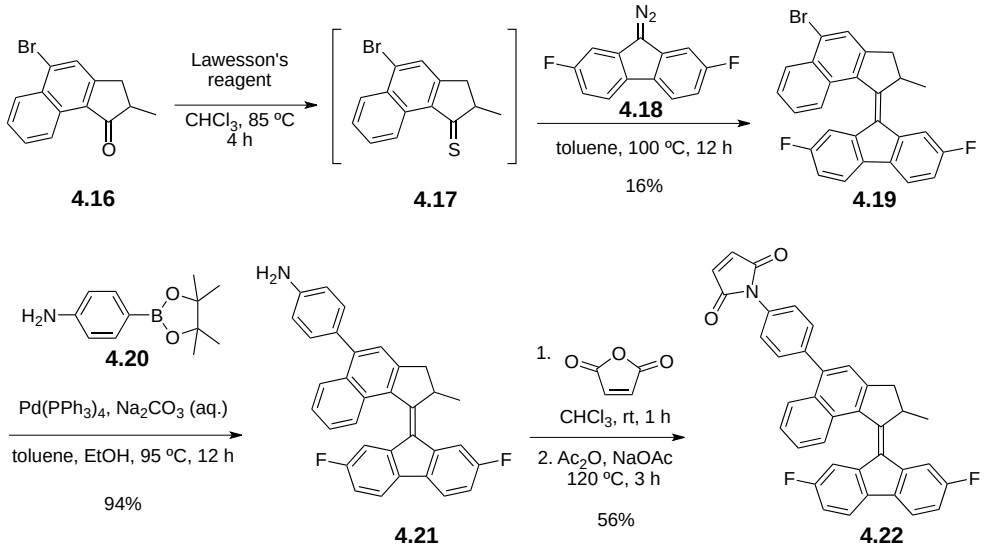

Scheme 4.6 Synthesis of a maleimide-functionalized molecular motor **4.22**.

The Diels-Alder strategy toward tetrapodal compounds **4.1**-**4.6** ultimately to be used for surface modification was tested by mixing diene **4.8** or **4.9** with *trans*-**4.11**, **4.15**, or **4.22** in CH_2Cl_2 under ambient conditions yielding *trans*-**4.1**, *trans*-**4.2**, **4.3**o, **4.4**o, stable-**4.5** and stable-**4.6** (Scheme 4.2). By monitoring the reaction by TLC and ^{1}H NMR, we observed full conversion in 1 h and the desired products were obtained in excellent isolated yield (> 95%). Although Diels-Alder reactions are known to be thermally reversible, no retro Diels-Alder reaction was observed upon standing of the NMR solutions of the the Diels-Alder products at rt for 72 h, showing the thermal stability of the Diels-Alder adducts.

4.3 Photochemical isomerization studies

4.3.1 Tetrapodal azobenzenes

The photochemical behavior of azobenzenes **4.1**, **4.2**, and **4.11** were analyzed by UV/vis absorption spectroscopy. The UV/vis absorption spectra of a sample of azobenzene *trans*-**4.1** or *trans*-**4.2** in CH_2Cl_2 showed absorption bands centered at 296 and 322 nm (Figure 4.2a and 4.2b, solid bold line). For *trans*-**4.11** the maximum absorption was centered at 329 nm (Figure 4.2c, solid bold line). Upon irradiation with UV light (λ_{max} = 365 nm), the major bands decreased in intensity and new bands centered at 437 nm appeared. This spectral change is indicative of the photochemically induced formation of the *cis* isomer (Scheme 4.1a, *cis*-**4.1**, *cis*-**4.2**, and *cis*-**4.11**).[17]

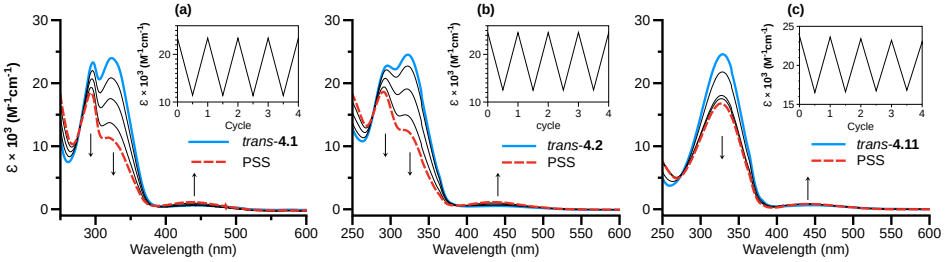

Figure 4.2 UV/vis absorption spectra (CH_2Cl_2, 283 K) of *trans*-**4.1** (a), *trans*-**4.2** (b), and *trans*-**4.11** (c) before UV irradiation (solid bold line) and at the photostationary state (PSS) (dashed line). Inserts: changes in molar absorptivity (ε) at 322 nm upon alternating irradiation with UV light and visible light over several cycles.

During the irradiation of each compound, clear isosbestic points were observed and each sample was irradiated until no further changes were observed, *i.e.* the photostationary state (PSS) was reached (Figure 4.2, dashed lines). Irradiation of the PSS mixture of *trans*-**4.1**/*cis*-**4.1**, *trans*-**4.2**/*cis*-**4.2**, or *trans*-**4.11**/*cis*-**4.11** with visible light (> 500 nm) resulted in the recovery of the original spectra, which is indicative of photoisomerization back to the original *trans* isomers. These switching cycles could be repeated several times without observing any sign of fatigue (Figure 4.2, insert).[‡]

4.3.2 Tetrapodal dithienylethenes

The photochemical behavior of dithienylethenes **4.3**, **4.4**, and **4.15** were analyzed in a similar manner. UV/vis absorption spectra of dithienylethene **4.3**o, **4.4**o, or **4.15**o (o: ring-opened form of the dithienylethenes) in CH_2Cl_2 showed absorption bands with maxima around 290 and 325 nm (Figure 4.3, solid bold line). Upon UV irradiation (λ_{max} = 312 nm), both major bands decreased in intensity and two new bands centered around 370 nm and 544 nm appeared simultaneously, which is indicative of the photochemically induced formation of the isomers in the ring-closed form (Scheme 4.1b, **4.3**c, **4.4**c and **4.15**c; c: ring-closed form of the dithienylethenes).[18]

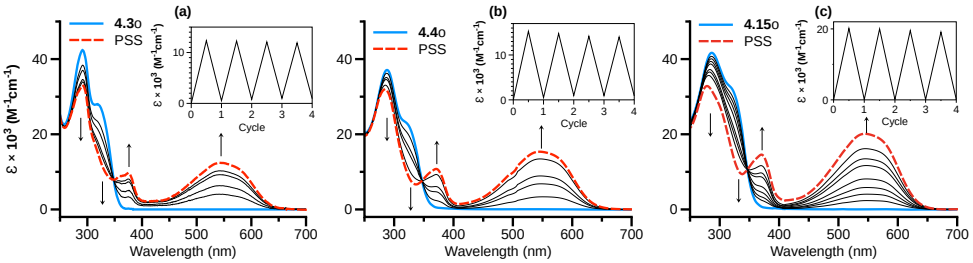

Figure 4.3 UV/vis absorption spectra (CH_2Cl_2, 283 K) of **4.3**o (a), **4.4**o (b), and **4.15**o (c) before UV irradiation (solid bold line) and at the PSS (dashed line). Inserts: changes in molar absorptivity (ε) at 550 nm upon alternating irradiation with UV and visible light over several cycles.

Isosbestic points were clearly visible during the irradiation and the PSS (Figure 4.3, dashed lines) was reached after 5 min. Irradiation of the PSS mixture of **4.3**o/**4.3**c, **4.4**o/**4.4**c or **4.15**o/**4.15**c with visible light (> 500 nm) regenerated the original spectra, indicating formation of the isomers in the ring-open form. The insert in Figure 4.3 shows that the switching cycles could be repeated several times without the observation of any fatigue, *i.e.* the tetrapodal dithienylethene switches are highly stable under photochemical conditions.[‡]

4.3.3 Tetrapodal molecular motors

Finally, the photochemical and thermal behavior of molecular motors **4.5**, **4.6**, and **4.22** were studied. The UV/vis absorption spectra of the stable form of molecular motors **4.5**, **4.6**, and **4.22** in CH_2Cl_2 show absorption bands centered at 405 nm (Figure 4.4; solid bold line). Irradiation of the samples with UV light (λ_{max} = 365 nm) led to a red-shift of the bands at 405 nm, indicating the photochemically induced formation of the unstable isomer (Scheme 4.1c, step 1; unstable-**4.5**, unstable-**4.6**, and unstable-**4.22**). This shift is consistent with increased strain at the central double bond, and the generation of a higher energy isomer.

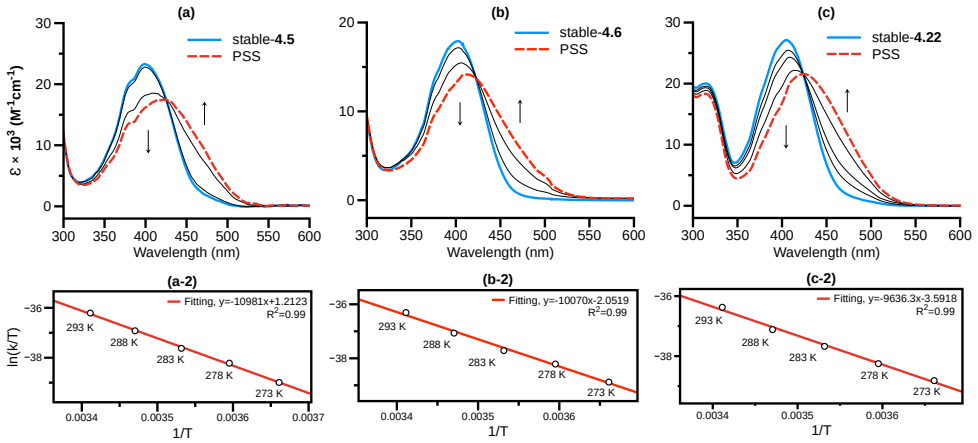

Figure 4.4 UV/vis absorption spectra (CH_2Cl_2, 283 K) of stable-**4.5** (a), stable-**4.6** (b), and stable-**4.22** (c) before irradiation (solid bold line) and at the PSS (dashed line); Eyring plot of the conversion of unstable-**4.5** → stable-**4.5** (a-2), unstable-**4.6** → stable-**4.6** (b-2), and unstable-**4.22** → stable-**4.22** (c-2) *via* thermal isomerization at different temperature.

During irradiation, clear isosbestic points were observed in each case and samples were irradiated until no further changes were observed, *i.e.* the PSS (Figure 4.4, dashed lines) was reached. Allowing the PSS mixtures to warm to rt resulted in a blue-shift of the bands back to their original position, which is consistent with thermal isomerization back to the corresponding stable isomers (Scheme 4.1c, step 2). The thermal isomerization steps (Scheme 4.1c, step 2) were followed over a range of temperatures and from these data the Eyring plots were obtained (Figure 4.4, lower panels; see experimental sections for details). For the unstable-**4.5** → stable-**4.5** conversion , the Gibbs free energy of activation ($\Delta^{\ddagger}G°$) was calculated to be 88.5 kJ/mol (half-life: $t_{1/2}$ = 625 s at rt) and for unstable-**4.6** →

stable-**4.6**, $\Delta^{\ddagger}G°$ = 89.1 kJ/mol ($t_{1/2}$ = 731 s at rt). These values are similar to the half-life of their parent motor **4.22** (unstable-**4.22** → stable-**4.22**, $\Delta^{\ddagger}G°$ = 89.2 kJ/mol; $t_{1/2}$ = 777 s at rt).

In summary, by studying the photochemical and thermal behavior of **4.5**, **4.6**, and **4.22** in solution by UV/vis absorption spectroscopy, and by analogy with similar motor systems reported previously,[27,53] it is anticipated that **4.5**, **4.6**, and **4.22** function as light-driven rotary motors in solution. The photochemical studies and the Eyring analyses show that the Diels-Alder adduct does not have a significant influence on the photochemical and thermal behaviors of the motors.[‡]

4.4 Conclusions

In conclusion, we have described a new surface attachment strategy for molecular switches and motors based on a Diels-Alder transformation. To achieve this we have developed tetrapodal anthracene units as dienes containing either thioacetate or azide pendant functional groups. These dienes were coupled to maleimide-functionalized molecular switches as well as a molecular motor. The tetrapodal molecular switches and motors produced by this method retained their ability to undergo photoisomerization in solution upon irradiation as was demonstrated by UV/vis absorption spectroscopy. The design and synthesis of these novel tetrapod functionalized photochromophores described herein will allow us to develop highly functional and photoresponsive surfaces for application in smart materials and nanotechnology research. Studies on the behavior of the systems when attached to surfaces are currently ongoing.

[‡] In our irradiation experiments, no noticeable degradation was observed; moreover, if the irradiation could induce dissociation, it would depend on which wavelength the structure of the Diels-Alder adduct absorbs. Raymo *et al.* ademonstrated that the maleimide/anthracene Diels-Alder adduct only dissociates upon irradiation with 254 nm UV light when directly connected with a strong electron donating group [*e.g.* 4-$(CH3)_2NC_6H_4$-maleimide/anthracene adduct]. This short wavelength does not overlap with the major absorption band of the tetrapodal azobenzene (296, 322 nm), dithienylethene (290, 325 nm), and molecular motors (405 nm). We irradiate our systems with 312 or 365 nm UV light, which is well below the reported energy used to dissociate Diels-Alder adducts containing electron donating groups. See also: Thapaliya, E. R.; Captain, B.; Raymo, F. M. *J. Org. Chem.* **2014**, *79*, 3973–3981.

4.5 Experimental Section

4.5.1 General remarks

All reactions were performed in oven-dried glassware under a nitrogen atmosphere, unless stated otherwise; solvents were reagent grade and commercially available reagents were used without purification. UVASOL grade solvents were used for spectroscopic measurements. UV irradiation experiments were performed using an ENB-280C/FE lamp (λ_{max} = 312 or 365 nm) and visible irradiation using a high intensity fiber optic white light source combined with a 500 nm long pass filter. Kinetic analysis of the thermal isomerization steps of the motors (unstable-**4.5** → stable-**4.5**, unstable-**4.6** → stable-**4.6**, and unstable-**4.22** → stable-**4.22**) were performed by UV/vis absorption spectroscopy. A long pass filter was mounted between the UV light source and the sample to cut off light with wavelengths below 460 nm to minimize photochemical isomerization occurring upon data recording. The thermal isomerization was followed by monitoring the change in absorption at 470 nm as a function of time at 273, 278, 283, 288, and 293 K. From the experimental data the rate constants (*k*) for the thermal isomerization steps were obtained and Eyring plots were derived from these data.

4.5.2 Synthesis of compounds and intermediates

Compound 4.8

A mixture of 2,3,6,7-tetrakis(6-bromohexyloxy)-9,10-dimethylanthracene **4.7**[47] (1.00 g, 1.08 mmol) and potassium thioacetate (656 mg, 5.75 mmol) in DMF (130 mL) was stirred for 10 h at rt. The mixture was treated with water (90 mL) and the water layer was extracted with CH_2Cl_2 (3 × 45 mL). The combined organic layers were washed with water (75 mL) and brine (75 mL), dried over $MgSO_4$ and concentrated. Flash column chromatography (SiO_2, CH_2Cl_2) gave **4.8** as pale yellow solid (930 mg, 1.03 mmol, 95%). M.p. 116.8 – 118.3 °C; ^{1}H NMR (400 MHz, $CDCl_3$) δ 7.39 (s, 4H, Ar-*H*), 4.17 (t, *J* = 6.5 Hz, 8H, ArOC-H_2), 2.90 (m, 14H, overlap of ArC-H_3 and AcSC-H_2), 2.33 (s, 12H, SC=OC-H_3), 1.99 – 1.87 (m, 8H, C-H_2), 1.69 – 1.43 (m, 24H, C-H_2); ^{13}C NMR (101 MHz, $CDCl_3$) 195.9, 148.5, 125.8, 123.6, 104.3, 68.5, 30.6, 29.5, 29.0, 28.6, 25.7, 14.7; UV/vis (CH_2Cl_2, 293 K): λ_{max} (ε) = 278 nm (143517 $M^{-1}cm^{-1}$); HRMS (ESI-ion trap) *m/z*: $[M]^+$ Calcd for $C_{48}H_{70}O_8S_4$ 902.3948, found 902.3922.

Compound 4.9

A mixture of 2,3,6,7-tetrakis(6-bromohexyloxy)-9,10-dimethylanthracene **4.7**[47] (85 mg, 0.092 mmol) and sodium azide (36 mg, 0.55 mmol) was heated at 80 ºC in DMF (30 mL) for 24 h. The solvent was evaporated and the residue was dissolved in CH_2Cl_2 (50 mL) and washed with water (50 mL). The organic phase was dried over $MgSO_4$ and filtered over a silica plug, then the residue was concentrated *in vacuo* affording **4.9** as pale yellow solid (65 mg, 0.085 mmol, 92%). M.p. 105.4 – 107.4 ºC; ^{1}H NMR (300 MHz, $CDCl_3$) δ 7.40 (s, 4H, Ar-*H*), 4.18 (t, *J* = 6.4 Hz, 8H, ArOC-H_2), 3.31 (t, *J* = 6.8 Hz, 8H, N_3C-H_2), 2.91 (s, 6H, ArC-H_3), 2.03 – 1.88 (m, 8H, C-H_2), 1.75 – 1.43 (m, 24H, C-H_2); ^{13}C NMR δ (75 MHz, $CDCl_3$) 148.8, 126.1, 123.8, 104.7, 68.7, 51.6, 29.3, 29.1, 26.8, 26.0, 14.9; UV/vis (CH_2Cl_2, 293 K): λ_{max} (ε) = 277 nm (100717 $M^{-1}cm^{-1}$); HRMS (ESI-ion-trap) *m/z*: $[M]^+$ Calcd for $C_{40}H_{58}N_{12}O_4$ 770.4698, found 770.4695.

Compound 4.11

(*E*)-4-((4-(Trifluoromethyl)phenyl)diazenyl)benzeneamine **4.10** (2.36 g, 24.1 mmol) in $CHCl_3$ (200 mL) was added dropwise to a stirred solution of maleic anhydride (6.39 g, 24.1 mmol) in $CHCl_3$ (40 mL) at rt, after which stirring was continued for 1 h. The solvent was evaporated and the residue was added to a solution of sodium acetate (3.95 g, 48.2 mmol) in acetic anhydride (2 mL). The resulting mixture was at 120 ºC for 3 h, cooled to rt and concentrated *in vacuo*. Flash column chromatography (SiO_2, CH_2Cl_2) provided *trans*-**4.11** as an orange solid (5.82 g, 16.9 mmol, 70%). M.p. 174.4 – 175.8 ºC; ^{1}H NMR (400 MHz, $CDCl_3$) δ 8.08-7.98 (m, 4H, Ar-*H*), 7.79 (d, *J* = 8.3 Hz, 2H, Ar-*H*), 7.62-7.57 (m, 2H, Ar-*H*), 6.90 (s, *J* = 3.6 Hz, 2H, *H*-C=C-*H*); ^{13}C NMR (101 MHz, $CDCl_3$) δ 169.1, 151.0, 134.4, 134.2, 126.3, 126.3, 126.2, 123.8, 123.1; ^{19}F NMR (376 MHz, $CDCl_3$) δ –62.60; UV/vis (CH_2Cl_2, 283K): λ_{max} (ε) = 445 (643), 329 nm (24648 $M^{-1}cm^{-1}$); HRMS (ESI-ion trap) *m/z*: $[M + H]^+$ Calcd for $C_{17}H_{11}F_3N_3O_2$ 346.0798, found 346.0787.

Compound 4.13

n-BuLi (1.6 M solution in hexane, 3.99 mL, 6.38 mmol) was added dropwise to a stirred solution of 1,2-bis(5-chloro-2-methylthiophen-3-yl)cyclopent-1-ene **4.12**[50] (2.00 g, 6.07 mmol) at rt in THF (80 mL), after which stirring was continued for 1 h. Subsequently, tributyl borate (1.96 g, 8.50 mmol) was added dropwise and the resulting mixture was deoxygenated by purging with argon for 5 min and then stirred for an additional 1 h (flask A). Meanwhile, in a separate flask (flask B), a

stirred mixture of *p*-$IC_6H_4CF_3$ (2.48 g, 9.11 mmol), $Pd(PPh_3)_4$ (0.19 g, 0.18 mmol), ethylene glycol (0.8 mL), and aqueous Na_2CO_3 (2 M, 32 mL) in THF (50 mL) was deoxygenated by purging with argon for 5 min and then heated to 70 ºC. The suspension in flask A was transferred to flask B by cannula and the combined mixture was heated at 70 ºC for 16 h under argon atmosphere. The mixture was diluted with Et_2O (200 mL) and washed with water (2 × 100 mL). The combined aqueous layers were extracted with Et_2O (100 mL), after which the combined organic layer was dried over $MgSO_4$ and concentrated *in vacuo*. Flash column chromatography (SiO_2, pentane) provided **4.13** as light brown solid (1.56 g, 3.55 mmol, 59%). M.p. 84.5 – 85.3 ºC; ^{1}H NMR (400 MHz, $CDCl_3$) δ 7.58 (s, 4H, Ar-*H*), 7.06 (s, 1H, thiophene-*H*), 6.62 (s, 1H, thiophene-*H*), 2.85-2.72 (m, 4H, C-H_2), 2.11-2.00 (m, 5H, overlap of C-H_2 and C-H_3), 1.89 (s, 3H, C-H_3); ^{13}C NMR (75 MHz, $CDCl_3$) δ 138.1, 137.8, 136.8, 136.1, 135.0, 135.0, 134.3, 133.29, 126.8, 125.9, 125.8, 125.8, 125.7, 125.3, 125.3, 125.2, 118.5, 115.8, 38.4, 38.4, 22.9, 14.5, 14.1; ^{19}F NMR (376 MHz, $CDCl_3$) δ –62.50 (d, *J* = 8.5 Hz); HRMS (ESI-ion trap) *m/z*: $[M + H]^+$ Calcd for $C_{22}H_{19}ClF_3S_2$ 439.0563, found 439.0567.

Compound 4.14

n-BuLi (1.6 M solution in hexane, 2.30 mL, 3.68 mmol) was added dropwise to a stirred solution of **4.13** (1.54 g, 3.51 mmol) at rt in THF (50 mL), after which stirring was continued for 1 h. Tributyl borate (1.13 g, 4.91 mmol) was added dropwise and the resulting mixture was deoxygenated by purging with argon for 5 min and then stirred for an additional 1 h (flask A). Meanwhile, in a separate flask (flask B), a stirred mixture of *p*-$IC_6H_4NH_2$ (1.54 g, 7.02 mmol), $Pd(PPh_3)_4$ (109 mg, 0.11 mmol), ethylene glycol (0.8 mL), and aqueous Na_2CO_3 (2 M, 18 mL), in THF (30 mL) was deoxygenated by purging with argon for 5 min and then heated to 70 ºC. The suspension in flask A was transferred to flask B by cannula and the resulting mixture was heated at 70 ºC for 16 h under argon atmosphere. The mixture was diluted with Et_2O (100 mL) and washed with water (2 × 100 mL). The combined aqueous layers were extracted with Et_2O (50 mL), after which the combined organic layers were dried over $MgSO_4$ and concentrated *in vacuo*. Flash column chromatography (SiO_2, 17:3 pentane:Et_2O) provided **4.14** as orange viscous oil (813 mg, 1.64 mmol, 47%). ^{1}H NMR (400 MHz, $CDCl_3$) δ 7.57 (s, 4H, Ar-*H*), 7.31 (d, *J* = 8.5 Hz, 2H, Ar-*H*), 7.11 (s, 1H, thiophene-*H*), 6.87 (s, 1H, thiophene-*H*), 6.66 (d, *J* = 8.6 Hz, 2H), 3.71 (br s, 2H, N-H_2), 2.84 (t, *J* = 7.4 Hz, 4H, C-H_2), 2.15-1.98 (m, 5H, overlap of C-H_2 and C-H_3), 1.96 (s, 3H, C-H_3); ^{13}C NMR (101 MHz, $CDCl_3$) δ 145.5, 140.4, 137.9, 137.7, 137.2, 136.2,

136.1, 135.4, 133.9, 132.6, 128.7, 128.4, 126.5, 125.8, 125.8, 125.7, 125.7, 125.6, 125.3, 125.2, 122.9, 122.0, 115.3, 38.5, 38.4, 23.0, 14.6, 14.3; ^{19}F NMR (376 MHz, $CDCl_3$) δ –62.45; HRMS (ESI-ion trap) *m/z*: $[M + H]^+$ Calcd for $C_{28}H_{25}F_3NS_2$ 496.1375, found 496.1361.

Compound 4.15

Compound **4.14** (300 mg, 0.61 mmol) in $CHCl_3$ (1 mL) was added dropwise to a stirred solution of maleic anhydride (60 mg, 0.61 mmol) in $CHCl_3$ (0.2 mL) at rt, after which stirring was continued for 1 h. The solution was concentrated and to the residue was added acetic anhydride (5 mL) and sodium acetate (99 mg, 1.21 mmol). The resulting mixture was heated at 120 ºC for 3 h, cooled to rt and concentrated *in vacuo*. Flash column chromatography (SiO_2, CH_2Cl_2) provided **4.15** as yellow solid (173 mg, 0.30 mmol, 50%). M.p. 186.0 – 187.6 ºC; ^{1}H NMR (400 MHz, $CDCl_3$) δ 7.60-7.54 (m, 6H, Ar-*H*), 7.32 (d, *J* = 8.5 Hz, 2H, Ar-*H*), 7.11 (s, 1H, thiophene-*H*), 7.03 (s, 1H, thiophene-*H*), 6.85 (s, 2H, *H*-C=C-*H*), 2.86 (t, *J* = 7.4 Hz, 4H, C-H_2), 2.15-2.05 (m, 2H, C-H_2), 2.02 (s, 6H, C-H_3); ^{13}C NMR (101 MHz, $CDCl_3$) δ 169.4, 138.6, 137.9, 137.8, 137.0, 136.7, 136.1, 135.2, 135.0, 134.5, 134.2, 134.2, 129.8, 128.8, 128.5, 128.1, 126.3, 125.9, 125.8, 125.8, 125.8, 125.7, 125.5, 125.4, 125.2, 124.6, 122.8, 38.4, 23.0, 14.5, 14.5; ^{19}F NMR (376 MHz, $CDCl_3$) δ –62.47; UV/vis (CH_2Cl_2, 283K): λ_{max} (ε) = 325 (30568), 287 nm (41446 $M^{-1}cm^{-1}$); HRMS (ESI-ion trap) *m/z*: $[M + H]^+$ Calcd for $C_{32}H_{25}F_3NO_2S_2$ 576.1273, found 576.1257.

Compound 4.19

To a solution of 5-bromo-2-methyl-2,3-dihydro-1*H*-cyclopenta[*a*]naphthalen-1-one **4.16**[51] (2.30 g, 8.4 mmol) in toluene (30 mL) was added Lawesson's reagent (4.15 g, 10.3 mmol). The mixture was heated at 90 ºC for 4 h. The solution was concentrated and the residue was purified by flash column chromatography (SiO_2, 1:1 pentane:CH_2Cl_2). The first red-wine band was collected (1.28 g), concentrated *in vacuo*, and added immediately to a solution of 9-diazo-2,7-difluoro-9*H*-fluorene **4.18**[52] (1.00 g, 4.4 mmol) in toluene (30 mL). The mixture was heated at 90 ºC for 12 h, cooled to rt and concentrated *in vacuo*. Flash column chromatography (SiO_2, 19:1 pentane:MTBE) afforded **4.19** as viscous orange oil (330 mg, 0.72 mmol, 16%). ^{1}H NMR (400 MHz, $CDCl_3$) δ 8.39 (d, *J* = 8.5 Hz, 1H, Ar-*H*), 7.93 (s, 1H, Ar-*H*), 7.77-7.66 (m, 2H, Ar-*H*), 7.65-7.56 (m, 3H, Ar-*H*), 7.43 (dd, *J* = 11.2, 4.0 Hz, 1H, Ar-*H*), 7.10 (td, *J* = 8.6, 2.2 Hz, 1H, Ar-*H*), 6.92 (td, *J* = 8.6, 2.3 Hz, 1H, Ar-*H*), 6.27 (dd, *J* = 10.7, 2.3 Hz, 1H, Ar-*H*), 4.32-4.21 (m, 1H, C-*H*), 3.58 (dd, *J*

= 15.3, 5.6 Hz, 1H, C-*H*), 2.77 (d, *J* = 15.3 Hz, 1H, C-*H*), 1.39 (d, *J* = 6.7 Hz, 3H, C-H_3); ^{13}C NMR (101 MHz, $CDCl_3$) δ 163.6, 162.7, 161.2, 160.3, 152.4, 147.9, 141.3, 141.3, 141.2, 138.7, 138.7, 138.6, 138.6, 135.6, 135.4, 135.4, 135.0, 135.0, 130.9, 130.8, 130.3, 129.9, 129.6, 128.3, 128.2, 127.8, 127.4, 127.3, 127.1, 126.9, 126.4, 125.3, 120.2, 120.1, 119.5, 119.4, 114.3, 114.0, 112.9, 112.7, 111.4, 111.2, 72.8, 49.5, 45.5, 45.2, 41.6, 27.0, 19.1; HRMS (APCI) *m/z*: $[M + H]^+$ Calcd for $C_{27}H_{18}BrF_2$ 459.0554, found 459.0547.

Compound 4.21

An aqueous solution of Na_2CO_3 (2 M, 1.36 mL), EtOH (1.5 mL) and 4-aminophenylboronic acid pinacol ester **4.20** (143 mg, 0.65 mmol) were added to a solution of **4.19** (250 mg, 0.55 mmol) and $Pd(PPh_3)_4$ (28 mg, 27 μmol) in toluene (5 mL). The reaction mixture was deoxygenated by purging with argon for 5 min and stirred at 95 ºC for 12 h. The mixture was diluted with water (20 mL) and EtOAc (20 mL), the layers were separated and the aqueous layer was extracted with EtOAc (3 × 20 mL). The combined organic layers were dried over $MgSO_4$ and concentrated *in vacuo*. Flash column chromatography (SiO_2, 1:1 pentane:CH_2Cl_2) provided **4.21** as orange sticky oil (173 mg, 0.30 mmol, 50%). ^{1}H NMR (400 MHz, $CDCl_3$) δ 8.09 (d, *J* = 8.3 Hz, 1H, Ar-*H*), 7.78-7.59 (m, 4H, Ar-*H*), 7.52 (s, 1H, Ar-*H*), 7.48-7.33 (m, 4H, Ar-*H*), 7.10 (td, *J* = 8.7, 2.2 Hz, 1H, Ar-*H*), 6.96-6.91 (m, 1H, Ar-*H*), 6.91-6.85 (m, 2H, Ar-*H*), 6.43 (dd, *J* = 10.9, 2.3 Hz, 1H, Ar-*H*), 4.29 (quin, *J* = 6.5 Hz, 1H, C-*H*), 3.98 (brs, 2H, N-H_2), 3.60 (dd, *J* = 15.1, 5.6 Hz, 1H, C-*H*), 2.81 (d, *J* = 15.2 Hz, 1H, C-*H*), 1.43 (d, *J* = 6.7 Hz, 3H, C-H_3); ^{13}C NMR (126 MHz, $CDCl_3$) δ 166.0, 165.2, 164.1, 163.3, 156.8, 150.4, 148.4, 146.9, 144.2, 144.1, 141.6, 141.6, 137.9, 137.4, 137.4, 137.3, 137.2, 137.1, 136.7, 133.9, 133.5, 132.9, 132.7, 131.3, 130.5, 130.5, 130.4, 130.4, 130.2, 130.0, 129.4, 128.2, 127.4, 122.8, 122.7, 122.0, 121.9, 117.8, 116.5, 116.3, 115.7, 115.5, 114.0, 113.8, 105.0, 47.8, 44.6, 22.1; HRMS (ESI-ion trap) *m/z*: $[M + H]^+$ Calcd for $C_{33}H_{24}F_2N$ 472.1871, found 472.1865.

Compound 4.22

Compound **4.21** (100 mg, 0.21 mmol) in $CHCl_3$ (1 mL) was added dropwise to a stirred solution of maleic anhydride (20.1 mg, 0.21 mmol) in $CHCl_3$ (0.2 mL) at rt, after which stirring was continued for 1 h. The solution was concentrated and the residue was treated with acetic anhydride (2 mL) and sodium acetate (34.8 mg, 0.42 mmol). This mixture was heated at 120 ºC for 3 h, cooled to rt and concentrated *in vacuo*. Flash column chromatography (SiO_2, CH_2Cl_2) provided

4.22 as yellow solid (65 mg, 0.12 mmol, 56%). M.p. 300.5 – 301.6 ºC; ^{1}H NMR (500 MHz, $CDCl_3$) δ 8.05 (d, *J* = 8.6 Hz, 1H, Ar-*H*), 7.82 (d, *J* = 8.4 Hz, 1H, Ar-*H*), 7.78-7.63 (m, 5H, Ar-*H*), 7.58 (d, *J* = 7.6 Hz, 3H, Ar-*H*), 7.49 (t, *J* = 7.6 Hz, 1H, Ar-*H*), 7.42 (t, *J* = 7.4 Hz, 1H, Ar-*H*), 7.29 (s, 1H, Ar-*H*), 7.13 (t, *J* = 8.3 Hz, 1H, Ar-*H*), 7.00-6.93 (m, 3H, overlap of Ar-*H* and *H*-C=C-*H*), 6.46 (d, *J* = 10.7 Hz, 1H, Ar-*H*), 4.41-4.28 (m, 1H, C-*H*), 3.65 (dd, *J* = 15.3, 5.3 Hz, 1H, C-*H*), 2.86 (d, *J* = 15.1 Hz, 1H, C-*H*), 1.47 (d, *J* = 6.4 Hz, 3H, C-H_3); ^{13}C NMR (125 MHz, $CDCl_3$) δ 172.2, 166.0, 165.2, 164.1, 163.3, 156.3, 150.1, 145.4, 144.1, 144.1, 142.9, 141.5, 141.5, 138.0, 137.9, 137.6, 137.0, 133.5, 133.5, 133.4, 132.5, 131.9, 130.0, 129.9, 129.7, 128.6, 128.6, 127.8, 122.8, 122.7, 122.1, 122.0, 116.7, 116.5, 115.8, 115.6, 114.1, 113.9, 47.9, 44.6, 22.0; UV/Vis (CH_2Cl_2, 283K): λ_{max} (ε) = 405 (27161), 314 nm (20017 $M^{-1}cm^{-1}$); HRMS (ESI-ion trap) *m/z*: $[M + H]^+$ Calcd for $C_{37}H_{23}F_2NO_2$ 551.1691, found 551.1681.

General method **for the synthesis of 4.1, 4.2, 4.3, 4.4, 4.5, 4.6**

A solution of diene (**4.8** or **4.9**, 25 mg) and dienophile (**4.11**, **4.15**, or **4.22**, 1.1 equiv) in CH_2Cl_2 (0.02 M) was stirred at rt until TLC and ^{1}H NMR indicated complete conversion. The solvent was evaporated to yield the crude product. The products were obtained after filtration of the crude material through a short plug of SiO_2 with CH_2Cl_2 as eluent to remove the unreacted dienophile, and subsequently using EtOAc to collect the product.

Compound *trans*-4.1

Following *general method*, *trans*-**4.1** was obtained (33 mg, 0.027 mmol, 96%) as an orange oil. ^{1}H NMR (400 MHz, $CDCl_3$) δ 7.98 (d, *J* = 8.3 Hz, 2H, Ar-*H*), 7.88 (d, *J* = 8.6 Hz, 2H, Ar-*H*), 7.77 (d, *J* = 8.4 Hz, 2H, Ar-*H*), 6.98 (s, 2H, Ar-*H*), 6.89 (s, 2H, Ar-*H*), 6.82 (d, *J* = 8.6 Hz, 2H, Ar-*H*), 4.05 – 3.86 (m, 8H, OC-H_2), 3.04 (s, 2H, C=OC-*H*), 2.86 (dt, *J* = 12.0, 7.3 Hz, 8H, C-H_2), 2.32 (s, 6H, SC=OC-H_3), 2.29 (s, 6H, SC=OC-H_3), 2.26 (s, 6H, ArCC-H_3), 1.84 – 1.71 (m, 8H, C-H_2), 1.65 – 1.35 (m, 24H, C-H_2); ^{13}C NMR (101 MHz, $CDCl_3$) δ 195.9, 195.9, 174.7, 154.2, 151.6, 147.8, 147.5, 138.0, 134.5, 134.3, 127.2, 126.3, 126.3, 123.7, 123.2, 109.7, 109.3, 69.8, 69.8, 52.8, 44.1, 30.6, 30.6, 29.5, 29.5, 29.3, 29.2, 29.0, 28.99, 28.5, 28.5, 25.6, 25.5, 16.0; ^{19}F NMR (376 MHz, $CDCl_3$) δ –62.60; UV/Vis (CH_2Cl_2, 283 K): λ_{max} (ε) = 454 (964), 322 (24068), 296 nm (23343 $M^{-1}cm^{-1}$); HRMS (ESI-ion trap) *m/z*: $[M + Na]^+$ Calcd for $C_{65}H_{80}F_3N_3O_{10}S_4Na$ 1270.4570, found 1270.4573.

Compound *trans*-4.2

Following *general method*, *trans*-**4.2** was obtained (34 mg, 0.031 mmol, 95%) as an orange oil. ^{1}H NMR (400 MHz, $CDCl_3$) δ 7.98 (d, *J* = 8.3 Hz, 2H, Ar-*H*), 7.88 (d, *J* = 8.7 Hz, 2H), 7.78 (d, *J* = 8.5 Hz, 2H, Ar-*H*), 6.99 (s, 2H, Ar-*H*), 6.90 (s, 2H, Ar-*H*), 6.83 (d, *J* = 8.7 Hz, 2H, Ar-*H*), 4.07 – 3.87 (m, 8H, OC-H_2), 3.27 (dt, *J* = 14.1, 6.9 Hz, 8H, C-H_2), 3.05 (s, 2H, C=OC-*H*), 2.27 (s, 6H, ArCC-H_3), 1.87 – 1.71 (m, 8H, C-H_2), 1.69 – 1.38 (m, 24H, C-H_2); ^{13}C NMR (101 MHz, $CDCl_3$) δ 174.7, 151.6, 147.8, 147.5, 138.0, 134.6, 134.3, 127.2, 126.3, 123.7, 123.1, 109.7, 109.3, 69.7, 52.8, 51.4, 51.3, 44.1, 29.3, 29.2, 28.8, 28.8, 26.5, 26.4, 25.7, 25.6, 16.0; UV/vis (CH_2Cl_2, 283 K): λ_{max} (ε) = 454 (1394), 322 (24559), 297 nm (23851 $M^{-1}cm^{-1}$); HRMS (ESI-ion trap) *m/z*: $[M + H]^+$ Calcd for $C_{57}H_{69}F_3N_{15}O_6$ 1116.5502, found 1116.5507.

Compound 4.3o

Following *general method*, **4.3**o was obtained (39 mg, 0.026 mmol, 94%) as a beige oil. ^{1}H NMR (400 MHz, $CDCl_3$) δ 7.56 (s, 4H, Ar-*H*), 7.40 (d, *J* = 8.5 Hz, 2H, Ar-*H*), 7.08 (s, 1H, thiophene-*H*), 6.97 (br s, 3H, overlap of Ar-*H* and thiophene-*H*), 6.87 (s, 2H, Ar-*H*), 6.56 (d, *J* = 8.5 Hz, 2H, Ar-*H*), 4.03 – 3.85 (m, 8H, OC-H_2), 3.01 (s, 2H, C=OC-*H*), 2.91 – 2.79 (m, 8H+4H, C-H_2), 2.32 (s, 6H, SC=OC-H_3), 2.30 (s, 6H, SC=OC-H_3), 2.25 (s, 6H, ArCC-H_3), 2.15 – 2.03 (m, 2H, C-H_2), 1.99 (s, 3H, thiophene-C-H_3), 1.98 (s, 3H, thiophene-C-H_3), 1.84 – 1.69 (m, 8H, C-H_2), 1.66 – 1.35 (m, 24H, C-H_2); ^{13}C NMR (101 MHz, $CDCl_3$) δ 195.9, 195.9, 175.0, 147.8, 147.5, 138.6, 138.1, 137.9, 137.8, 137.0, 136.7, 136.1, 135.2, 135.0, 134.8, 134.6, 134.5, 130.1, 128.7, 128.4, 128.2, 128.1, 126.8, 125.8, 125.8, 125.8, 125.7, 125.5, 125.4, 125.2, 124.5, 122.8, 109.6, 109.3, 69.8, 69.8, 52.7, 44.0, 38.4, 30.6, 30.6, 29.5, 29.5, 29.3, 29.2, 29.0, 28.5, 28.5, 25.6, 25.5, 23.0, 16.0, 14.5, 14.4; ^{19}F NMR (376 MHz, $CDCl_3$) δ –62.45; UV/vis (CH_2Cl_2, 283 K): λ_{max} (ε) = 325 (34875), 290 nm (42534 $M^{-1}cm^{-1}$); HRMS (ESI-ion trap) *m/z*: $[M + Na]^+$ Calcd for $C_{80}H_{94}F_3NO_{10}S_6Na$ 1500.5046, found 1500.5050.

Compound 4.4o

Following *general method*, **4.4**o was obtained (43 mg, 0.032 mmol, 98%) as an beige oil. ^{1}H NMR (400 MHz, $CDCl_3$) δ 7.56 (s, 4H, Ar-*H*), 7.39 (d, *J* = 8.5 Hz, 2H, Ar-*H*), 7.07 (s, 1H, thiophene-*H*), 6.97 (s, 2H, Ar-*H*), 6.96 (s, 1H, thiophene-*H*), 6.88 (s, 2H, Ar-*H*), 6.56 (d, *J* = 8.6 Hz, 2H, Ar-*H*), 4.05 – 3.84 (m, 8H, OC-H_2), 3.26 (dt, *J* = 14.1, 6.9 Hz, 8H, C-H_2), 3.01 (s, 2H, C=OC-*H*), 2.83 (s, 4H, C-H_2), 2.25 (s, 6H, ArCC-H_3), 2.14 – 2.04 (m, 2H, C-H_2), 1.99 (s, 3H, thiophene-C-

H$_3$), 1.98 (s, 3H, thiophene-C-*H*$_3$), 1.86 – 1.70 (m, 8H, C-*H*$_2$), 1.68 – 1.34 (m, 24H, C-*H*$_2$); ^{13}C NMR (101 MHz, $CDCl_3$) δ 175.0, 174.9, 147.7, 147.4, 138.6, 138.1, 137.9, 137.8, 136.9, 136.7, 136.1, 135.3, 134.9, 134.8, 134.6, 134.5, 130.1, 126.8, 125.8, 125.8, 125.4, 125.2, 124.6, 109.6, 109.3, 69.7, 69.7, 52.7, 51.4, 51.3, 44.0, 38.4, 29.3, 29.2, 28.8, 28.8, 26.5, 26.4, 25.7, 25.6, 23.0, 16.0, 14.4, 14.4; ^{19}F NMR (376 MHz, $CDCl_3$) δ –62.45; UV/vis (CH_2Cl_2, 283 K): λ_{max} (ε) = 325 (21568), 290 nm (36490 $M^{-1}cm^{-1}$); HRMS (ESI-ion trap) *m/z*: $[M + H]^+$ Calcd for $C_{72}H_{83}F_3N_{13}O_6S_2$ 1346.5977, found 1346.5992.

Compound stable-4.5

Following *general method*, stable-**4.5** was obtained (39 mg, 0.027 mmol, 97%) as an yellow oil. ^{1}H NMR (400 MHz, CD_2Cl_2) δ 7.96 (d, *J* = 8.4 Hz, 1H, Ar-*H*), 7.81 – 7.73 (m, 2H, Ar-*H*), 7.72 – 7.64 (m, 2H, Ar-*H*), 7.59 (d, *J* = 8.2 Hz, 2H, Ar-*H*), 7.55 (s, 1H, Ar-*H*), 7.47 (t, *J* = 7.2 Hz, 1H, Ar-*H*), 7.40 (t, *J* = 7.2 Hz, 1H, Ar-*H*), 7.13 (td, *J* = 8.7, 2.2 Hz, 1H, Ar-*H*), 7.04 (s, 2H, Ar-*H*), 7.00 – 6.91 (m, 3H, Ar-*H*), 6.83 (d, *J* = 8.3 Hz, 2H, Ar-*H*), 6.43 (dd, *J* = 10.9, 2.3 Hz, 1H, Ar-*H*), 4.33 (quin, *J* = 6.6 Hz, 1H, C-*H*), 4.09 – 3.88 (m, 9H, OC-*H*$_2$), 3.64 (dd, *J* = 15.1, 5.6 Hz, 1H, C-*H*), 3.11 (s, 2H, C=OC-*H*), 2.92 – 2.79 (m, 8H, C-*H*$_2$), 2.32 (s, 6H, SC=OC-*H*$_3$), 2.30 (s, 6H, SC=OC-*H*$_3$), 2.27 (s, 3H, ArCC-*H*$_3$), 2.25 (s, 3H, ArCC-*H*$_3$), 1.85 – 1.70 (m, 8H, C-*H*$_2$), 1.68 – 1.25 (m, 24+3H, overlap of C-*H*$_2$ and C-*H*$_3$); ^{13}C NMR (101 MHz, CD_2Cl_2) δ 195.5, 195.4, 174.9, 163.5, 162.7, 161.1, 160.3, 153.9, 147.9, 147.8, 147.5, 142.7, 141.4, 140.8, 138.8, 138.2, 135.2, 134.9, 131.4, 130.7, 130.6, 129.8, 129.0, 127.2, 127.0, 126.8, 126.6, 125.8, 125.2, 120.1, 119.4, 113.9, 113.6, 112.8, 111.3, 110.0, 109.4, 70.0, 69.8, 45.2, 44.0, 41.9, 30.4, 30.4, 29.5, 29.5, 29.4, 29.3, 28.9, 28.9, 28.5, 28.5, 25.6, 25.5, 25.5, 19.0, 15.8; UV/vis (CH_2Cl_2, 283 K): λ_{max} (ε) = 402 nm (23194 $M^{-1}cm^{-1}$); HRMS (ESI-ion trap) *m/z*: $[M + Na]^+$ Calcd for $C_{85}H_{93}F_2NO_{10}S_4Na$ 1476.5542, found 1476.5531.

Compound stable-4.6

Following *general method*, stable-**4.6** was obtained (42 mg, 0.031 mmol, 97%) as a yellow oil. ^{1}H NMR (400 MHz, CD_2Cl_2) δ 7.95 (d, *J* = 7.9 Hz, 1H, Ar-*H*), 7.79 – 7.72 (m, 2H, Ar-*H*), 7.71 – 7.64 (m, 2H, Ar-*H*), 7.61 – 7.56 (m, 2H, Ar-*H*), 7.55 (s, 1H, Ar-*H*), 7.46 (dd, *J* = 11.2, 4.2 Hz, 1H, Ar-*H*), 7.42 – 7.36 (m, 2H, Ar-*H*), 7.13 (td, *J* = 8.8, 2.2 Hz, 1H, Ar-*H*), 7.03 (s, 2H, Ar-*H*), 6.99 – 6.92 (m, 2H, Ar-*H*), 6.82 (d, *J* = 8.5 Hz, 2H, Ar-*H*), 6.42 (dd, *J* = 10.9, 2.3 Hz, 1H, Ar-*H*), 4.36 – 4.28 (m, 1H, C-*H*), 4.09 – 3.90 (m, 8H, OC-*H*$_2$), 3.63 (dd, *J* = 15.2, 5.5 Hz, 1H, C-*H*), 3.35 – 3.16 (m, 8H, C-*H*$_2$), 3.11 (s, 2H, C=OC-*H*), 2.85 (d, *J* = 15.3 Hz, 1H, C-*H*), 2.30

(s, 6H, ArCC-H_3), 1.89 – 1.71 (m, 8H, C-H_2), 1.71 – 1.23 (m, 24+3H, overlap of C-H_2 and C-H_3); ^{13}C NMR (101 MHz, CD_2Cl_2) δ 174.9, 163.6, 162.7, 161.2, 160.3, 153.9, 147.9, 147.8, 147.5, 142.6, 141.5, 141.4, 140.9, 138.9, 138.8, 138.2, 135.3, 135.2, 135.0, 134.9, 131.4, 130.7, 130.6, 129.8, 129.0, 127.3, 127.0, 126.8, 126.6, 125.8, 125.2, 120.2, 120.1, 119.5, 119.4, 113.9, 113.6, 112.8, 112.5, 111.3, 111.1, 110.0, 109.4, 69.9, 69.8, 51.4, 51.4, 51.3, 45.2, 44.0, 41.9, 29.4, 28.8, 26.47, 26.43, 25.63, 18.99, 15.82; UV/vis (CH_2Cl_2, 283 K): λ_{max} (ε) = 402 nm (18104 $M^{-1}cm^{-1}$); HRMS (ESI-ion trap) *m/z*: $[M + H]^+$ Calcd for $C_{77}H_{81}F_2N_{13}O_6$ 1322.6474, found 1322.6489.

4.5.3 DFT calculations[§]

The Gaussian 09 program was used for geometry optimizations and the calculation of energies. Initial geometries were optimized at the semi-empirical PM6 level. Further geometry optimizations were performed at the DFT B3LYP/6-31G(d,p) level with tight convergence criteria; -O$(CH_2)_6$SAc or -O$(CH_2)_6N_3$ groups were replaced with -OCH3 groups to reduce calculation cost. Two planes are defined, the first plane through the four oxygen atoms on the tetrapod, the second plane defined by the seven atoms making up the maleimide group. The angle between the two planes is calculated from their normal vectors. Vibrational analyses have been performed to ascertain minimum energy geometries.

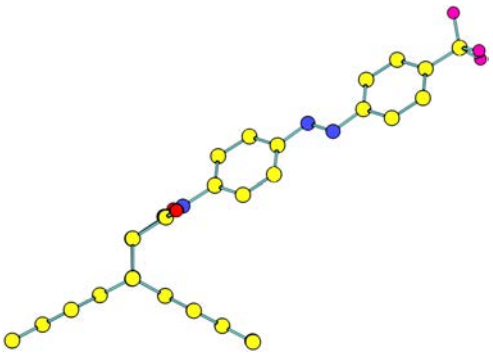

Figure 4.5 B3LYP/6-31G(d,p) optimized structure for tetrapodal azobenzene. H-atoms are all omitted. The angle between the two defined planes is 33.7 º.

[§] Jos C. M. Kistemaker is acknowledged for the computational chemistry.

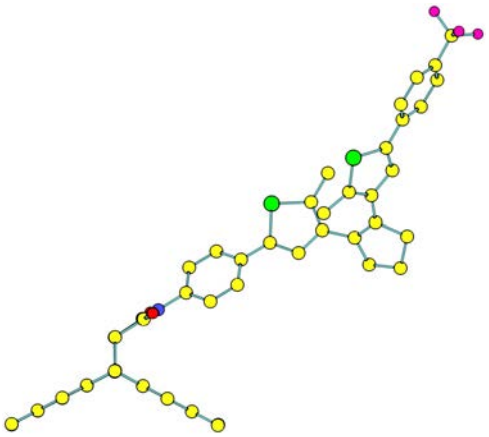

Figure 4.6 B3LYP/6-31G(d,p) optimized structure for tetrapodal dithienylethene. H-atoms are all omitted. The angle between the two defined planes is 33.3 º.

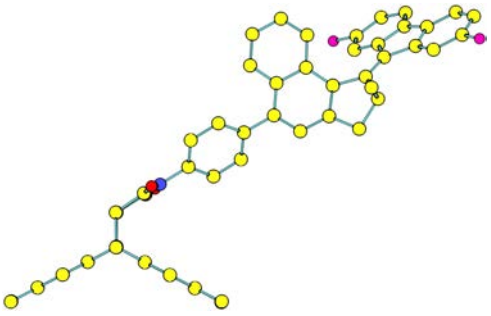

Figure 4.7 B3LYP/6-31G(d,p) optimized structure for tetrapodal molecular motor. H-atoms are all omitted. The angle between the two defined planes is 33.5 º.

4.6 References

[1] Saha, S.; Stoddart, J. F. *Chem. Soc. Rev.* **2006**, *36*, 77–92.

[2] Browne, W. R.; Feringa, B. L. *Nat. Nanotechnol.* **2006**, *1*, 25–35.

[3] Kay, E. R.; Leigh, D. A.; Zerbetto, F. *Angew. Chem. Int. Ed.* **2007**, *46*, 72–191.

[4] *Molecular Devices and Machines: Concepts and Perspectives for the Nanoworld*; Balzani, V., Credi, A., Venturi, M., Eds.; Wiley-VCH: Weinheim, **2008**.

[5] *From Non-Covalent Assemblies to Molecular Machines*; Sauvage, J.-P., Gaspard, P.; Wiley-VCH: Weinheim, **2010**.

[6] Coskun, A.; Banaszak, M.; Astumian, R. D.; Stoddart, J. F.; Grzybowski, B. A. *Chem. Soc. Rev.* **2012**, *41*, 19–30.

[7] Berná, J.; Leigh, D. A.; Lubomska, M.; Mendoza, S. M.; Pérez, E. M.; Teobaldi, G.; Zerbetto, F. *Nat. Mater.* **2005**, *4*, 704–710.

[8] Tian, D.; Song, Y.; Jiang, L. *Chem. Soc. Rev.* **2013**, *42*, 5184–5209.

[9] Hutchison, J. A.; Uji-i, H.; Deres, A.; Vosch, T.; Rocha, S.; Müller, S.; Bastian, A. A.; Enderlein, J.; Nourouzi, H.; Li, C.; Herrmann, A.; Müllen, K.; De Schryver, F.; Hofkens, J. *Nat. Nanotechnol.* **2014**, *9*, 131–136.

[10] Klajn, R. *Chem. Soc. Rev.* **2014**, *43*, 148–184.

[11] Donhauser, Z. J.; Mantooth, B. A.; Kelly, K. F.; Bumm, L. A.; Monnell, J. D.; Stapleton, J. J.; Price, D. W., Jr; Rawlett, A. M.; Allara, D. L.; Tour, J. M.; Weiss, P. S. *Science* **2001**, *292*, 2303–2307.

[12] Katsonis, N.; Kudernac, T.; Walko, M.; van der Molen, S. J.; van Wees, B. J.; Feringa, B. L. *Adv. Mater.* **2006**, *18*, 1397–1400.

[13] Moore, A. M.; Dameron, A. A.; Mantooth, B. A.; Smith, R. K.; Fuchs, D. J.; Ciszek, J. W.; Maya, F.; Yao, Y.; Tour, J. M.; Weiss, P. S. *J. Am. Chem. Soc.* **2006**, *128*, 1959–1967.

[14] Nakanishi, H.; Bishop, K. J. M.; Kowalczyk, B.; Nitzan, A.; Weiss, E. A.; Tretiakov, K. V.; Apodaca, M. M.; Klajn, R.; Stoddart, J. F.; Grzybowski, B. A. *Nature* **2009**, *460*, 371–375.

[15] Göstl, R.; Senf, A.; Hecht, S. *Chem. Soc. Rev.* **2014**, *43*, 1982–1996.

[16] *Molecular Switches, 2nd Ed*; Browne, W. R., Feringa, B. L., Eds; Wiley-VCH: Weinheim, **2011**.

[17] Klajn, R. *Pure Appl. Chem.* **2010**, *82*, 2247–2279.

[18] Irie, M.; Mohri, M. *J. Org. Chem.* **1988**, *53*, 803–808.

[19] Castellanos, S.; Vieira, A. A.; Illescas, B. M.; Sacchetti, V.; Schubert, C. Moreno, J.; Guldi, D. M.; Hecht, S.; Martín, N. *Angew. Chem. Int. Ed.* **2013**, *52*, 13985–13990.

[20] Kudernac, T.; Ruangsupapichat, N.; Parschau, M.; Maciá, B.; Katsonis, N.; Harutyunyan, S. R.; Ernst, K.-H.; Feringa, B. L. *Nature* **2011**, *479*, 208–211.

[21] Wang, J.; Feringa, B. L. *Science* **2011**, *331*, 1429–1432.

[22] Hugel, T.; Holland, N. B.; Cattani, A.; Moroder, L.; Seitz, M.; Gaub, H. E. *Science* **2002**, *296*, 1103–1106.

[23] Liu, Y.; Flood, A. H.; Bonvallet, P. A.; Vignon, S. A.; Northrop, B. H.; Tseng, H.-R.; Jeppesen, J. O.; Huang, T. J.; Brough, B.; Baller, M.; Magonov, S.; Solares, S. D.; Goddard, W. A.; Ho, C.-M.; Stoddart, J. F. *J. Am. Chem. Soc.* **2005**, *127*, 9745–9759.

[24] Ferri, V.; Elbing, M.; Pace, G.; Dickey, M. D.; Zharnikov, M.; Samorì, P.; Mayor, M.; Rampi, M. A. *Angew. Chem. Int. Ed.* **2008**, *47*, 3407–3409.

[25] Balzani, V.; Credi, A.; Venturi, M. *ChemPhysChem* **2008**, *9*, 202–220.

[26] Browne, W. R.; Feringa, B. L. *Annu. Rev. Phys. Chem.* **2009**, *60*, 407–428.

[27] Chen, K.-Y.; Ivashenko, O.; Carroll, G. T.; Robertus, J.; Kistemaker, J. C. M.; London, G.; Browne, W. R.; Rudolf, P.; Feringa, B. L. *J. Am. Chem. Soc.* **2014**, *136*, 3219–3224.

[28] Sun, R.; Xue, C.; Ma, X.; Gao, M.; Tian, H.; Li, Q. *J. Am. Chem. Soc.* **2013**, *135*, 5990–5993.

[29] Ichimura, K.; Oh, S. K.; Nakagawa, M. *Science* **2000**, *288*, 1624–1626.

[30] Kumar, A. S.; Ye, T.; Takami, T.; Yu, B. C.; Flatt, A. K.; Tour, J. M.; Weiss, P. S. *Nano Lett.* **2008**, *8*, 1644–1648.

[31] Han, M.; Ishikawa, D.; Honda, T.; Ito, E.; Hara, M. *Chem. Commum.* **2010**, *46*, 3598–600.

[32] Lim, H. S.; Lee, W. H.; Lee, S. G.; Lee, D.; Jeon, S.; Cho, K. *Chem. Commun.* **2010**, *46*, 4336–4338.

[33] Min, M.; Bang, G. S.; Lee, H.; Yu, B. C. *Chem. Commum.* **2010**, *46*, 5232–5234.

[34] Han, M. N.; Honda, T.; Ishikawa, D.; Ito, E.; Hara, M.; Norikane, Y. *J. Mater. Chem.* **2011**, *21*, 4696–4702.

[35] Valley, D. T.; Onstott, M.; Malyk, S.; Benderskii A. V. *Langmuir*, **2013**, *29*, 11623−11631.

[36] Carroll, G. T.; London, G.; Landaluce, T. F.; Rudolf, P.; Feringa, B. L. *ACS Nano* **2011**, *5*, 622–630.

[37] London, G.; Chen, K.-Y.; Carroll, G. T.; Feringa, B. L. *Chem. Eur. J.* **2013**, *19*, 10690–10697.

[38] Pijper, T. C.; Kudernac, T.; Browne, W. R.; Feringa B. L. *J. Phys. Chem. C* **2013**, *117*, 17623−17632.

[39] Zhang, J.; Zou, Q.; Tian, H. *Adv. Mater.* **2013**, *25*, 378–399.

[40] Love, J. C.; Estroff, L. A.; Kriebel, J. K.; Nuzzo, R. G.; Whitesides, G. M. *Chem. Rev.* **2005**, *105*, 1103–1169.

[41] Shirai, Y.; Cheng, L.; Chen, B.; Tour, J. M. *J. Am. Chem. Soc.* **2006**, *128*, 13479–13489.

[42] Kolb, H. C.; Finn, M. G.; Sharpless, K. B. *Angew. Chem. Int. Ed.* **2001**, *40*, 2004–2021.

[43] Vachon, J.; Carroll, G. T.; Pollard, M. M.; Mes, E. M.; Brouwer, A. M.; Feringa, B. L. *Photochem. Photobiol. Sci.* **2014**, *13*, 241–246.

[44] Such, G. K.; Quinn, J. F.; Quinn, A.; Tjipto, E.; Caruso, F. *J. Am. Chem. Soc.* **2006**, *128*, 9318–9319.

[45] Ranjan, R.; Brittain, W. J. *Macromolecules* **2007**, *40*, 6217–6223.

[46] Bova, S.; Saponara, S.; Rampa, A.; Gobbi, S.; Cima, L.; Fusi, F.; Sgaragli, G.; Cavalli, M.; de los Rios, C.; Striessnig, J.; Bisi, A. *Org. Lett.* **2009**, *52*, 1259–1262.

[47] Han, T.; Chen, C.-F. *J. Org. Chem.* **2008**, *73*, 7735–7742.

[48] Yoshimitsu, Z.; Nakajima, A.; Watanabe, T.; Hashimoto, K. *Langmuir* **2002**, *18*, 5818–5822.

[49] Yu, B.-C.; Shirai, Y.; Tour, J. M. *Tetrahedron* **2006**, *62*, 10303–10310.

[50] Lucas, L. N.; van Esch, J.; Kellogg, R. M.; Feringa, B. L. *Chem. Commum.* **1998**, 2313–2314.

[51] Ruangsupapichat, N. Controlling the Motion of Molecular Machines at the Nanoscale. Ph.D. Thesis, University of Groningen, page 76, April **2012**.

[52] DuPriest, M. T.; Griffin, B. W.; Kuzmich, D.; McNatt, L. G. *J. Med. Chem.* **1991**, *34*, 3229–3234.

[53] Cnossen, A.; Hou, L.; Pollard, M. M.; Wesenhagen, P. V.; Browne, W. R.; Feringa, B. L. *J. Am. Chem. Soc.* **2012**, *134*, 17613–17619.

Chapter 5

Facile Assembly of Light-Driven Molecular Motors onto a Solid Surface

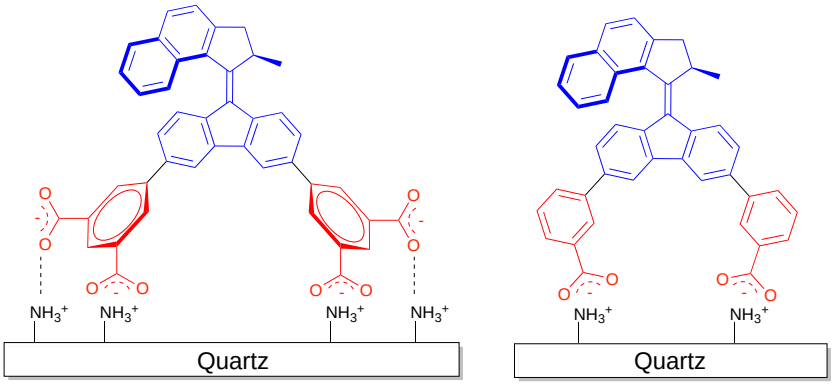

In order to improve the rotary motion of surface assembled light-driven molecular motors, tetraacid functionalized motors were bound to amine-coated surfaces without prior activation of the acid groups. In contrast to an earlier bipodal motor, the tetravalent motor showed no significant reduction on the rotation speed when attached to a surface.

This chapter has been published:
Chen, J.†; Chen, K.-Y.†; Carroll, G. T.; Feringa, B. L., *Chem. Commun.* **2014**, DOI: 10.1039/C4CC04440A
† Co-first authors

5.1 Introduction

A major challenge in nanotechnology is to build stimuli-responsive molecules to perform useful work.[1] Among the various organic molecules that have been proposed as components of future molecular devices and machines,[1] molecular motors based on overcrowded alkenes (motors) are highly promising systems.[2] These motors are able to convert light energy into repetitive unidirectional rotation, which occurs through a series of four steps involving photo-induced geometric isomerization and irreversible thermal isomerization reactions. It has been shown that molecular motors can be used to perform various tasks, such as propelling single molecules with control of directionality,[3a] controlling the chiral space in which a catalytic reaction takes place,[3b] inducing morphological changes in thin films,[3c] rotating micro-objects,[3d] and switching surface wettability in a reversible manner.[4e]

By confining rotary molecular motors on a surface, the relative rotation of one part of the molecule with respect to the other can be converted to absolute rotation of the rotor relative to the surface. We have previously designed a series of motors that can be attached to gold and quartz surfaces that bear alkyne, azide and amine functionalities *via* covalent binding.[4] When these molecules are attached to a surface, two types of orientations can be distinguished: azimuthal[4a,b,c] and altitudinal[4d,e] (Scheme 5.1). Molecular motors with rotors in either orientation were shown to undergo rotary motion upon irradiation, however, the rotary speed of a previously designed bipodal motor was found to reduce significantly due to interference as a result of close packing of these motors on the surface (Scheme 5.1b).[4d] Currently, among the key challenges in developing surface-bound devices based on molecular motors is the development of new and efficient strategies for surface preparation and to demonstrate unobstructed rotary motion in surface-bound systems.

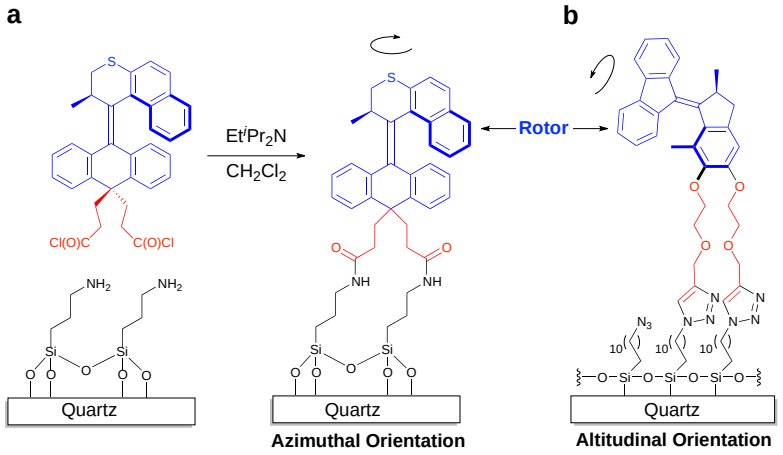

Scheme 5.1 Azimuthal (a) and altitudinal (b) rotary motors on surfaces.

Here we report novel molecular motors containing a stator functionalized with multivalent acid groups for electrostatic attachment to amine-coated surfaces (Scheme 5.2).[1e,5] The carboxylic acids do not require further activation prior to surface preparation, making this system advantageous over a previously reported system involving the reaction of carboxylic acid motors with amine-coated surfaces *via* an unstable acid chloride intermediate (Scheme 5.1a).[4b]

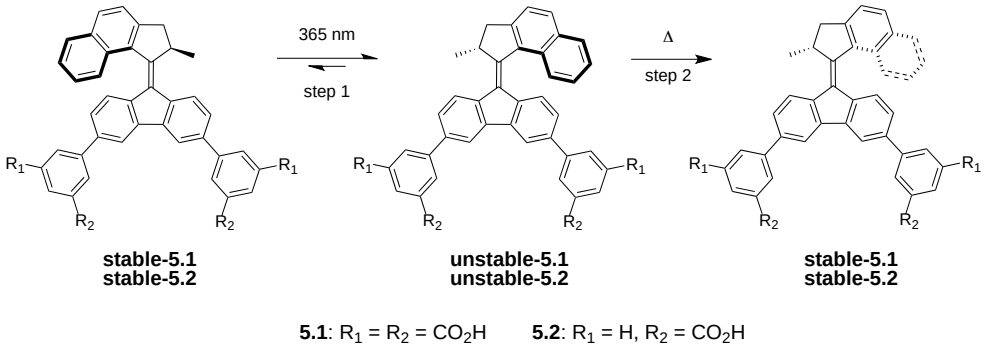

Scheme 5.2 Photochemical and thermal isomerization steps of motors **5.1** and **5.2**

Reduction in rotary speed can be overcome by designing motors **5.1** with tetravalent stators to increase the free volume between the surface-bound motors and therefore minimize intermolecular interactions.[4e] Molecular models show that meta-substitution of the biaryl units in the stator part of **5.1** with two carboxylates favors an azimuthal orientation of the rotor relative to the surface. A related

bivalent motor **5.2** was also prepared, in order to compare and understand the effect of the valency of surface attachment on the rotary speed of the surface-bound motors. The photochemically and thermally driven isomerization of these tetra- and bivalent motors **5.1** and **5.2** were compared both in solution and when attached to surfaces.

5.2 Synthesis of the tetra- and bivalent molecular motors

The approach toward the synthesis of motor **5.1** and **5.2**, which bears either four or two carboxylic acid groups at the meta-position of the biaryl units in the stator repectively, is depicted in scheme 5.3.

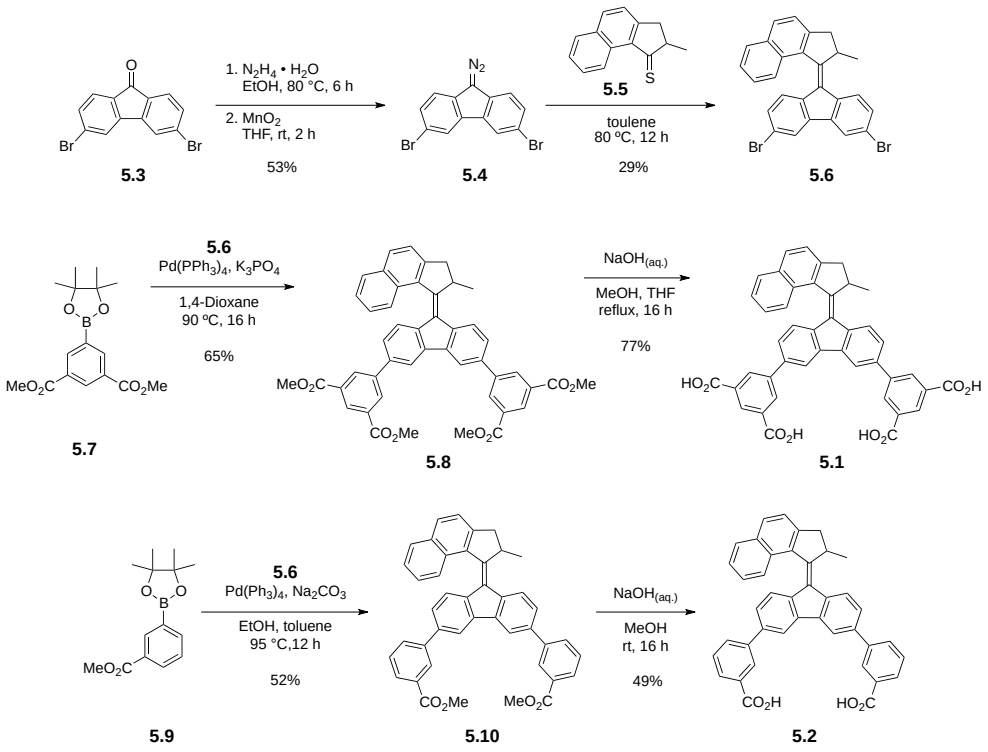

Scheme 5.3 Synthesis of molecular motors **5.1** and **5.2**.[†]

† Jiawen Chen is acknowledged for the synthesis and characterization of **5.8** and **5.1**.

3,6-Dibromo-9-fluorenone **5.3**[6] was converted to the corresponding hydrazone by heating at reflux in EtOH in the presence of hydrazine-monohydrate followed by oxidation to the diazo derivative **5.4** with manganese oxide (MnO_2) in THF. Thioketone **5.5**[7a] was reacted with diazo compound **5.4** in a Barton-Kellogg reaction,[8] followed by desulfurization, yielding dibromo motor **5.6** in 29% yield over two steps. The dibromo compound **5.6** was first functionalized with two dimethyl isophthalate groups through a Suzuki cross-coupling affording compound **5.8**, followed by hydrolysis of the ester groups yielding tetrapodal molecular motor **5.1**. The related bivalent motor **5.2** was also prepared using a similar procedure to the synthesis of **5.1**.

5.3 Photochemical and thermal isomerization studies in solution

The photochemical and thermal properties of molecular motors **5.1** and **5.2** were studied by UV/vis absorption spectroscopy. The UV/vis absorption spectra of stable-**5.1** (2.02×10^{-6} M) and stable-**5.2** (1.92×10^{-6} M) in MeOH at 278 K show absorption bands centred at 399 and 402 nm, respectively (Figure 5.1a and 5.1b, solid lines).

Irradiation with UV light (λ_{max} = 365 nm) led to a red-shift of the bands at 399 and 402 nm, indicating photochemically induced formation of the unstable isomer (Scheme 5.2, step1). This red shift is consistent with increased strain at the central double bond, and hence the generation of an isomer with a higher energy ground state.[2b] During irradiation, isosbestic points were maintained in each case. Each sample was irradiated until no further change was observed, *i.e.* the photostationary state (PSS) was reached (Scheme 5.1a and 5.1b, dashed lines). Allowing the PSS mixture of stable-**5.1**/unstable-**5.1** or stable-**5.2**/unstable-**5.2** to warm to rt resulted in a blue-shift of the bands to their original positions at 399 and 402 nm, which is consistent with thermal isomerization back to the corresponding stable isomers (Scheme 5.2, step 2).

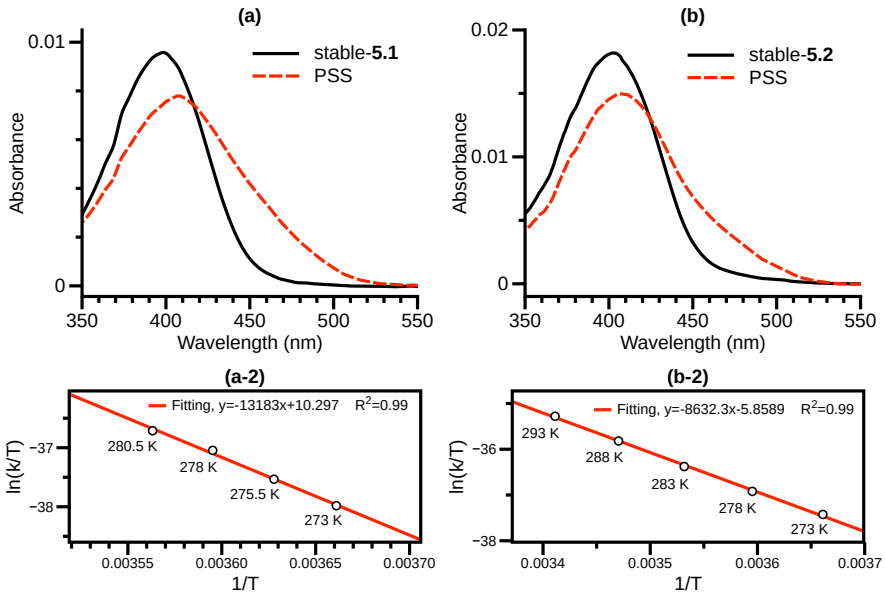

Figure 5.1 UV/vis absorption spectra (MeOH, 278 K) of stable-**5.1** (a) and stable-**5.2** (b) before irradiation (solid lines) and at the photostationary state (dashed lines). Eyring plot of the conversion of unstable-**5.1** → stable-**5.1** (a-2) and unstable-**5.2** → stable-**5.2** (b-2) *via* thermal isomerization at different temperatures.

Kinetic analyses were performed on the thermal isomerization steps of both motors (Scheme 5.2, step 2) at several temperatures by monitoring the change in absorbance at 475 nm as a function of time. The data obtained was fitted with a monoexponential decay and the rate constants (k) for the thermal isomerization steps and the Eyring plots were obtained (Figure 5.1a-2 and 5.1b-2). Using the Eyring equation, it was determined that the thermal isomerization of unstable-**5.1** → stable-**5.1** has a Gibbs free energy of activation ($\Delta^{\ddagger}G°$) of 84.5 kJ/mol ($t_{1/2}$ = 130 s at 293 K). Using the same procedure, the $\Delta^{\ddagger}G°$ of the thermal isomerization of unstable-**5.2** → stable-**5.2** was calculated to be 86.0 kJ/mol ($t_{1/2}$ = 227 s at 293 K). These values are similar to those obtained from structurally related motors.[2b,4e,7]

By studying the photochemical and thermal behaviour of **5.1** and **5.2** in solution using UV/vis absorption spectroscopy, and by analogy with similar motor systems reported previously,[2,4,7] it was anticipated that **5.1** and **5.2** function as light-driven rotary motors in solution.[2] The introduction of the carboxylic acid groups on the motor moiety does not have a significant influence on the photochemical and thermal behaviour of the molecular motors.

5.4 Surface attachment and characterization

In order to compare the photochemical and thermal behaviour of the motors in solution to those on the surfaces, surface-attached motor assemblies **5.1 MS** and **5.2 MS** were prepared (Scheme 5.4; **MS** = **M**otor **S**urface, for further details on surface preparation, see experimental section). Following literature procedures,[4c] amine-coated surfaces were prepared by immersing piranha-cleaned quartz slides in a 1 mM solution of 3-aminopropyl (diethoxy)methylsilane in toluene at rt for 12 h. The substrates were then rinsed extensively with toluene and MeOH and dried under a stream of argon. Motors **5.1** and **5.2** were grafted to amine-coated surfaces by immersing the slides in a solution of CH_2Cl_2 (10^{-4} M) containing stable-**5.1** or stable-**5.2** at rt for 6 h, followed by extensive rinsing with CH_2Cl_2 and drying under a stream of argon.

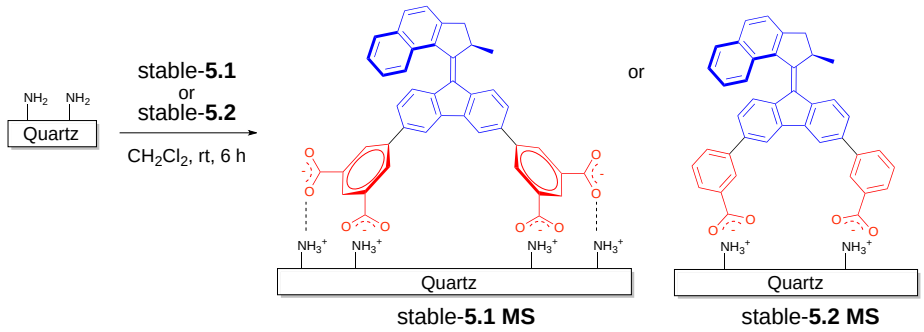

Scheme 5.4 Attachment of the tetra- and bivalent motors **5.1** and **5.2** to amine-coated quartz.

The presence of the motor on the surface was confirmed by UV/vis absorption spectroscopy and water contact angle measurements. The UV/vis absorption spectra of stable-**5.1 MS** or stable-**5.2 MS** showed the characteristic absorption bands of the motors (Figure 5.2, solid lines). The maxima of the major absorption band and the absorption profile are similar to that observed in MeOH solution (Scheme 5.1a and 5.1b, solid lines), indicating that the motors were attached to the amine-coated surface successfully.

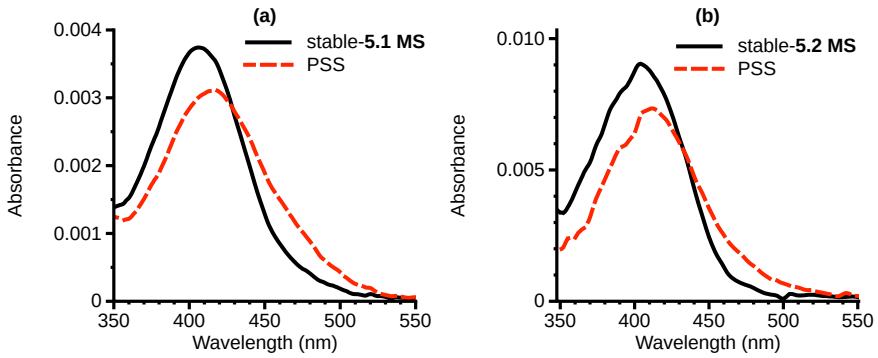

Figure 5.2 UV/vis absorption spectra (278 K) of stable-**5.1 MS** (a) and stable-**5.2 MS** (b) before irradiation (solid line) and the spectra at the photostationary state (dashed line).

Water contact angles (WCA) of the amine and motor-coated surfaces were determined by contact-angle goniometry studies using the Sessile drop method.[9] Coating an amine-functionalized surface with molecular motor **5.1** or **5.2** resulted in an increase in WCA from 40 ± 1º for the amine-coated surface to 63 ± 1º and 73 ± 1º for **5.1 MS** and **5.2 MS**, respectively (Figure 5.3). The lower WCA of **5.1 MS** compared to **5.2 MS** is likely due to the presence of two additional carboxylic acids per motor and the additional free volume between the surface-bound motors, which might allow the water to more easily access free amine groups.

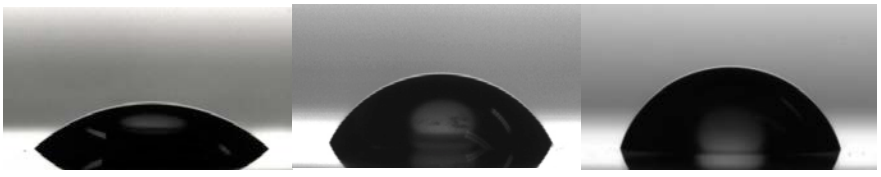

Figure 5.3 Water droplets on amine-coated quartz (left), **5.1 MS** (middle), and **5.2 MS** (right). Water contact angles of 40º, 63º and 73º were measured, respectively.

Stable-**5.1 MS** and stable-**5.2 MS** were irradiated with UV light for 15 min (λ_{max} = 365 nm, 278 K, N_2 atmosphere), which led to a red-shift in the long-wavelength absorption bands in the UV/vis absorption spectra (Figure 5.2, dashed lines), indicating the formation of the unstable-isomers of the surface-bound motors (Scheme 5.2, step 1; stable-**5.1 MS** → unstable-**5.1 MS** and stable-**5.2 MS** → unstable-**5.2 MS**). Allowing the substrate to warm to rt restored the original spectra, indicating thermal isomerization back to stable-**5.1 MS** and stable-**5.2 MS**

(Scheme 5.2, step 2). These observations are consistent with the thermal behaviour of unstable-**5.1** and unstable-**5.2** in MeOH.

To determine whether or not the surface immobilization compromises the rotary speed of the motors, the thermal isomerization step (Scheme 5.2, step 2) was measured by monitoring the decay of the absorbance at 475 nm as a function of time (Figure 5.4). The decrease in the absorbance for unstable-**5.1 MS** → stable-**5.1 MS** was fitted with a monoexponential decay, as for its solution analogue, and the half-life ($t_{1/2}$ = 161 s at rt) was extracted. This value is similar to the half-life observed in MeOH solution for unstable-**5.1** → stable-**5.1** ($t_{1/2}$ = 130 s at rt), indicating that the rotary motion of the tetravalent motor **5.1** shows minimal, if any, inhibition from neighbouring surface-bound motors.

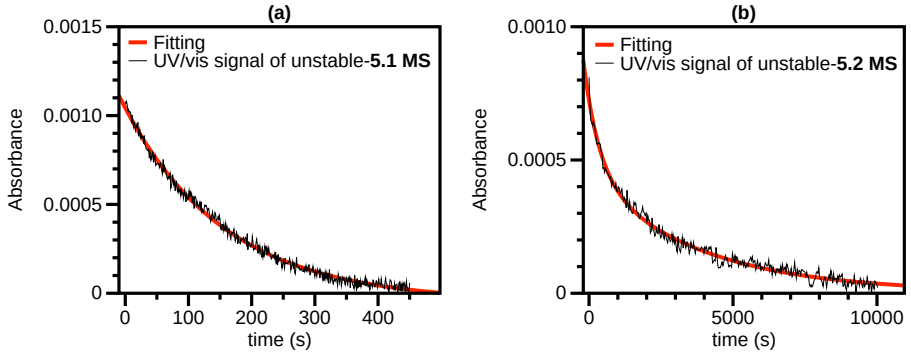

Figure 5.4 Thermal decay of UV/vis signals at 475 nm (293 K, in the dark, N_2 atmosphere) during thermal isomerization of the motors as a function of time. The thermal decay of the signals were fitted (red lines), and hence the half-lives for the rate of thermal isomerization for unstable-**5.1 MS** → stable-**5.1 MS** ($t_{1/2}$= 161 s at 293 K) and unstable-**5.2 MS** → stable-**2 MS** (T_1= 544 s; T_2= 3855 s at 293 K) were extracted.

However, in contrast to solution phase experiments, the thermal decay for unstable-**5.2 MS** → stable-**5.2 MS** suggests more complicated dynamics when the bivalent motor **5.2** binds to the surface. The time dependent change in the UV/vis signal at 475 nm was found to fit a biexponential decay and two-half lives were extracted that differ by an order of magnitude at 293 K, suggesting that at least two processes occurred during thermal isomerization. The first half-life had a value of 544 s, which is approximately 2 times than the half-life observed in solution for unstable-**5.2** → stable-**5.2** ($t_{1/2}$ = 227 s at 293 K). The second half-life had a value of 3855 s, which indicates the thermal isomerization of the surface-bound motors is slowed down considerably compared to their solution analogue.

The UV/Vis absorption of **5.1 MS** is lower in intensity than the absorption than for **5.2 MS**. We attribute the lower UV/vis signal to a lower surface coverage, although orientation can also affect the UV/vis absorbance. The lower surface coverage is most probably due to twisting of the diacid-benzene rings approximately 90 º relative to the benzene rings of the fluorene, creating more free volume between the rotors and forcing the motors to stand upright. In the case of **5.2 MS**, the surface-binding benzoic acid units occupy less space and can assume more configurations compared to a fully bound divalent unit, maximizing the number of motors that can bind to a given area of the substrate. The more complicated exponential decay may reflect a non-uniform distribution and inhomogeneity (*i.e.* various tilt angles, supramolecular interactions) of free volume in the surface-bound ensemble. Non-monoexponential kinetics were previously observed when azobenzene-side chains were bound to the polymer films. The rate of *cis* → *trans* thermal isomerization in these azobenzene films was found to deviate from a simple monoexponential decay due to neighbouring effects on the motion of the azobenzene groups.[10]

5.5 Conclusions

In conclusion, we described novel light-driven molecular motors containing either four or two carboxylic acid groups on the stator. The carboxylic acids allow for the motors to be attached to surfaces bearing amines without the need to activate the carboxylic acid (Scheme 5.1a). Both motors preserved their rotary function when attached to the amine-coated surface. Thermal isomerization of **5.1 MS** containing a tetravalent stator was not inhibited significantly by surface immobilization; however, **5.2 MS**, which contains a bivalent stator, showed a large reduction in the speed of thermal isomerization, demonstrating how subtle differences in molecular structure can considerably impact dynamic processes at interfaces in nanoscale systems. These observations and the current design feature will be key in developing advanced, dynamic surface-anchored systems.

5.6 Experimental Section

5.6.1 General remarks

For general remarks on the synthesis and characterization of compounds and intermediates, see Chapter 2. Contact Angles were measured under ambient conditions on a Dataphysics contact angle goniometer with SCA20, version 3.60.2, and software supplied by Dataphysics. Equilibrium contact angles were obtained on 1 μL water droplets on amine-coated quartz, **5.1 MS**, and **5.2 MS** using the sessile drop method. The contact angle was measured at four different locations on each surface and the results were averaged. UV/vis absorption spectra were measured with a Jasco V-630 spectrophotometer attached with NCP-706 Cell holders for maintaining samples at a fixed and uniform temperature. To generate the motors in the unstable forms, samples were irradiated with UV light (Spectroline model ENB-280C/FE lamp, λ_{max} = 365 nm; intensity ≈ 1.0 mW/cm^2) at a distance of 3 cm from the centre of the lamp. For monitoring the decay of the UV signals for unstable-**5.1** → stable-**5.1**, unstable-**5.2** → stable-**5.2**, unstable-**5.1 MS** → stable-**5.1 MS**, and unstable-**5.2 MS** → stable-**5.2 MS** at 475 nm as a function of time, a high-pass filter was mounted between the UV light source and the sample to cut off light with wavelengths below 460 nm to minimize photochemical isomerization occurring upon data recording.

5.6.2 Synthesis of compounds and intermediates

Compound 5.4

To a solution of dibromo fluorenone **5.3**[6] (800 mg, 2.4 mmol) in EtOH (280 mL), N_2H_4•H_2O (20 mL) was added and the solution was heated at 80 ºC for 6 h. Addition of water (10 mL) to the hot mixture followed by cooling to rt resulted in the precipitation of a pale yellow solid. The solid was filtered, washed with cold MeOH and dried *in vacuo*. MnO_2 (0.5 g, 5.75 mmol) was added to a stirred solution of this pale yellow solid in THF (20 mL) at rt for 2 h. The mixture was then filtered over a plug of SiO_2 and the solvent was removed under reduced pressure to afford diazo **5.4** (435 mg, 1.2 mmol, 60%) as an orange solid. (*This compound is not stable under ambient conditions and was used immediately for the synthses of* ***5.6***). ^{1}H NMR (400 MHz, $CDCl_3$) δ 8.01 (d, *J* = 1.5 Hz, 2H, Ar-*H*), 7.51 (dd, *J* = 8.3, 1.4 Hz, 2H, Ar-*H*), 7.36 (d, *J* = 8.3 Hz, 2H, Ar-*H*); ^{13}C NMR

(101 MHz, $CDCl_3$) δ 132.7, 131.8, 129.7, 125.7, 124.3, 124.1, 120.5, 118.3; HRMS (APCI-ion trap) *m/z*: $[M - N_2 + H]^+$ Calcd for $C_{13}H_7Br_2$ 320.8909, found 320.8919.

Compound 5.6

Diazo **5.4** (400 mg, 1.15 mmol) was added to a solution of thioketone **5.5**[7a] (485 mg, 2.30 mmol) in toluene (120 mL). The mixture was heated at 90 ºC for 12 h and then PPh_3 (300 mg, 1.15 mmol) was added, followed by an additional 4 h heating at 90 °C. The mixture was cooled down to rt and CH_3I (3 mL, 48 mmol) was added, followed by stirring at rt for 1 h. The mixture was concentrated *in vacuo* and purified by flash column chromatography (SiO_2, 20:1 pentane:CH_2Cl_2) affording dibromo **5.6** (169 mg, 0.34 mmol, 29%) as an orange oil. ^{1}H NMR (400 MHz, $CDCl_3$) δ 7.98 – 7.91 (m, 3H, Ar-*H*), 7.86 – 7.80 (m, 2H, Ar-*H*), 7.66 (d, *J* = 8.4 Hz, 1H, Ar-*H*), 7.59 (d, *J* = 8.2 Hz, 1H, Ar-*H*), 7.55 – 7.46 (m, 2H, Ar-*H*), 7.36 (m, 1H, Ar-*H*), 6.94 (dd, *J* = 8.5, 1.9 Hz, 1H, Ar-*H*), 6.56 (d, *J* = 8.5 Hz, 1H, Ar-*H*), 4.26 (p, *J* = 6.6 Hz, 1H, C-*H*), 3.57 (dd, *J* = 15.2, 5.6 Hz, 1H, C-*H*), 2.78 (d, *J* = 15.2 Hz, 1H, C-*H*), 1.37 (d, *J* = 6.7 Hz, 3H, C-H_3); ^{13}C NMR (101 MHz, $CDCl_3$) δ 153.0, 148.0, 140.5, 140.0, 138.6, 135.9, 135.7, 132.7, 131.6, 130.3, 129.6, 129.2, 128.9, 128.5, 127.1, 127.1, 127.0, 125.6, 125.3, 124.1, 123.1, 122.3, 121.0, 120.9, 45.5, 42.0, 19.3; HRMS (APCI-ion trap) *m/z*: $[M + H]^+$ Calcd for $C_{27}H_{19}Br_2$ 500.9848, found 500.9895.

Compound 5.10

A stirred mixture of **5.6** (300 mg, 0.60 mmol), $Pd(PPh_3)_4$ (92 mg, 0.09 mmol), EtOH (1.5 mL), aqueous $Na_2CO_{3(aq.)}$ (2 M, 3 mL), and toluene (80 mL) was purged with argon for 15 min and then heated to 95 ºC. Pinacol ester **5.9** (438 mg, 1.67 mmol) was added and the resulting mixture was heated at reflux for 16 h under argon atmosphere. The mixture was cooled down to rt and the water layer was removed. The organic layers were dried over $MgSO_4$ and concentrated *in vacuo*. Column chromatography (SiO_2, 1:1 pentane: CH_2Cl_2) afforded diester **5.10** as an orange sticky oil (190 mg, 0.31 mmol, 52%). ^{1}H NMR (400 MHz, $CDCl_3$) δ 8.48 (s, 1H, Ar-*H*), 8.35 (s, 1H, Ar-*H*), 8.21 (d, *J* = 1.2 Hz, 1H, Ar-*H*), 8.14 – 8.04 (m, 3H, Ar-*H*), 8.02 – 7.93 (m, 4H, Ar-*H*), 7.84 (dd, *J* = 14.7, 8.1 Hz, 2H, Ar-*H*), 7.72 (dd, *J* = 8.1, 1.5 Hz, 1H, Ar-*H*), 7.64 – 7.55 (m, 2H, Ar-*H*), 7.50 (t, *J* = 7.9 Hz, 2H, Ar-*H*), 7.38 (t, *J* = 7.6 Hz, 1H, Ar-*H*), 7.15 (dd, *J* = 8.2, 1.6 Hz, 1H, Ar-*H*), 6.82 (d, *J* = 8.3 Hz, 1H, Ar-*H*), 4.39 (dd, *J* = 12.7, 6.5 Hz, 1H, C-*H*), 4.00 (s, 3H, CO_2C-H_3), 3.95 (s, 3H, CO_2C-H_3), 3.63 (dd, *J* = 15.1, 5.5 Hz, 1H, C-*H*), 2.81

(d, *J* = 15.1 Hz, 1H, C-*H*), 1.44 (d, *J* = 6.7 Hz, 3H, C-H_3); ^{13}C NMR (101 MHz, $CDCl_3$) δ 167.2, 167.1, 152.2, 147.8, 141.5, 141.4, 140.5, 140.0, 139.7, 138.7, 138.5, 137.1, 136.2, 132.7, 131.6, 131.5, 131.2, 130.8, 130.6, 129.8, 129.6, 129.0, 128.8, 128.8, 128.4, 128.2, 128.1, 127.4, 126.8, 126.3, 126.2, 125.4, 125.1, 124.5, 124.0, 118.4, 117.6, 53.4, 52.3, 52.2, 45.5, 42.0, 19.5; HRMS (ESI-ion trap) *m/z*: $[M + H]^+$ Calcd for $C_{43}H_{33}O_4$ 613.2365, found 613.2373.

Compound 5.2

Diester **5.10** (300 mg, 0.49 mmol), NaOH (196 mg, 4.90 mmol), MeOH (3 mL), and H_2O (1 mL) were heated to 95 ºC for 12 h. The resulting mixture was then cooled to 5 ºC for 3 h and white precipitates were formed. The precipitates were filtered, washed with cold MeOH (5 mL), and redissolved in water (2 mL). The solution was acidified with $HCl_{(aq.)}$ (2 M) until pH = 1, and the solid was isolated by filtration, washed with cold water (10 mL) and dried *in vacuo* affording diacid **5.2** (140 mg, 0.24 mmol, 49%). ^{1}H NMR (500 MHz, DMSO-d_6) δ 8.65 (s, 1H, Ar-*H*), 8.57 (s, 1H, Ar-*H*), 8.45 (s, 1H, Ar-*H*), 8.30 (s, 1H, Ar-*H*), 8.17 (d, *J* = 7.7 Hz, 1H, Ar-*H*), 8.14 – 8.09 (m, 3H, Ar-*H*), 8.02 (t, *J* = 7.9 Hz, 2H, Ar-*H*), 7.94 (d, *J* = 7.7 Hz, 1H, Ar-*H*), 7.85 (d, *J* = 8.1 Hz, 1H, Ar-*H*), 7.76 (d, *J* = 8.2 Hz, 1H, Ar-*H*), 7.71 – 7.66 (m, 2H, Ar-*H*), 7.62 – 7.53 (m, 2H, Ar-*H*), 7.44 (t, *J* = 7.6 Hz, 1H, Ar-*H*), 7.23 (d, *J* = 8.3 Hz, 1H, Ar-*H*), 6.70 (d, *J* = 8.3 Hz, 1H, Ar-*H*), 4.40 – 4.30 (m, 1H, C-*H*), 3.63 (dd, *J* = 15.4, 5.3 Hz, 1H, C-*H*), 3.35 (brs, 3H, CO_2-*H*), 2.85 (d, *J* = 15.5 Hz, 1H, C-*H*), 1.37 (d, *J* = 6.6 Hz, 3H, C-H_3); ^{13}C NMR (101 MHz, DMSO-d_6) δ 167.9, 167.8, 152.4, 148.5, 140.9, 140.7, 140.6, 140.4, 139.4, 138.5, 138.4, 136.7, 135.7, 132.8, 132.1, 132.0, 131.9, 131.6, 131.5, 129.7, 129.6, 129.5, 129.3, 128.8, 128.7, 127.9, 127.8, 127.3, 127.0, 126.5, 126.0, 126.0, 124.9, 124.8, 124.7, 119.2, 118.6, 45.5, 41.9, 19.7; HRMS (ESI-ion trap) *m/z*: $[M + H]^+$ Calcd for $C_{41}H_{28}O_4$ 585.2050, found 585.2060.

5.6.3 Preparation of the surface

Quartz slides (Ted Pella, Inc) were cleaned by immersing in a piranha solution (3/7 ratio of 30% H_2O_2 in H_2SO_4) at 90 ºC for 1 h and rinsed copiously first with doubly distilled water (3 times), then with MeOH and dried under a stream of N_2 before surface modification (*Caution! Piranha solution is highly corrosive and reactive toward organics*). The piranha-cleaned quartz slides were silanized by[11] immersing in a 1 mM solution of 3-aminopropyl(diethoxy)methylsilane in freshly

distilled toluene at rt for 12 h, then rinsed copiously with toluene and MeOH, sonicated first in toluene, then in MeOH and dried under a stream of argon. The amine-coated slides were immersed in dried CH_2Cl_2 solution (10 mL) containing **5.1** or **5.2** (10^{-4} M) at rt for 6 h, then the slides were removed, washed with copious CH_2Cl_2 and dried under a stream of argon.

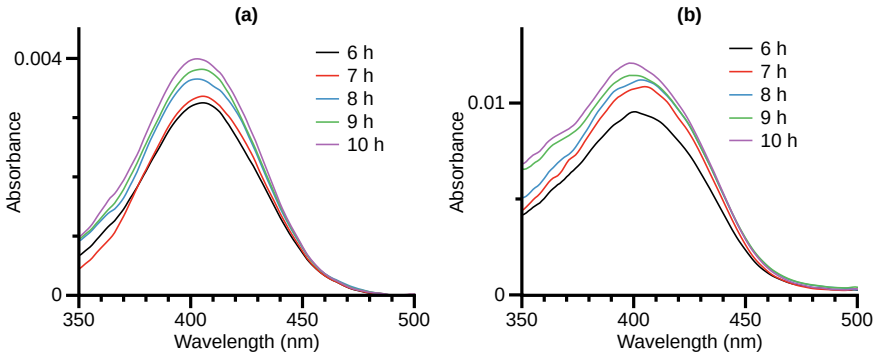

Figure 5.5 UV/vis absorption spectra of **5.1 MS** (a) and **5.2 MS** (b) after reaction with amine-coated quartz slides for various amounts of time. The signal increases with reaction time.

5.7 References

[1] (a) Saha, S.; Stoddart, J. F. *Chem. Soc. Rev.* **2007**, *36*, 77–92. (b) Browne, W. R.; Feringa, B. L. *Nat. Nanotech.* **2006**, *1*, 25–35. (c) Kay, E. R.; Leigh, D. A.; Zerbetto, F. *Angew. Chem. Int. Ed.* **2007**, *46*, 72–191. (d) *Molecular Devices and Machines: Concepts and Perspectives for the Nanoworld*; Balzani, V., Credi, A., Venturi, M., Eds.; Wiley-VCH: Weinheim, **2008**. (e) *From Non-Covalent Assemblies to Molecular Machines*; Sauvage, J.-P., Gaspard, P., Eds.; Wiley-VCH: Weinheim, **2010**. (f) Coskun, A.; Banaszak, M.; Astumian, R. D.; Stoddart, J. F.; Grzybowski, B. A. *Chem. Soc. Rev.* **2012**, *41*, 19–30.

[2] (a) Koumura, N.; Zijlstra, R. W.; van Delden, R. A.; Harada, N.; Feringa, B. L. *Nature* **1999**, *401*, 152–155. (b) Koumura, N.; Geertsema, E. M.; van Gelder, M. B.; Meetsma, A.; Feringa, B. L. *J. Am. Chem. Soc.* **2002**, *124*, 5037–5051.

[3] (a) Kudernac, T.; Ruangsupapichat, N.; Parschau, M.; Maciá, B.; Katsonis, N.; Harutyunyan, S. R.; Ernst, K.-H.; Feringa, B. L. *Nature* **2011**, *479*, 208–211. (b) Wang, J.; Feringa, B. L. *Science* **2011**, *331*, 1429–1432. (c) Carroll, G. T.; Feringa, B. L. *Org. Biomol. Chem.* **2013**, *11*, 3477–3483. (d) Eelkema, R.; Pollard, M. M.; Vicario, J.; Katsonis, N.; Ramon, B. S.; Bastiaansen, C. W. M.; Broer, D. J.; Feringa, B. L. *Nature* **2006**, *440*, 163–163.

[4] (a) van Delden, R. A.; Wiel, ter, M. K. J.; Pollard, M. M.; Vicario, J.; Koumura, N.; Feringa, B. L. *Nature* **2005**, *437*, 1337–1340. (b) Pollard, M. M.; Lubomska, M.; Rudolf, P.; Feringa, B. L. *Angew. Chem.* **2007**, *119*, 1300–1302. (c) Carroll, G. T.; Pollard, M. M.; van Delden, R.; Feringa, B. L. *Chem. Sci.* **2010**, *1*, 97–101. (d) Carroll, G. T.; London, G.; Landaluce, T. F.; Rudolf, P.; Feringa, B. L. *ACS Nano* **2011**, *5*, 622–630. (e) Chen, K.-Y.; Ivashenko, O.; Carroll, G. T.; Robertus, J.; Kistemaker, J. C. M.; London, G.; Browne, W. R.; Rudolf, P.; Feringa, B. L. *J. Am. Chem. Soc.* **2014**, *136*, 3219–3224.

[5] (a) Berná, J.; Leigh, D. A.; Lubomska, M.; Mendoza, S. M.; Pérez, E. M.; Rudolf, P.; Teobaldi, G.; Zerbetto, F. *Nat. Mater.* **2005**, *4*, 704–710. (b) Hutchison, J. A.; Uji-i, H.; Deres, A.; Vosch, T.; Rocha, S.; Müller, S.; Bastian, A. A.; Enderlein, J.; Nourouzi, H.; Li, C.; Herrmann, A.; Müllen, K.; De Schryver, F.; Hofkens, J. *Nat. Nanotech.* **2014**, *9*, 131–136.

[6] Cnossen, A. Overcrowded alkene-based molecular motors: from single molecule to multimotor systems. Ph.D. Thesis, University of Groningen, page 36, March **2013**.

[7] (a) Pijper, D.; Feringa, B. L. *Angew. Chem. Int. Ed. Engl.* **2007**, *46*, 3693–3696. (b) Vicario, J.; Walko, M.; Meetsma, A.; Feringa, B. L. *J. Am. Chem. Soc.* **2006**, *128*, 5127–5135.

[8] (a) Barton, D. H. R.; Willis, B. J. *J. Chem. Soc. –Perkin Trans. 1* **1972**, 305–310. (b) Buter, J.; Wassenaar, S.; Kellogg, R. M. *J. Org. Chem.* **1972**, *37*, 4045–4060.

[9] Ivashenko, O.; Logtenberg, H.; Areephong, J.; Coleman, A. C.; Wesenhagen, P. V.; Geertsema, E. M.; Heureux, N.; Feringa, B. L.; Rudolf, P.; Browne, W. R. *J. Phys. Chem. C* **2011**, *115*, 22965–22975.

[10] (a) Barrett, C.; Natansohn, A.; Rochon, P. *Macromolecules* **1994**, *27*, 4781–4786. (b) Priimagi, A.; Lindfors, K.; Kaivola, M.; Rochon, P. *ACS Appl. Mater. Interfaces* **2009**, *1*, 1183–1189.

[11] Doron-Mor, I.; Barkay, Z.; Filip-Granit, N.; Vaskevich, A.; Rubinstein, I. *Chem. Mater.* **2004**, *16*, 3476–3483.

English Summary

Molecular motors are a unique group of photoresponsive organic molecules that are able to convert light energy into repetitive unidirectional rotary motion which is controlled by the stereogenic center in the rotor moiety.

The full 360º unidirectional rotary cycle occurs through a four-step switching cycle. These steps involve two energetically uphill photochemical isomerization steps (Scheme 1, step 1 and 3), each followed by an energetically downhill and irreversible thermal isomerization step (Scheme 1, step 2 and 4), resulting in a full 360º rotation of the rotor relative to the stator. The irreversibility of the thermal isomerization steps is key to the unidirectionality of the rotary cycle.

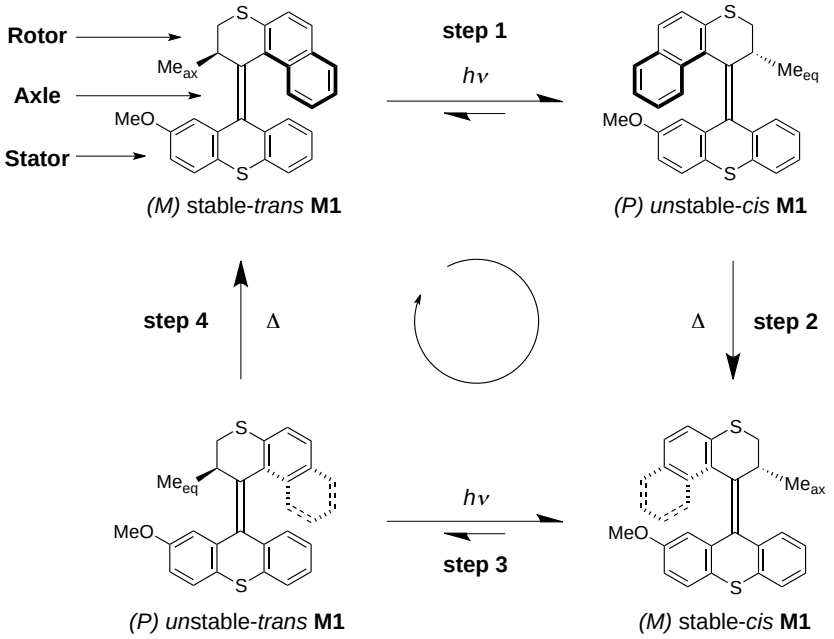

Scheme 1 Photochemical and thermal isomerization processes of molecular motors.

A major challenge in developing photo-driven systems based on molecular motors is to exploit their collective rotary motion in order to interact with external, micro- or macro-objects in a dynamic manner. However, the rotary motion of molecular motors is overwhelmed by Brownian motion when the molecules are in solution. Confining molecular motors to surfaces could inhibit Brownian motion

and hence the relative rotation of one part of the molecule with respect to the other could be converted to absolute rotation of the rotor relative to the surface.

When molecular motors are attached to the surface, two kinds of orientations could be envisioned: azimuthal and altitudinal (Figure 1). In the azimuthal orientation the axis of rotation is perpendicular to the surface, while in the altitudinal orientation it is parallel to the surface.

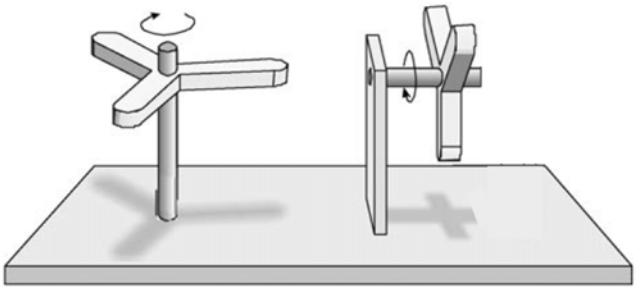

Figure 1 A schematic view of azimuthal (left) and altitudinal (right) orientations.

The proper assembly of light-driven molecular motors on surfaces while retaining their rotary motion is particularly challenging and of great importance for harnessing their collective motion to perform work. To avoid interference effects, orientation with respect to surface, mode of attachment (number of legs), distance from the surface, rigidity of anchoring groups, and packing density of the rotor moieties are all basic issues to be considered and addressed for the successful construction of new surface-bound systems based on molecular motors for dynamic nanoscale applications.

In Chapter 2, the first concept of surface wettability control using light-driven molecular motors is demonstrated. In this design, a surface functionalized with *cis* or *trans* isomers of altitudinal motor with a hydrophobic chain on the rotor shows a difference of 12º in WCA between the *cis* and *trans* isomers. However, once the motors are assembled on the surface, the wettability cannot be modulated by UV irradiation.

In Chapter 3, the design, preparation, and characterization of tripodal molecular motors for surface wettability control is described. The design comprises a molecular motor with a hydrophobic perfluorobutyl chain on the rotor and a tripodal stator containing thiol groups for self-assembly on gold. The bulky stator dictates the orientation and increases the spacing between the rotors of the surface-bound motors sufficiently to facilitate unobstructed rotary motion. This is

the first example of dynamic wettability control of solid surfaces using molecular motors decorated with a hydrophobic functional group on the rotor part.

In Chapter 4, the synthesis and photochemistry of novel molecular switches and motors bearing tetrapodal anchoring units are described. The anchoring units consist of anthracene molecules with four “legs” that are terminated with functional groups appropriate for surface attachment. A facile Diels-Alder reaction under mild conditions allows for the attachment of molecular switches and motors to the anthracene anchoring units in high yield. Studies on the photochemical and/or thermal isomerization processes of these tetrapodal molecular switches and motors are included, showing that their dynamic properties are not affected. The tetrapodal system provides an excellent platform for surface assembly of photoresponsive molecules with high control over anchoring at the surfaces.

In Chapter 5, molecular motors containing multivalent carboxylic acid groups on the stator for surface attachment is described. The acids allow for the motors to be attached to an amine-coated surface without prior activation of the acid groups. Thermal isomerization of tetravalently attached motors was not inhibited considerably by surface immobilization; however, bivalently attached motors showed a large reduction in the speed of thermal isomerization, demonstrating how subtle differences in molecular structure can considerably impact dynamic processes in nanoscale systems.

With these studies we have made major steps in the design of surface assembled molecular motors and elucidated how dynamic behavior can be fully retained in surface-bound systems. The work described in this thesis sets the stage for the control of various functions using molecular motors including the control of interaction with surface adsorbates while it also provides the stepping stone to detailed studies of single motor rotation.

Nederlandse Samenvatting

Moleculaire motoren zijn een unieke groep fotoresponsieve organische verbindingen die in staat zijn licht energie om te zetten in repetitieve unidirectionele draaiende beweging, hetgeen gecontrolleerd is door het stereogene centrum van de rotor groep.

De volledige 360º unidirectionele roterende cyclus bestaat uit vier stappen. Deze stappen behelzen twee energetisch bergopwaartse fotochemische isomerisatie stappen (Schema 1, stap 1 en 3), beide gevolgd door een energetisch bergafwaartse en irreversibele thermische isomerisatie stap (Schema 1 stap 2 en 4), resulterend in een volledige 360º rotatie van de rotor ten opzichte van de stator. De irreversibiliteit van de thermische stappen is de sleutel voor de unidirectionaltieit van de roterende cyclus.

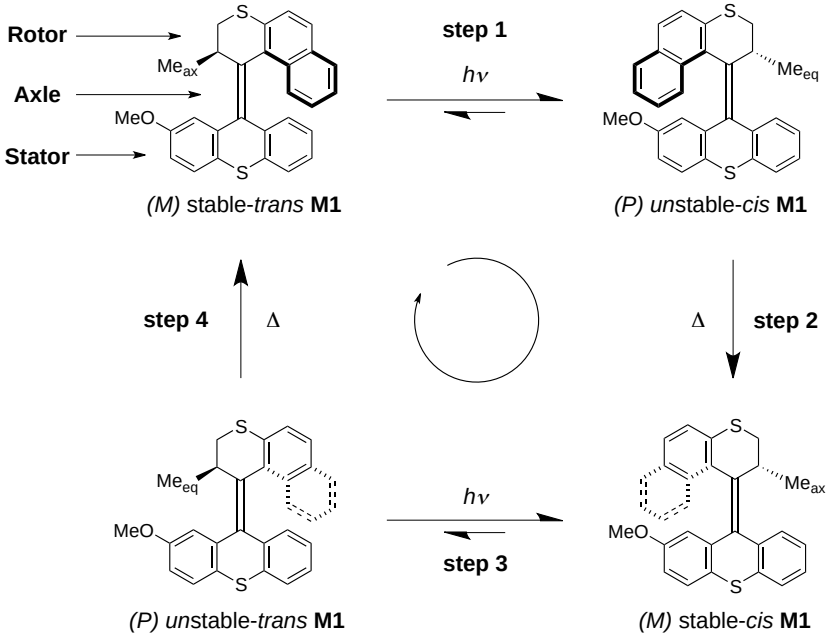

Schema 1 Fotochemische en thermische processen van de moleculaire motor.

Een belangrijke uitdaging in het ontwikkelen van lichtgestuurde systemen gebaseerd op moleculaire motoren is het exploiteren van de collectieve roterende beweging om in te werken op micro- of macro-objecten op een dynamische manier. Echter, de roterende beweging van moleculaire motoren wordt overweldigd door Browniaanse beweging wanneer de moleculen in oplossing zijn.

Moleculaire motoren immobiliseren op oppervlaktes zou de Browniaanse beweging kunnen onderdrukken en zodoende is het mogelijk om de relatieve rotatie van één deel van het molecuul ten opzichte van het andere, om te zetten in absolute rotatie van de rotor ten opzichte van het oppervlak.

Er zijn twee manieren om moleculaire motoren op een oppervlak te bevestigen: azimutaal en altitudinaal (Figuur 1). In de azimutale oriëntatie staat de as van rotatie loodrecht op het oppervlak, terwijl in de altitudinale oriëntatie de as evenwijdig is aan het oppervlak.

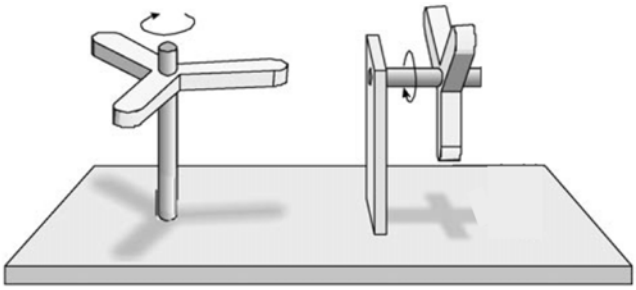

Figuur 1 Een schematische weergave van een azimutale (links) en een altitudinale (rechts) orientatie.

De juiste assemblage van met licht aangedreven moleculaire motoren op oppervlakken met behoud van hun roterende beweging is bijzonder uitdagend en van grote betekenis voor het benutten van de collectieve beweging om arbeid te verrichten. Het verhinderen van interferentie effecten, de oriëntatie ten opzichte van het oppervlak, de wijze van bevestiging (aantal poten), de afstand tot het oppervlak, de rigiditeit van de verankeringsgroepen, en de bepakkingsdichtheid van de rotor groepen zijn allemaal fundamentele kwesties die overwogen en aangepakt dienen te worden om zodoende nieuwe, op moleculaire motoren gebaseerde, aan het oppervlak gebonden systemen te maken voor dynamische nanoschaal toepassingen.

In hoofdstuk 2 is het eerste concept van de controle over de bevochtbaarheid van het oppervlak door middel van moleculaire motoren gedemonstreerd. Een oppervlak gefunctionaliseerd met het *cis* of de *trans* isomeer van een altitudinale motor met een hydrofobe groep aan de rotor een verschil van 12° WCA tussen de cis en trans isomeer. Echter, zodra de motoren zijn geassembleerd op het oppervlak, kan de bevochtbaarheid niet meer worden gemoduleerd met UV bestraling.

In hoofdstuk 3 is het ontwerp, de synthese en de karakterisatie van een driepotige moleculaire motor voor de controle over de oppervlakte bevochtbaarheid beschreven. Het ontwerp bestaat uit een moleculaire motor met een hydrofobe perfluorobutyl groep aan de rotor en een driepotige stator met thiol groepen voor de zelf-assemblage op goud. De sterisch grote stator dicteert de oriëntatie en vergroot de afstand tussen de rotors van de aan het oppervlak

gebonden motors voldoende om de ongehinderde roterende beweging mogelijk te maken. Dit is het eerste voorbeeld van dynamische controle over de bevochtbaarheid van oppervlaktes met moleculaire motoren die een hydrofobe functionele groep hebben aan het rotor deel.

In hoofdstuk 4 wordt de synthese en fotochemie van nieuwe moleculaire schakelaars en motors met een vierpotige verankeringsgroep beschreven. De verankeringsgroep bestaat uit een antraceen molecuul met vier “poten” die aan hun uiteinde functionele groepen hebben geschikt voor hechting aan oppervlak. Een eenvoudige Diels-Alder reactie onder milde condities biedt toegang tot de bevestiging van moleculaire schakelaars en motors aan de antraceen verankeringsgroep in hoge opbrengst. Het bijgevoegde onderzoek naar de fotochemische en/of thermische isomerisatie processen van deze vierpotige moleculaire schakelaars en motoren laat zien dat de dynamische eigenschappen niet beïnvloed worden. Het vierpotige systeem biedt een uitstekend platform voor oppervlak assemblage van fotoresponsieve moleculen met een hoge mate van controle over de verankering aan het oppervlak.

In hoofdstuk 5, worden moleculaire motoren met multivalente carbonzuurgroepen aan de stator voor hechting aan het oppervlak beschreven. De zuurgroepen kunnen verbonden worden aan een met amine bedekte oppervlak zonder activering van de zuurgroepen. De thermische isomerisatie van de tetravalent verbonden motoren wordt niet aanzienlijk gehinderd door immobilisatie op het oppervlak; bivalent verbonden motoren tonen echter een grote vertraging van de thermische isomerisatie, daarmee aantonend hoe subtiele verschillen in de moleculaire structuur een aanzienlijke invloed hebben op de dynamische processen op nanoschaal systemen.

Met deze studies hebben we grote vooruitgang geboekt richting het ontwerp van moleculaire motoren die op het oppervlak geassembleerd zijn en we hebben ons licht geworpen op hoe het dynamische gedrag van systemen die aan het oppervlak gebonden worden, volledig behouden kunnen blijven. Het werk beschreven in dit proefschrift heeft de weg geëffend voor de controle met moleculaire motoren over verschillende functies, inclusief de interactie van oppervlak adsorbaten. Dit proefschrift biedt eveneens een opstap naar gedetailleerde studies naar de rotatie van een enkele motor.

Acknowledgement

Life itself is amazing and deeply fascinates me. However, our knowledge of life to date is mostly built on empirical observations from which we tend to draw some conclusions even though with flaw. Shall life be part of the science? I was ready to go to Austin for my Ph.D. studies but ended up staying in Groningen for the past four years. Needless to say, I can never finish this thesis without the helps from the following people:

First of all I am grateful to my promoter, Prof. Ben Feringa, for changing my life in 2009, doing a Ph.D. in this fantastic group is for sure the highlight in my life. I always receive substantial supports from you, in all kind of aspects. I hope you are fine with my “brilliant” decoration to your cover picture. I hope that you won’t lock me in your office again, otherwise I have to call Tineke for help.

Wesley, thanks for always being helpful and efficient in correcting and improving my manuscripts and chapters. I do learn a lot from you, including how to use the laser pointer and the Mac. I also enjoyed a lot your sense of humor (Irish jokes).

I would like to thank my reading committee Prof. Wesley R. Browne, Prof. Petra Rudolf, and Prof. Jurriaan Huskens for correcting my thesis.

Thanks my neighbor Prof. Engberts for sharing the eastern poems and philosophies which enriches and inspires my life.

Tineke and Alphons, thanks for being very professional and efficient in handling many tedious works and tasks I requested, especially during my final stage.

The analytical group, Pieter, Theodora, Hans, and, Wim, is also acknowledged for their technical supports.

Gábor, thank you for the daily guidance and your contribution to my research. I enjoyed the discussions with you about the molecules on the surfaces. You also acted as a beacon in my desperate first year. Needless to say, my PhD would never be successful without the participation of you.

Jos, thank you for always being very straight and for teaching me how to solve issues and conflicts with others in a real-man way. You are the first and the only one that made me cry in the borrel. My English and Dutch also improved

significantly during the past four years due to your help (in both good and bad ways). I enjoyed climbing with you and I will never forget your “Angry Dragon” you showed me last time. I also thank Esther for teaching me “always climb until you fall down”. It was an unforgettable experience to do rock-climbing with you two in Warstein.

Tom, although you “impressed” me a lot for the first time we met in 238N (I just wanted to discuss with you about the synthesis of 2-bromofluorenone), we turned out to be the best friends. I appreciate every moment with you and sincerely hope that we can drink beers and watch football together again in the bar. I also want to thank the hospitality of Dorien which made me believe that Groningen is my second home.

Jort, you are like a big brother, teaching me many lessons in all kind of aspects (ranging from how to solve conflicts with colleagues to how to flirt a girl). You also read me quite well, and providing helpful suggestions when I am stuck in my life. My tolerance to noise and annoyance is also one level higher since we share the office together. I actually worked more efficiently without you being in the office, but felt bored at the same time (so did you, vice versa). I have to say sorry for leaving Groningen so soon, but when it’s time to move on, it’s time to go, right?

Oleksii, I still remember the way we started our collaboration, just by some simple chatting in front of our posters in Vlieland. There is no better candidate like you who can repeatedly examine my surfaces for more than 10 times. Our JACS paper was for sure a great hit due to your perseverance. When I felt stressful due to overwork, you simply told me to just work harder, and all my pressure actually disappeared this way! Hope you enjoy your life and the dark metal in Canada well.

Greg, you have invisible hands to direct my Ph.D. in the correct path. No one would believe that we published 4 papers together, and we never met and talked with each other in the real life! It only means one thing: you put significant input and effort to my researches.

Robby, thanks for inviting me being your paranymphs, Jurica and me had a lot of fun. Orange also wants to thank you for feeding her during my holiday. You just make me to miss the nasi without the hams.

Matea (panda family), no one can travel like us: going to so many places in the Netherland in one day. It was also a nice experience to cook and watch movies

with you. I saw you becoming a better chemist these days, and I firmly believe that you will be an excellent teacher in the future.

Martín, at the moment you moved to my next fumehood, everything in my world changed. I cannot imagine what kind of person I would become if you did not move to 238N three years ago, do you know the answer?

Anouk, due to your Friday-afternoon-playlist in the 238N (sometimes accompanied with your dance), the echo of these music always haunted me during my nights or holidays. Besides this, thank you for the unlimited “gay” or “banana” stickers all over the lab, I got no trouble to find my own chemicals and lab equipments since then. Oh! It was an “unforgettable” night we spent in the tent. Most importantly, you are the best and the sweetest ZaalAssistant!

Sander, my skills in academic writing improved significantly due to your training. You also helped me a lot in making the right decisions by evaluating fairly all kind of aspect that I should be concerned about. I also appreciate your way in selling an idea in a paper in the most appropriate and safest way (Please don’t finish all the Haribo in the office).

Ana (panda family), I enjoyed climbing with you in both Gropo and ACLO, thanks for accidentally remembered to put the rope into the carabiner, in our first top-rope climbing, hence I could complete this thesis in one piece today. It is also very nice that you always came with a smile :) which really cheered me up while I was struggling in the writing. Drinking beers with you with a Panda face was also a lot of fun.

Petra, thanks for providing us unlimited Haribo, which was very essential for many desperate PhDs like us. I believe that all the people around gained averagely 3 kilogram, from your candies. Besides that, your idea of playing Xmas music during summer time was quite “refreshing”.

Thomas, thanks for taking care of Orange when I was on holiday, our trip to Emmen zoo and the bird park was also an special experience. Your tips in applying jobs and postdocs are always helpful. Your special trick to grow fibers in the cuvette is invaluable, and will be very useful to the motor group.

Jochem, thanks for teaching me many lessons in “how to survive” in this group.

Thom, I enjoyed the discussions of photochemistry, molecular switches, and metal music with you.

It was a nice experience to play football with many people from all around the world, special thanks go to Arjen and Jos for organizing the football subgroup.

The past and current members of the Motor-subgroup, Gábor, Tom, Jos, Jort, Arjen, Giuseppe, Jurica, Nop, Jaiwei, Jiaobi, Lili, Anouk, Matea, Luca, Wen-Hao, Thomas, Betric, Stefano, Peter, Petra, and Sander, and the whole Feringa-group are all acknowledged for their contributions to my research, we did learn a lot from each other.

Thanks my Taiwanese fellows in Groningen, Wayne, Belinda, Sisi, Ming-Yi, Yi-Chun, Judy, Johnny, Tiffany Shu, PiawPiaw, Wan-Yun, Megon, Sophia, Larry, Mu-Chieh, Bin-Yan, Wen-Hao, Chewing, I don't feel lonely anymore because you guys are always around. Special thanks go to Flora van der Wei and Tiffany Hsu for the nice times we had together.

To my best Chinese friends in Groningen: Ning, Frankie, Bin, Runtian, Xiaoyu, thanks for always being supportive and kind to me. Hope we can meet each one day in either China or Taiwan.

Special thanks go to my brother, Klára Smolná for always sending me cute stuffs like postcards, calendar, and T-shirt, hope we will see each other soon.

Orange (a lutino cockatiel), my best companion, wish you a good second life in Rotterdam with your new friend (an albino cockatiel), I will visit soon!

Anegg, I could never be the Kuang-Yen today without your participation in my life.

No matter what decisions I made, thanks my parents for always supporting me. I want to say sorry to my sister that I cannot take care of you well while I am abroad.

陳光彥 Kuang-Yen Chen

31/08/2014 at Tiefenbrunnen, Zürich

Kuang-Yen Chen

Born March 11, 1986 **Nationality** Taiwanese

Email peterchen0311@gmail.com

EDUCATION

Ph.D. / Chemistry / University of Groningen / The Netherlands	Jul 2010 – Jul 2014
B.Sc. / Chemistry / National Taiwan University / Taiwan	Sept 2004 – Jun 2008

APPOINTMENTS

Postdoctoral Associate / ETH Zürich / Switzerland	Sept 2014 – Aug 2015
Full-time Teaching Assistant / National Taiwan University	Aug 2009 – Jul 2010
Military Service / Taiwan	Sep 2008 – Aug 2009
Chairman / 10th National Chemistry Winter School / Taiwan	Sep 2006 – Feb 2007

AWARDS AND HONORS

- Government Scholarship for Overseas Ph.D. Studies / Taiwan 2013 – 2014
- Selected for 125th BASF International Summer Course / Germany 2013
- Ubbo Emmius Ph.D. Scholarship / University of Groningen 2010 – 2014
- Dean's Award, College of Science / National Taiwan University 2008
- Research Creativity Award, National Science Council / Taiwan 2008

PUBLICATIONS

- K. -Y. Chen, O. Ivashenko, G. T. Carroll, J. Robertus, J. C. M. Kistemaker, G. London, W. R. Browne, P. Rudolf, B. L. Feringa, *J. Am. Chem. Soc.*, **2014**, *136*, 3219-3224.
- K. -Y. Chen, S. J. Wenzenberg, G. T. Carroll, G. London, J. C. M. Kistemaker, T. C. Pijper, B. L. Feringa, *J. Org. Chem.* **2014**, *79*, 7032-7040.
- J. Chen†, K. -Y. Chen†, G. T. Carroll, B. L. Feringa, *Chem. Comm.* **2014**, DOI: 10.1039/C4CC04440A.
- G. London†, K. -Y. Chen†, G. T. Carroll, B. L. Feringa, *Chem. Eur. J.*, **2013**, *19*, 10690-10697.
- H. -C. Lin, J. -H. Hsu, C. -K. Lee, O. Y. -H. Tai, C. -H. Wang, C. -M. Chou, K. -Y. Chen, Y. -L. Wu, T. -Y. Luh, *Chem. Eur. J.* **2009**, *15*, 13201-13209.

† Co-first authors / equal contributions